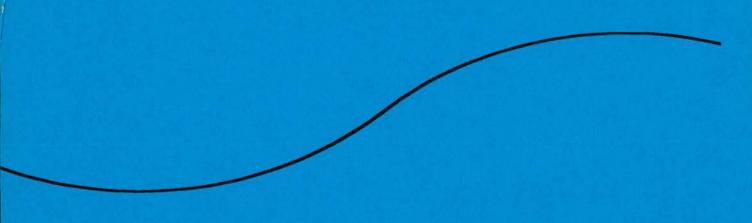
DI: 235691 -1



## INSTITUUT VOOR MARIEN EN ATMOSFERISCH ONDERZOEK UTRECHT



De functie en het gedrag van kortsluitgeulen in het westelijk deel van de Westerschelde (eindrapport contract ZL-3612)

Deel 1: tekst

drs M.C.J.L. Jeuken

R 98-06

# DE FUNCTIE EN HET GEDRAG VAN KORTSLUITGEULEN IN HET WESTELIJK DEEL VAN DE WESTERSCHELDE.

Deel 1: tekst

Eindrapport voor het contract ZL-3612

Juli 1998

M.C.J.L. Jeuken

## INHOUDSOPGAVE

Lists of Figures, Tables, Appendices and Photos

1	INLEIDIN	IG			
	1.1 Achter	rgrond en opzet van dit rapport	1		
		cadering en verkenning van het onderzoeksthema (hoofdstuk 2)	1		
		1.3 De morfologische ontwikkeling van het geulenstelsel sinds 1955 (hoofdstuk 3			
		terbeweging in enkele kortsluitgeulen gebaseerd op veldmetingen			
		stuk 4)	6		
		berekeningen (hoofdstuk 5, in voorbereiding)	8		
		van kortsluitgeulen in de morfologische ontwikkeling van het			
	geulsy		10		
		opige conclusies	11		
2	<b>MORPHO</b>	DYNAMICS OF TIDAL CHANNELS AND SHOALS IN THE			
	WESTERS	SCHELDE	14		
	2.1 Introdu	action	14		
	2.2 Morph	ologic phenomena and behaviour	14		
	2.2.1	General geomorphologic characteristics of the Schelde estuary	14		
	2.2.2	Geomorphologic characteristics of the tidal channels in the			
		Westerschelde	15		
	2.2.3	Outline of the morphological behaviour of the tidal channels in the	:		
		Westerschelde	19		
	2.2.4	Some important aspects of morphodynamic behaviour	23		
	2.3 Hydrod	dynamics and sediment transport in the Terneuzen section	26		
	2.3.1	Introduction	26		
	2.3.2	The general morphological differences between the main ebb and			
		flood channels in relation to the deformation of the tidal wave	26		
	2.3.3	The effect of channel dimensions on the primary flow pattern - a			
		preliminary analysis	28		
	2.3.4	Secondary flow phenomena	33		
	2.3.5	Sediment transport capacities in the main channels at maximum			
		flow	35		
	2.4 Resear	ch questions	38		
3	THE MORPHOLOGICAL BEHAVIOUR OF THE TIDAL CHANNELS				
	3.1 Introduction				
	3.2 Survey methods, accuracy, data sets and data processing				
	Charles of the Charles of the Charles	ds for quantitative morphological analyses	47		
	3.3.1	Introduction	47		
	3.3.2	The computation of sediment budgets	48		
	3.3.3	The computation of the cross-sectional channel geometry	49		
	3.3.4	The computation of the migration of the connecting channels	50		
	3.3.5	The assesment of dredging and dumping on the evolution of the			
		connecting channel	51		
	3.3.6	The computation of the sediment reworking	52		

		orphological evolution of the main channels in the Terneuzen and		
		veert section	52	
	3.4.1	The evolution of the planform channel geometry	52	
	3.4.2	Large-scale and small-scale variations in the sediment budgets	53	
	3.4.3	The evolution of the cross-sectional channel geometry	56	
	3.4.4	Discussion and conclusions	58	
		orphological evolution of the bar channels in the Terneuzen section	60	
	3.5.1	The evolution of the planform channel geometry	60	
	3.5.2	The evolution of the cross-sectional channel geometry	61	
	3.5.3	The reworking of sediment	64	
	3.5.4	Discussion and conclusion	64	
		orphological evolution of the cross channel in the Terneuzen section	66	
	3.6.1	The evolution of the planform channel geometry	66	
	3.6.2	The evolution of the cross-sectional channel geometry	66	
	3.6.3	Discussion and conclusion	67	
	3.7 Conclu	isions	68	
4	HYDROD	YNAMIC PROCESSES - FIELD OBSERVATIONS	71	
	4.1 Introdu	action	71	
	4.2 Measu	rement locations and methods	74	
	4.2.1	Introduction	74	
	4.2.2	Tidal water levels	75	
	4.2.3	Tidal currents	76	
	4.3 Data a	nalysis	78	
	4.3.1	The analysis of water level measurements	78	
	4.3.2	The analysis of current measurements	79	
	4.4 The ge	eneral flow pattern in the study area	83	
	4.4.1	Introduction	83	
	4.4.2	Temporal variations of tidal flow	84	
	4.4.3	Current patterns during ebb	88	
	4.4.4	Current patterns during flood	91	
	4.4.5	Tidal current asymmetry and residual flow	93	
	4.4.6	Discussion and conclusion	95	
	4.5 Hydrod	dynamics of the cross channel	97	
	4.5.1	Introduction	97	
	4.5.2	Current patterns during ebb	98	
	4.5.3	Current patterns during flood	101	
	4.5.4	Tidal current asymmetry and residual flow.	102	
	4.5.5	Discussion	103	
	4.6 Hydro	dynamics of the ebb bar channel	104	
	4.6.1	Introduction	104	
	4.6.2	Current patterns during ebb	104	
	4.6.3	Current patterns during flood	109	
	4.6.4	Current asymmetry and residual flow	112	
	4.6.5	Discussion and conclusion	113	
	4.7 Hydrod	dynamics of the flood bar channel	115	
		Introduction	115	

4.7.2	Current patterns during ebb	115
4.7.3	Current patterns during flood	118
4.7.4	Tidal current asymmetry and residual flow	120
4.7.5	Discussion and conclusion	121
4.8 Discus	121	

## Literatuur

## List of Figures

- 2.1 Schematic representation of a morphodynamic system
- 2.2 The funnel shaped geometry of the Schelde estuary and the four morphologically distinct zones:
  - a) tidal delta;
  - b) multiple tidal channel system in the Westerschelde;
  - c) single tidal channel system;
  - 4) tidal channel directly linked to the river channel.
- 2.3 The three recurring arrangements of ebb and flood channels according to van Veen (1950):
  - a) the forked tongue pattern
  - b) the flanking attack pattern
  - c) the wide estuary pattern
- 2.4 Tidal meanders.
  - a) the ideal channel pattern of Van Veen (1950), consisting of sine-shaped ebb channels and straight flood channels that start in each bend. The arrows show the expected circulation cells.
  - b) 'the estuarine meander' of Ahnert (1960).
  - c) the cuspate 'estuarine meanders' of South Alligator River. The arrows show the course of the maximum flood velocity path and the large eddies around mid the channel flats (after Vertessy, 1990, in Carter and Woodroffe, 1994).
- 2.5 Bathymetric map of the Westerschelde in greyshades. Dark shades indicate deep areas, light shades are shallow areas. White spots indicate 'no data areas'.
- 2.6 Schematized geomorphology of the various ebb and flood channels within the Westerschelde. The bathymetric map of 1990 was used as a basis for schematizing. Three different types of tidal channels exist: main channels, secondary channels and connecting channels.
- 2.7 Subdivision into three different types of connecting channels based on the geographical location within the main channel system. a) bar channels, b) cross channels, c) margin channels.
- 2.8 The subdivision of the channel and flat system into six estuarine sections. Each estuarine section has a mutually evasive meandering ebb channel and a straight flood channel separated by tidal flats and connected by connecting channels. 1= Vlissingen section, 2= Terneuzen section, 3= Hansweert section, 4= Baalhoek section, 5= Bath section, 6= border section.
- 2.9 The meandering of the main ebb channels, and accompanied extension of the flood channels and flats between 1860 and 1994 (after Van den Berg. et.al., in prep.).
- 2.10 Time and space scales of the estuarine morphology
- 2.11 Time and space scales of the estuarine hydrodynamics.
- 2.12 Deformation of the tidal wave along the Schelde estuary.
  - a) vertical tide along the Schelde with the horizontal tide at Vlissinge.
  - b) tidal range.
  - c) mean high water and mean low water along the estuary.

- d) tidal basin storage and flood volume along the estuary.
- 2.13 The subdivision of the channels into channel sections according to the Duflow schematization. The heavy, interrupted lines indicate the channel axes. Two depth contours of the bathymetric map of 1982 are indicated: ----- = Mean Low Water Spring (NAP-2.5m), —— = Mean Low Water Spring -8m (NAP-10.5m).
- 2.14 Along channel morphometry based on the Duflow schematization.
  - a) the ebb channel;
  - b) the flood channel;
  - c) the channel sections and nodes according to Duflow;

A dimensionless hydraulic radius (R/Rmean) shows the averaged depth along the channel. The cross-sectional area is divided by the averaged cross-sectional area of the entire ebb channel. The averaged cross-sectional area and hydraulic radius are weighted for the channel length as

$$A_{mean} = \sum_{i=28}^{i=37} \left( \frac{L_{section\ i}}{L_{channel}} * A_{section\ i} \right)$$

The dimensionless parameter (1-(R/Ro) visualizes the channel bed (Ro=30m). The sections 45 and 52 are joined by considering the averaged depth and the sum of the cross-sectional areas. The values of the parameters are plotted in the middle of esch channel section.

- 2.15 Water levels and current velocities in the main ebb and flood channel at maximum tidal flow.
  - a) flow response in the ebb channel at maximum flood
  - b) flow response in the flood channel at maximum flood
  - c) flow response in the ebb channel during maximum ebb
  - d) flow response in the flood channel during maximum ebb. The waterlevel of section 45 is plotted. (R=hydraulic radius,

Ro=30m). Note that the ebb values are negative and flood values positive.

- Values of the variables in the simplified momentum equation at maximum flow  $(\Delta h/\Delta L = Q^2/A^2R^2C^2)$ .
  - a) Values of the various variables at maximum ebb flow
  - b) Values of the various variables at maximum flood flow.

The variables discharge (Q), cross-sectional area (A), cross-sectional velocity (U), and hydraulic radius (R), are weighted for the length of the

specific channel section, according to e.g. 
$$A_{mean} = \sum_{i=28}^{i=37} \left( \frac{L_{section\ i}}{L_{channel}} * A_{section\ i} \right)$$

- 2.17 The initial adaptations in flow pattern and water level pattern due to morphological changes. Each figure presents the following four situations:

  A) reference situation. B) the channel pattern without the large cross channel, C) the effect of a clockwise rotation of the cross channel of 30°.

  D) the effect of a deepening of the flood channel bar by 15 %. Solid heavy line = increase with respect to the reference situation, dotted line indicates a decrease.
  - a) situation at maximum ebb;
  - b) situation at maximum flood;

- 2.18 Calculated sediment transport capacity (kg/s) according to Van Rijn (1990) at maximum flow, using the flow response of Duflow. (R=hydraulic radius, Ro=30m).
  - a) flood transport capacity in the ebb channel
  - b) flood transport capacity in the flood channel
  - c) ebb transport capacity in the ebb channel
  - d) ebb transport capacity in the flood channel.
- 2.19 Calculated est ion and sedimentation pattern near the flood channel bar. Calculation of the sediment transport is based on a Duflow simulation and the application of Van Rijn's (1990) formula for suspended and bed load transport.
  - a) bar morphology and the channel sections according to Duflow
  - b) erosion and sedimentation at maximum flood and ebb
- 2.20 Expected patterns of primary flow and erosion and sedimentation related to the morphology of bar channels
  - a) channel morphology of the bar channels at flood channel bar in 1982 and 1992.
  - b) flow pattern at ebb and flood across the bar channel morphology in 1992.
  - c) expected patterns of erosion and sedimentation at ebb and flood.
- 2.21 Expected patterns of flow and erosion and sedimentation in the ebbdominated bar channel.
  - a) Channel morphology of 1992
  - b) expected secondary flow phenomena and the course of the primary flow at ebb and flood.
  - c) expected locations of erosion and sedimentation at ebb and flood
- 2.22 Expected patterns of flow and erosion and sedimentation in the ebb-dominated cross channel.
  - a) Channel morphology of 1992
  - b) expected secondary flow phenomena and the course of the primary flow at ebb and flood.
  - c) expected locations of erosion and sedimentation at ebb and flood
- Bathymetric maps of the Westerschelde in 1994 (a), the Terneuzen and Hansweert section in 1994 (b) and the bar channels in 1974 (c) and 1994 (d).

FC#= main flood channel (and number)

EC=main ebb channel

BC & CC = connecting channels: CC = cross channel BC= bar channel (+number)

B#= bar in main channel.

NAP= Dutch Ordnance level.

These abbreviations of the channel types are used throughout the chapter.

- 3.2 The schematisation of the main channels into channel sections, to compute the changes in the sediment budgets and the average cross-sectional channel geometry.
- 3.3 Definition sketch of the computation of the channel migration.

- 3.4 The total sediment reworking at the bar B1 in the main flood channel FC1(section 4, Fig. 3.2) versus time interval.
- 3.5 Erosion-sedimentation patterns over the period 1955-1996.
- 3.6 Large-scale changes in the sediment budget (in Mm<sup>3</sup>) in the Terneuzen and Hansweert section between 1955 and 1996. The changes refer to the water volume below NAP+2.5m
- 3.7 Small-scale changes in the sediment budget (in Mm³) in the Terneuzen and Hanswell section between 1955 and 1996. The changes refer to the water volume below NAP+2.5m
- 3.8 Small-scale evolution of the sediment budgets (in Mm<sup>3</sup>) in the main flood channel FC1 in the Terneuzen section between 1955 and 1996. FC1 is the entire main flood channel (= sum of changes in sections 1,2,3 and 4).
  - a) changes in the channel volume (water volume below NAP-2m)
  - b) changes in the intertidal shoal volume (sand volume above NAP-2m)
  - c) cumulative net magnitude of dredging and dumping. Positive values mean a net dredging, whereas negative values indicate a net dumping.
- 3.9 Small-scale evolution of the sediment budgets (in Mm³) in the main ebb channel EC1 in the Terneuzen section between 1955 and 1996. EC1 is the entire main ebb channel (= sum of changes in sections 5,6,7,8 and 9).
  - a) changes in the channel volume (water volume below NAP-2m)
  - b) changes in the intertidal shoal volume (sand volume above NAP-2m)
  - c) cumulative net magnitude of dredging and dumping. Positive values mean a net dredging, whereas negative values indicate a net dumping.
- 3.10 Small-scale evolution of the sediment budgets (in Mm<sup>3</sup>) in the main flood channel FC2 in the Hansweert section between 1955 and 1996. FC2 is the entire main flood channel (= sum of changes in sections 15, 16 and 17).
  - a) changes in the channel volume (water volume below NAP-2m)
  - b) changes in the intertidal shoal volume (sand volume above NAP-2m)
  - c) cumulative net magnitude of dredging and dumping. Positive values mean a net dredging, whereas negative values indicate a net dumping.
- 3.11 Small-scale evolution of the sediment budgets (in Mm³) in the main ebb channel EC2 in the Hansweert section between 1955 and 1996. EC2 is the entire main ebb channel (= sum of changes in sections 11, 12, 13 and 14).
  - a) changes in the channel volume (water volume below NAP-2m)
  - b) changes in the intertidal shoal volume (sand volume above NAP-2m)
  - c) cumulative net magnitude of dredging and dumping. Positive values mean a net dredging, whereas negative values indicate a net dumping.
- 3.12 Evolution of the cross-sectional channel geometry of the main channels FC1 and EC1 in the Terneuzen section between 1955 and 1996. FC1 = entire main flood channel, EC1=entire main ebb channel
  - a) average cross sectional area of the main flood channel
  - b) average hydraulic radius of the main flood channel
  - c) average cross sectional area of the main ebb channel
  - d) average hydraulic radius of the main ebb channel
- 3.13 Evolution of the cross-sectional channel geometry of the main channels FC2 and EC2 in the Hansweert section between 1955 and 1996. FC2 = entire main flood channel, EC2=entire main ebb channel

- a) average cross sectional area of the main flood channel
- b) average hydraulic radius of the main flood channel
- c) average cross sectional area of the main ebb channel
- d) average hydraulic radius of the main ebb channel
- 3.14 Changes in the distribution of the tidal volumes (in Mm³) between the main ebb and flood channel in the Terneuzen and Hansweert section since 1932, based on discharge measurements.
  - a) ebb volumes in the main channels of the Terneuzen section
  - b) flood volumes in the main channels of the Terneuzen section
  - c) ebb volumes in the main channels of the Hansweert section
  - d flood volumes in the main channels of the Hansweert section
- 3.15 The three patterns of bar channels between 1955 and 1996.
- 3.16 The morphological evolution of channel pattern 1 in the Terneuzen section.
  - a) changes in the average cross-sectional area of the channels.
  - b) changes in the average hydraulic radius of the channels.
  - c) average migration rates and cumulative channel displacement
  - d) changes in the location of the channel axis.
- 3.17 The observed changes in the cross sectional area of channel pattern 1 (in %) and the potential changes in the channel cross section as result of dredging and dumping. Positive values indicate an increase of the channel cross section.

  Negative values indicate a decrease of the channel cross section.
  - a) the flood bar channel BC1
  - b) the ebb bar channel BC2
- 3.18 The morphological evolution of channel pattern 2 in the Terneuzen section.
  - a) changes in the average cross-sectional area of the channels.
  - b) changes in the average hydraulic radius of the channels.
  - c) average migration rates and cumulative channel displacement
  - d) changes in the location of the channel axis.
- 3.19 The observed changes in the cross sectional area of the bar channels of pattern 1 (in %) and the potential changes in the channel cross section as result of dredging and dumping. Positive values indicate an increase of the channel cross section. Negative values indicate a decrease of the channel cross section.
  - a) the ebb bar channel BC3
  - b) the flood bar channel BC4
  - c) the flood bar channel BC5
- 3.20 The total sediment reworking at the bar B1 together with the reworking induced by the migration of the bar channels BC1, BC2, BC12, BC3, BC4.
  - sediment reworking during pattern 1 (based on the 'standard echosoundings').
  - sediment reworking during pattern 2 (based on the 'specific echosoundings').
- 3.21 The morphological evolution of the cross channel (cc in Fig. 3.1) in the Terneuzen section
  - a) changes in the location of the channel axis.
  - b) average migration rates and cumulative channel displacement
  - c) changes in the average cross-sectional area and hydraulic radius of the

- d) net changes in cross-sectional area and the potential changes of dredging.
- 4.1 The location and morphology of the three different types of connecting channels in 1994/1995
- 4.2 The general hydrodynamics in the study area: overview of the measurements.
- 4.3 Overview of the measurements in the connecting channels in 1994
- 4.4 Overview of the measurements in the connecting channels in 1995
- 4.5 Overview of the measurements in the connecting channels in 1996
- 4.6 Definition sketch of the coordinate systems used in the analysis of discharge measurements and ADCP observations of the vertical current structure.
- 4.7 Relationships between channel geometry and tidal flow parameters for the Westerschelde and measurement values obtained in the present study (for location of transects see Figure 4.2).
  a) ebb volume versus cross-sectional area, b) flood volume versus cross-

sectional area, c) dominant volume versus cross-sectional area, d) dominant volume versus streampower.

- 4.8 Tidal wave propagation along the estuary during neap, mean and spring tide. a) tidal range, b) delay of high water with respect to Vlissingen (hours), c) delay of low water with repsect to Vlissingen d) difference in delay between low water and high water (hours), e) duration of tidal rise, f) duration of tidal fall, g) duration difference between fall and rise, h) tidal period, i) discharge and
  - water level at the landward boundary, j) discharge and water level at the seaward boundary.
- 4.9 Water levels at the seaward and landward boundary of the study area and the water level difference (water level station 1 and 2, for locations see Fig. 4.2).a) spring tide, b) mean tide, c) neap tide.
- 4.10 Duration of tidal fall and tidal rise versus tidal range at Terneuzen, as occurred during the water level measurements.
- 4.11 Temporal variation in falls along the five channel sections in the study area.

  During spring tide (a & b), during mean tide (c & d) and during neap tide (e & f).
- 4.12 Temporal variation in discharge and cross-sectional velocities as occurred during the measurements (for locations see Fig. 4.2).
  - a) discharges in transect 1, b) velocities in transect 1
  - c) discharges in transect 2, d) velocities in transect 2
  - e) discharges in transect 4, f) velocities in transect 4
  - g) discharges in transect 3, h) velocities in transect 3
  - i) discharges in transect 5, j) velocities in transect 5
  - i) discharges in transect 6, k) velocities in transect 6
- 4.13 Overview of the time of maximum flood and maximum ebb flow in the studya area.
- 4.14 Temporal variation in depth-averaged current velocities and falls in the cross channel (for locations see Fig. 4.3 and 4.4).a) current velocities at location 5 and 6, b) current velocities at location 13 and falls along the channel.
- 4.15 Variation in mean and maximum falls and surface slopes along the five channel sections during ebb. Maximum refers to the condition of maximum

- currents (= 4 hours after high water). Mean refers to the average values over the ebb period.
- 4.16 Spatial patterns of ebb volumes for neap, mean and spring tide together with the water budgets for mean tide.
- 4.17 Spatial patterns of maximum ebb discharges during mean, neap and spring tide.
- 4.18 Variation in mean and maximum falls and surface slopes along the five channel sections during flood. Maximum refers to the condition of maximum flood currents (= 11.6 hours after high water). Mean refers to the average values over the flood period.
- 4.19 Spatial patterns of flood volumes for neap, mean and spring tide together with the water budgets for mean tide.
- 4.20 Spatial patterns of maximum flood discharges during mean, neap and pring tide.
- 4.21 Spatial patterns of current asymmetry and the maximum values of tidal flow during ebb and flood for mean, neap and spring tide. a) tidal volumes, b) maximum discharges, c)cross-sectional velocities.
- 4.22 Residual cross-sectional velocities as occured during the measurements.
- 4.23 Spatial pattern of residual water transports and transport velocities for mean, neap and spring tide.
- 4.24 Mean lagrangian current patterns in the cross channel during ebb.
- 4.25 Depth-averaged tidal current patterns in the cross channel during ebb and mean tidal conditions in April 1994 (locations 5 and 6) and November 1994 (11 to 13).
- 4.26 Differences in current direction between near-surface and near-bed significant current vectors versus near-bed current velocity and velocity difference in the cross channel during ebb (locations 11 and 13, Figure 4.3).
- 4.27 Mean lagrangian current patterns in the cross channel during flood and mean tidal conditions.
- 4.28 Depth-averaged tidal current patterns in the cross channel during flood and mean tidal conditions in April 1994 (locations 5 and 6) and November 1994 (11 to 13).
- 4.29 Current asymmetry in the cross channel. a) measurement locations, b) significant current vector and asymmetry ratio's during mean tide, c) asymmetry ratio's for neap and spring tide, d) significant velocity and asymmetry versus tidal range.
- 4.30 Long-term mean depth-averaged residual current vectors in the cross channel.
  a) measurement locations, b) residual currents.
- 4.31 Mean lagrangian current patterns in the ebb bar channel during accelerating ebb on 4 November 1994.
- 4.32 Mean lagrangian current patterns in the ebb bar channel during maximum and decelerating ebb on 8 November 1994
- 4.33 Depth-averaged current current patterns in the ebb bar channel during ebb and mean tidal conditions in November 1994
- 4.34 Depth-averaged current current patterns in the ebb bar channel during ebb and mean tidal conditions in June 1995.
- 4.35 Cross-sectionally averaged and depth-averaged currents in the ebb bar channel along transect 5 2 and 5 3 during ebb. a) locations and orientations of ADCP-

- transects, b) time-series of the cross-sectionally averaged currents, c) magintude of depth-averaged current vectors along transect 5\_2. d) direction of depth-averaged current vectors along transect 5\_2. e) magintude of depth-averaged current vectors along transect 5\_3. f) direction of depth-averaged current vectors along transect 5\_3.
- 4.36 Depth-averaged along-channel and cross-channel velocity patterns over the bar of the ebb bar channel during ebb (transect 5\_1), ac= acceleration of the flow, dc=deceleration of the flow, dsb=downstream side of the bar, usb=ustream side of the bar. Negative along-channel component is ebb, positive component is flood.
- 4.37 Countour plots of the relative magnitude of the secondary flow (in % of the magnitude of the depth-averaged current velocity) and current veering with repect to the depth-averaged current direction in the central part of the ebb bar channel (transect 5\_2, Fig. 5.4). a & b) accelerating ebb, c & d) maximum ebb, e & f) decelerating ebb.
- 4.38 Contourplots of the relative magnitude of secondary flow and current veering near the bar in the ebb bar channel durinf ebb (transect 5\_3, for location see Fig. 4.5).
- 4.39 Mean lagrangian current patterns in the ebb bar channel during flood on 4 November 1994
- 4.40 Depth-averaged current current patterns in the ebb bar channel during flood and mean tidal conditions in November 1994
- 4.41 Depth-averaged current current patterns in the ebb bar channel during flood and mean tidal conditions in June 1995.
- 4.42 Cross-sectionally averaged and depth-averaged currents in the ebb bar channel along transect 5\_2 and 5\_3 during flood. a) locations and orientations of ADCP-transects, b) time-series of the cross-sectionally averaged currents, c) magintude of depth-averaged current vectors along transect 5\_2. d) direction of depth-averaged current vectors along transect 5\_2. e) magintude of depth-averaged current vectors along transect 5\_3. f) direction of depth-averaged current vectors along transect 5\_3. f) direction of depth-averaged current vectors along transect 5\_3.
- 4.43 Depth-averaged along-channel and cross-channel velocity patterns over the bar of the ebb bar channel during flood (transect 5\_1), ac= acceleration of the flow, dc=deceleration of the flow, dsb=downstream side of the bar, usb=ustream side of the bar. Negative along-channel component is ebb, positive component is flood.
- 4.44 Countour plots of the relative magnitude of the secondary flow (in % of the magnitude of the depth-averaged current velocity) and current veering with repect to the depth-averaged current direction in the central part of the ebb bar channel during flood (transect 5\_2, Fig. 5.4). a & b) accelerating flood, c & d) maximum flood, e & f) decelerating flood.
- 4.45 Contourplots of the relative magnitude of secondary flow and current veering near the bar in the ebb bar channel during flood (transect 5\_3, for location see Fig. 4.5).
- 4.46 Current asymmetry in the ebb bar channel channel in November 1994 and June 1995. a & b) measurement locations, c & d) significant current vector and

- asymmetry ratio's during mean tide, e & f) asymmetry ratio's for neap and spring tide
- 4.47 Residual current vectors in the ebb bar channel channel in November 1994 and June 1995. a & b) measurement locations, c & d) long-term mean residual current vectors.
- 4.48 Depth-averaged current current patterns in the flood bar channel during ebb and mean tidal conditions in August 1995.
- 4.49 Depth-averaged current current patterns in the flood bar channel during ebb and mean tidal conditions in February 1996.
- 4.50 Cross-sectionally averaged and depth-averaged currents in the flood bar channel along transect 6\_2 and 6\_3 during ebb. a) locations and orientations of ADCP-transects, b) time-series of the cross-sectionally averaged currents, c) magintude of depth-averaged current vectors along transect 6\_2. d) direction of depth-averaged current vectors along transect 6\_2. e) magintude of depth-averaged current vectors along transect 6\_3. f) direction of depth-averaged current vectors along transect 6\_3. f) direction of depth-averaged current vectors along transect 6\_3.
- 4.51 Depth-averaged along-channel and cross-channel velocity patterns over the bar of the ebb bar channel during ebb (transect 6\_1), ac= acceleration of the flow, dc=deceleration of the flow, dsb=downstream side of the bar, usb=ustream side of the bar. Negative along-channel component is ebb, positive component is flood.
- 4.52 Countour plots of the relative magnitude of the secondary flow (in %) and current veering in the central part of the flood bar channel (transect 6\_2, Fig. 5.4) during maximum ebb flow. a & b) transect 6\_2, c & d) transect 6\_3.
- 4.53 Depth-averaged current current patterns in the flood bar channel during flood and mean tidal conditions in August 1995.
- 4.54 Depth-averaged current current patterns in the flood bar channel during flood and mean tidal conditions in February 1996.
- 4.55 Cross-sectionally averaged and depth-averaged currents in the flood bar channel along transect 6\_2 and 6\_3 during flood. a) locations and orientations of ADCP-transects, b) time-series of the cross-sectionally averaged currents, c) magintude of depth-averaged current vectors along transect 6\_2. d) direction of depth-averaged current vectors along transect 6\_2. e) magintude of depth-averaged current vectors along transect 6\_3. f) direction of depth-averaged current vectors along transect 6\_3. f) direction of depth-averaged current vectors along transect 6\_3.
- 4.56 Depth-averaged along-channel and cross-channel velocity patterns over the bar in the flood bar channel during flood (transect 6\_1), ac= acceleration of the flow, dc=deceleration of the flow, dsb=downstream side of the bar, usb=ustream side of the bar. Negative along-channel component is ebb, positive component is flood.
- 4.57 Countour plots of the relative magnitude of the secondary flow (in %) and current veering in the central part of the flood bar channel (transect 6\_2, Fig. 5.4) near maximum flood flow. a & b) transect 6\_2, c & d) transect 6\_3.
- 4.58 Current asymmetry in the flood bar channel channel in August 1995 and February 1996. a & b) measurement locations, c & d) significant current vector and asymmetry ratio's during mean tide, e & f) asymmetry ratio's for neap and spring tide

- 4.59 Residual current vectors in the flood bar channel channel in August 1995 and February 1996. a & b) measurement locations, c & d) long-term mean residual current vectors.
- 4.60 Large and small-scale circulations of flow in the study area.

#### List of Tables

- 3.1 Budget changes (in Mm³) in the Terneuzen and Hansweert section between 1955 and 1996
- 3.2 Budget changes (in Mm<sup>3</sup>) in the Terneuzen section between 1955 and 1996
- 3.3 Budget changes (in Mm<sup>3</sup>) in the Hansweert section between 1955 and 1996
- 4.1 Hydrodynamic and meteorological conditions during the discharge measurements
- 4.2 Accuracy of water level measurements
- 4.3 System configurations during the two ADCP surveys
- 4.4 Configuration and summary of the smapling procedures of the EMF-frame.
- 4.5 Current veering in the cross channel based on significant current vectors at 'Flachsee' locations 11 and 13 during ebb.
- 4.6 Overview of the conditions and observations during the near-bed current measurements in the channel bend of the cross channel.
- 4.7 Current veering in the cross channel based on significant current vectors at 'Flachsee' locations 11 and 13 during flood.
- 4.8 Comparison of measured and computed secondary flow in the central part of the ebb bar channel during ebb and flood.

## List of Appendices

- 3.0 Computation of the average cross-sectional area and hydraulic radius.
- 3.1 Location and legend of Enclosures 2 and 3
- 3.2 Bathymetric maps of the Terneuzen and the Hansweert section in 1955, 1964, 1974, 1982, 1990, 1996.
- 3.3 Bathymetric maps of the bar area in the main flood channel in the Terneuzen section during the period 1955 up to 1996 (based on 'standard' echosoundings).
- 4.1 Overview of measurement locations and periods (ontbreekt)
- 4.2 Filtering of the ADCP-velocity profiles (ontbreekt)
- 4.3 Application of the shape-function approach to the filtered ADCP profiles (ontbreekt).
- A Congrespublikatie
- B Vrdere uitwerking van de verkennende modelsommen uit hoofdstuk 2.

## List of Photos

- 4.1 Water level station 3 (ontbreekt)
- 4.2 EMF-frame (ontbreekt)

#### 1 INLEIDING

### 1.1 Achtergrond en opzet van dit rapport

In opdracht van Rijkswaterstaat Directie Zeeland heeft de vakgroep Fysische Geografie van de Universiteit Utrecht onderzoek verricht naar het geulgedrag in het westelijk deel van de Westerschelde. Het voorliggende rapport is bedoeld als eindrapport voor het contract ZL-3612. Een verdere wetenschappelijke verdieping en uitbreiding van het onderzoek, met als beoogd resultaat een proefschrift, volgen nog.

De opzet van de rapportage is als volgt. De paragrafen 1.2 t/m 1.4 van dit hoofdstuk geven een (nederlandse) samenvatting van het onderzoek. Paragraaf 1.5 geeft de stand van zaken met betrekking tot de modelberekeningen weer. Een hypothese over het functioneren van de kortsluitgeulen binnen het geulenstelsel en enkele *voorlopige* conclusies worden gegeven in de paragrafen 1.6 en 1.7. De hoofdstukken 2 t/m 4 beschrijven de voorlopige resultaten van het onderzoek (in het engels). Een publikatie over de waterbeweging in twee kortsluitgeulen, in de proceedings van de "International Conference on Coastal Engineering 1996", is opgenomen in bijlage A. Bijlage B bevat een voorlopige verdere uitwerking van de verkennende stroomberekeningen uit hoofdstuk 2.

1.2 De inkadering en verkenning van het onderzoeksthema (hoofdstuk 2, Bijlage B)

Opmerking: de namen van de geulen (FC#, EC#, BC# en CC) verwijzen naar figuur 3.1

Het algemene doel van het onderzoek is het vergroten van de kennis over het geulgedrag in de Westerschelde op de tijdschaal van jaren tot decennia. Meer specifiek richt het onderzoek zich op het begrijpen van de functie en het gedrag van de kortsluitgeulen in de morfologische ontwikkeling van het geulsysteem in het westelijk deel van de Westerschelde. Met gedrag wordt hier bedoeld de interactie tussen waterbeweging, sediment transport en morfologie en de terugkoppeling van de morfologische veranderingen op de hydrodynamische en sediment transport processen.

Er is nog vrij weinig bekend over stroom- en transportprocessen in relatie tot de morfologie en het morfologisch gedrag van geulsystemen in getijdemilieus. Zeker is wel dat het hier een tamelijk complexe materie betreft. Van meet af aan is daarom de noodzaak gevoeld om het onderzoek in te perken tot enkele onderdelen van het morfologisch systeem. De inperkingen en de formulering van de onderzoeksvragen zijn voornamelijk gebaseerd op een morfologische classificatie van het geulsysteem en enkele verkennende stroomberekeningen. Het classificeren van de geulen is geen doel op zich. Het moet worden gezien als een hulpmiddel bij het inperken en verkennen van de probleemstelling van het onderzoek.

De morfologische classificatie, gebaseerd op eerder werk van Van Veen (1950), laat zien dat het geulenstelsel van de Westerschelde zeer regelmatig is en in essentie uit drie verschillende geultypen bestaat (fig. 2.6 en 2.7):

- 1) hoofdgeulen ('main channels')
- 2) secundaire geulen ('secondary channels')
- 3) kortsluitgeulen ('connecting channels'), op basis van hun ligging onder te verdelen in:
  - drempelgeulen ('bar channels')
  - dwarsgeulen ('cross channel')
  - randgeulen ('margin channels')

Op basis van de locatie van de drempels, aan de zeewaartse of landwaartse zijde van een geul, kunnen de geulen verder worden onderverdeeld in eb- en vloedgeulen. De hoofdgeulen en kortsluitgeulen vormen samen een elementair geulpatroon, aangeduid als estuariene sectie. De regel-

maat van het geulenstelsel in de Westerschelde komt tot uitdrukking in de aanwezigheid van zes estuariene secties (fig.2.8). Iedere estuariene sectie bestaat uit twee hoofdgeulen, een rechte vloedgeul en een gekromde ebgeul, die op diverse plaatsen met elkaar verbonden zijn/waren door één of twee typen kortsluitgeulen (drempelgeulen en eventueel dwarsgeulen). De regelmaat in het geulenstelsel suggereert de aanwezigheid van bepaalde morfodynamische processen die in iedere estuariene sectie werkzaam zijn. Dit betekent dat een analyse van morfodynamische geulgedrag van één estuariene sectie leidt tot inzichten die naar verwachting ook bruikbaar zijn voor andere delen (secties) van de Westerschelde (inductieve benadering). Op basis hiervan is het geulsysteem nabij Terneuzen, de Terneuzen sectie, gekozen als hoofdonderzoeksgebied. Deze estuariene sectie wordt gekenmerkt door diverse kortsluitgeulen, zowel drempelgeulen (BC#) als dwarsgeulen (CC), in en nabij het ondiepe drempelgebied (B1) van de grote vloedgeul (FC1, fig. 3.1).

Ter verkenning zijn enkele 1D-stroomberekeningen uitgevoerd voor het geulsysteem van de Terneuzen sectie. Hieruit blijkt dat het ondiepe drempelgebied B1 (fig.3.1) in de grote vloedgeul FC1 een sturend element is in de waterbeweging tijdens de bed-vormende condities rond maximum stroom (bijlage B). Door de relatief grote bodemwrijving die de getijstroom boven het drempelgenied B1 ondervindt, beïnvloedt de drempel de debietverdeling in de gehele estuariene sectie. Met name de waterbeweging in de kortsluitgeul Zuid-Everingen (CC in fig. 3.1, dwarsgeul) en het drempelgebied B1 hangen nauw met elkaar samen. Verder blijkt dat de waterbeweging in de hoofdgeulen is aangepast aan de aanwezigheid van de kortsluitgeulen. Deze observaties suggereren dat de drempel (B1) in de vloedgeul (FC1) en de kortsluitgeulen (BC#, CC) een belangrijke rol spelen in de waterbeweging en daarmee de morfologische ontwikkeling van het geulsysteem. Met name de kortsluitgeulen zouden wel eens belangrijke rol kunnen spelen in de ontwikkeling van het geulsysteem omdat ze het uiterlijk, en naar verwachting ook de morfologische veranderingen, van het drempelgebied B1 in de vloedgeul FC1 bepalen.

Het potentiële belang van de kortsluitgeulen en de drempel in de vloedgeul voor de morfologische ontwikkeling van het geulsysteem is niet eerder onderkend en daardoor ook niet systematisch onderzocht. Het huidige onderzoek richt zich op deze kennislacune. Tijdens de formulering van de probleemstelling van het onderzoek zijn met betrekking tot dit centrale onderzoeksthema de volgende hypothesen geformuleerd:

- 1 de eb- en vloedgedomineerde drempelgeulen zorgen voor de instandhouding en de veranderingen in het sedimentbudget en de gemiddelde geometrie van de drempel B1 in de vloedgeul FC1.
- 2 de kortsluitgeul Zuid-Everingen (dwarsgeul) is mede verantwoordelijk voor de instandhouding en morfologische veranderingen van de drempel in de vloedgeul en versterkt het eb-vloedschaar karakter van de hoofdgeulen.

Tijdens het onderzoek werd al vrij snel duidelijk dat deze hypothese moeilijk te toetsen is op basis van veldwaarnemingen. Dit komt doordat de werkelijke morfologische veranderingen van de kortsluitgeul kleiner (minder extreem) en meer geleidelijk verlopen dan in de verkennende modelberekeningen. Bovendien suggereert het verschil in afmeting tussen de kortsluitgeul en de drempel, dat het waarschijnlijker is dat de kortsluitgeul de morfologische veranderingen van het drempelgebied volgt in plaats van andersom. Daarom is de nadruk gelegd op het herkennen en verklaren van een samenhang in de morfologische ontwikkeling van de kortsluitgeul en het drempelgebied in plaats van het toetsen van de hypothese. Of de kortsluitgeul het eb- vloedschaar karakter van de hoofdgeulen versterkt is alleen te onderbouwen met gevoeligheidsberekeningen met een morfodynamisch model. Dit heeft vooralsnog een lagere prioriteit.

3 Transversale secundaire circulaties zorgen voor de migratie van de kortsluitgeulen in de huidige

situatie (1995).

De probleemstelling van het onderzoek beperkt zich dus tot het begrijpen van het gedrag en de functie van de kortsluitgeulen in de morfologische ontwikkeling van het geulsysteem in de Terneuzen sectie. Hierbij zijn drie verschillende onderzoeksmethoden togepast: 1) het analyseren van het opgetreden morfologische geulgedrag, 2) het vergroten van de hydrodynamische proceskennis op basis van veldmetingen, en 3) modelberekeningen. De kracht van het onderzoek ligt in de integratie van deze drie methoden. De volgende doelen en onderzoeksvragen komen aan de orde:

- De morfologische analyses hadden tot doel het bepalen van de ruimtelijke en temporele samenhang in de morfologische ontwikkeling van de kortsluitgeulen en hoofdgeulen in de Terneuzen sectie (hoofdstuk 3).
  - Door welke ruimtelijke en temporele variaties worden de sedimentbudgetten van de hoofdgeulen gekenmerkt? Wordt de drempel in de grote vloedgeul gekarakteriseerd door perioden van erosie en/of sedimentatie? Bestaat er een temporele samenhang tussen de budget veranderingen van de drempel en de budgetveranderingen elders in de hoofdgeulen? Hoe verhouden de waargenomen budgetveranderingen zich tot de ingrepen? Zijn de budgetveranderingen gepaard gegaan met duidelijke veranderingen in de gemiddelde geometrie van de geulen?
  - Welke temporele variaties treden op in het patroon van kortsluitgeulen? Door welke stadia en tijdschalen wordt de morfologische ontwikkeling van de individuele kortsluitgeulen gekenmerkt? Op welke manier en met welke snelheden migreren de kortsluitgeulen? Bestaat er een samenhang tussen de ontwikkeling van de individuele kortsluitgeulen. Hebben bagger- en stortactiviteiten de geulontwikkeling gestuurd?
  - Is er een temporele samenhang tussen het gedrag van de verschillende kortsluitgeulen en dat van de hoofdgeulen? In hoeverre gaan de morfologische veranderingen van de kortsluitgeulen gepaard met veranderingen in het sedimentbudget en de gemiddelde geometrie van de drempel B1 in de vloedgeul? Zijn er bepaalde condities waaronder kortsluitgeulen ontstaan?

Eerdere grootschalige zandbalansstudies suggereren dat de morfologische ontwikkelingen in Terneuzen sectie sinds 1955 samenhangen met de bodemveranderingen in de landwaarts aangrenzende Hansweert sectie. De volgende vragen dienen daarom ook te worden beantwoord:

- Wat is het geulgedrag in de Hansweert sectie en hoe hangt dit eventueel samen met de geulontwikkeling in de Terneuzen sectie?
- De hydrodynamische veldmetingen hadden tot doel de kennis over de ruimtelijke en temporele variabiliteit in de instantane en getijmiddelde stroompatronen en -processen in relatie tot de morfologie van de (kortsluit)geulen, te vergroten (hoofdstuk 4). De verkregen proceskennis draagt bij aan de toetsing van de hypothesen 1 en 3 en wordt gebruikt voor het verklaren van het waargenomen geulgedrag (hoofdstuk 3) op basis van modelberekeningen (hoofdstuk 5).
  - In hoeverre wordt de instantane waterbeweging in de geulen gekenmerkt door stroomversnellingen en -vertragingen en stroomconvergentie en -divergentie? Wat zijn de verschillen en overeenkomsten in het stroompatroon tijdens eb en vloed en tijdens doodtij en springtij? Zijn de drempels in de geulen versnellings- of vertragingsgebieden, geen van beiden of allebei?
  - Wordt de instantane waterbeweging gekenmerkt door transversale secundaire circulaties. Zijn er aanwijzingen voor het optreden van residuele longitudinale secundaire circulaties?

- Worden de stroomasymmetrie en residuele stroming in de geulen gekenmerkt door ruimtelijke en temporele variaties die gerelateerd zijn aan de geulmorfologie? Zo, ja hoe zien deze variaties eruit?
- Het bepalen van de ruimtelijke en temporele variabiliteit in de instantane en residuele transportpatronen in relatie tot de morfologie en het waargenomen gedrag van de geulen op basis van modelberekeningen (hoofdstuk 5 in voorbereiding).

Het belangrijkste doel van de berekeningen bestaat uit het verklaren van de waargenomen samenhang in de geulontwikkeling en de meest elementaire aspecten van het morfologische gedrag van de kortsluitgeulen. Dit betekent tevens een verdere toetsing van de hypothesen.

1.3 De morfologische ontwikkeling van het geulenstelsel sinds 1955 (hoofdstuk 3).

Het doel van hoofdstuk 3 bestond uit het bepalen van de ruimtelijke en temporele samenhang in het morfologische gedrag van de geulen (en platen) in de Terneuzen sectie en de Hansweert sectie, op basis van een kwantitatieve analyse. Het tot nu toe ontbreken van een dergelijke analyse is inherent aan de beschikbaarheid van de dieptekaarten. De kaarten vanaf 1955 zijn sinds 1994 geleidelijk in digitaal formaat beschikbaar gekomen.

De morfologische analyse heeft een beschrijvend karakter doordat hydrodynamische en sediment transport processen grotendeels buiten beschouwing blijven. Een samenhang in de ontwikkeling van de geulen kan daardoor alleen worden afgeleid uit de temporele opeenvolging van morfologische processen en globale inzichten uit de verkennende stroomberekeningen (hoofdstuk 2) en beschikbare debietmetingen. Op basis van de stroommetingen in combinatie met modelberekeningen wordt geprobeerd de afgeleide samenhang in de geulontwikkeling en de meest elementaire aspecten van het geulgedrag te verklaren.

Uit de analyses komt een uitgesproken geulgedrag in de Hansweert sectie naar voren dat van invloed lijkt te zijn geweest op de geulontwikkeling in het drempelgebied B1 van de vloedgeul FC1 in de Terneuzen sectie. Op een paar plaatsen na lijkt het baggeren en storten niet sturend te zijn geweest in de geulontwikkeling. Dat wil zeggen dat storten niet gepaard ging met een verondieping van de geulen en dat baggeren niet resulteerde in erosie.

Het geulsysteem in de Hansweert sectie wordt gekenmerkt door een netto sedimentatie die het gevolg is geweest van een functiewisseling tussen de grote ebgeul EC2 en vloedgeul FC2. De functiewisseling bestaat in feite uit een bochtafsnijding van de ebgeul door het ontstaan van een kortsluitgeul BC in het drempelgebied B3 van de vloedgeul rond 1951. Het daarop volgende aanpassingsproces van de twee hoofdgeulen duurde van 1955 tot ongeveer 1986. De geulaanpassing ging gepaard met een aanzienlijke sedimentatie in de ebgeul EC2, een netto erosie van de vloedgeul FC2 en een duidelijke herverdeling van de debieten ten gunste van de vloedgeul FC2. De sedimentatie in de ebgeul was groter dan de erosie in de vloedgeul. Dit betekent dat er een aanvoer van sediment is geweest vanuit de aangrenzende estuariene sectie(s). De tendens van een landwaarts gericht netto sedimenttransport (Vroon et.al. 1997), zoals afgeleid in eerdere zandbalansstudies, suggereert dat de resterende hoeveelheid sediment afkomstig is geweest uit de Terneuzen sectie.

De Terneuzen sectie kan sediment hebben geleverd aan de Hansweert sectie. Tussen 1960 en 1986/1988 wordt het geulsysteem gekenmerkt door erosie van met name het drempelgebied B1 in de vloedgeul FC1. Na 1988 stagneerde de erosie en lijkt er sprake te zijn van een geringe sedimentatie. De erosie van het drempelgebied ging niet gepaard met duidelijke en systematische

morfologische veranderingen van de overige (delen) van de hoofdgeulen. De erosie van de drempel B1 valt samen met de sedimentatie in de ebgeul EC2 en een afname van de erosiesnelheid in de vloedgeul FC2 van de Hansweert sectie. Deze samenhang en het netto landwaarts gericht sediment transport in de Westerschelde suggereren dat de erosie van de drempel is geïnitieerd door de morfologische veranderingen in de Hansweert sectie en dat het drempelgebied als sedimentbron heeft gefungeerd voor de Hansweert sectie. De kortsluitgeulen in de Terneuzen sectie, met name de drempelgeulen, lijken hierin een belangrijke rol te hebben gespeeld.

De kortsluitgeulen in het drempelgebied van de vloedgeul, de drempelgeulen (BC1 t/m BC5), vertonen de meest uitgesproken morfologische veranderingen. Het patroon van deze geulen is in de tijd duidelijk veranderd (Fig.3.1 en 3.15). Bovendien vallen deze patroonvariaties samen met de temporele veranderingen in het sedimentbudget en de sedimentomwerking (bruto sedimentbudget, morfologische dynamiek) op de drempel:

- Het ontstaan en de ontwikkeling van geulpatroon 1 (1964-1986) viel samen met de erosie van de drempel. Het geulpatroon bestond uit een grote vloedgeul (BC1) en ebgeul (BC2) die bijna haaks op elkaar stonden. De relatief lage migratiesnelheden (20-40m/jr) van de beide geulen resulteerde in een geringe sedimentomwerking.
- De stagnatie van de erosie van de drempel valt samen met het ontstaan en de ontwikkeling van geulpatroon 2. Dit patroon bestond aanvankelijk uit 4 kleine kortsluitgeulen (2 ebgeulen: BC12, BC3, 2 vloedgeulen: BC4, BC5) die evenwijdig naast elkaar lagen. De hoge migratiesnelheden (140-130m/jr) leidden tot een grote sedimentomwerking.

Deze samenhang tussen enerzijds het patroon en de migratie van de drempelgeulen en anderzijds de netto en bruto veranderingen in het sedimentbudget van de drempel, suggereert dat de drempelgeulen voor de uiteindelijk erosie of sedimentatie van de drempel zorgen (ondersteuning hypothese 1).

De meest opmerkelijke morfologische veranderingen van de drempelgeulen en de evolutie van de geulpatronen hangen samen met het quasi-cyclisch gedrag van de snelst migrerende kortsluitgeul in elk geulpatroon. Dit gedrag bestaat uit een transversale verplaatsing van de geul in zeewaartse richting, waarbij de geul na een aanvankelijk expansie geleidelijk verzandt. Tijdens patroon 1 vertoonde de drempelgeul BC1 (Straatje van Willem) dit quasi-cyclisch gedrag op een tijdsschaal van ongeveer 22 jaar. Tijdens patroon 2 was het de ebgedomineerde kortsluitgeul BC3 die, op een tijdsschaal van ongeveer 9 jaar, gekenmerkt werd door een cyclisch geulgedrag. Opmerkelijk is verder het morfologisch gedrag van de kleine drempels in de kortsluitgeulen. Afgezien van kleine longitudinale verplaatsingen en transversale verplaatsingen ten gevolge van geulmigratie, lijken ook de drempels in de kortsluitgeulen morfologisch stabiele verschijnselen te zijn: ze verdwijnen pas als de geul verzandt<sup>1</sup>.

De zeewaarts migrerende kortsluitgeul Zuid-Everingen (dwarsgeul CC) vertoont geen duidelijke veranderingen in het doorstroomoppervlak die samenhangen met de erosie van de vloedgeuldrempel B1. De erosie (15-20%) van het drempelgbied B1 tussen 1964 en 1988 suggereert een forse afname van de debieten door de kortsluitgeul CC en als gevolg daarvan een afname van het doorstroomoppervlak van de kortsluitgeul (hoofdstuk 2). Een dergelijke relatie wordt alleen waargenomen tijdens de periode 1966-1972, waarin geulpatroon 1 ontstond en zich snel ontwikkelde. De meest waarschijnlijke verklaringen voor het ontbreken van deze samenhang tussen 1972 en 1988 zijn:

• ondanks de erosie zijn de totale debieten over de vloedgeuldrempel B1 niet wezenlijk veranderd.

Dit zou betekenen dat een toename van het gemiddelde doorstroomoppervlak op de drempel is gecompenseerd door een toename van de bodemwrijving: veel kleine kortsluitgeulen hebben samen een groter doorstroomoppervlak maar een kleinere geuldiepte (=grotere wrijving) dan twee grote kortsluitgeulen.

• de sedimentatie in de kortsluitgeul CC is gecompenseerd door de zandwinning. Het potentiële lange-termijn effect van de zandwinning is een toename van het doorstroomoppervlak van 20%.

De hierboven geschetste samenhang in de geulontwikkeling moet nog worden onderbouwd/verklaard. De te beantwoorden de geulontwikkeling moet nog worden onderbouwd/ver-

- 3.1 Is de drempel B1 in de vloedgeul FC1 van de Terneuzen sectie een sedimentbron geweest voor de verondiepende ebgeul EC2 in de Hansweert sectie? Zo ja, op welke manier?;
- 3.2 Is het patroon en gedrag van de drempelgeulen (BC#) bepalend geweest voor:
  - de temporele variaties in het sedimentbudget van de vloedgeuldrempel B1? Zo ja, op welke wijze?
  - temporele variaties in het totale debiet over de drempel B1 en daarmee de ontwikkeling van de dwarsgeul Zuid-Everingen (CC)? Zo ja, op welke manier?
- 3.3 Heeft zandwinning in de Zuid-Everingen (CC) een natuurlijke sedimentatie in de geul gecompenseerd?

Hiervoor is inzicht in de instantane en residuele stroom- en sedimenttransportpatronen nodig voor de situatie van 1974 en 1995. Deze informatie is deels verkregen uit stroommetingen en uit de modelberekeningen.

<sup>1</sup> Opmerking: deze observatie met betrekking tot het gedrag van de drempels in de kortsluitgeulen volgt uit een kwalitatieve analyse van diepte- en verschilkaarten die niet wordt beschreven in hoofdstuk 3.

1.4 De waterbeweging in enkele geulen gebaseerd op veldmetingen (hoofdstuk 4).

Het doel van de stroommetingen was tweeledig: 1) het vergroten van de kennis over de hydrodynamische stroomprocessen in de geulen en daarmee 2) het deels onderbouwen van de hypothesen 1 en 3. Hiervoor zijn in 1994 en 1995 diverse metingen in met name de drempelgeulen uitgevoerd (zie ook bijlage A). Daarnaast is het algemene stroompatroon in termen van waterstanden, vervallen en debieten, in de gehele Terneuzen sectie gemeten. De resultaten van deze laatste metingen, die vooral bedoeld zijn voor de verificatie van stroommodellen, zijn eveneens als referentiekader in hoofdstuk 4 gepresenteerd (paragraaf 4.4).

De algemene stroommetingen laten zien dat de getijvoortplanting in het estuarium verantwoordelijk is voor de elementaire temporele variaties in waterbeweging die tot uitdrukking komen in de grootte van o.a. de stroomasymmetrie en residuele stroming. De richting van de stroomasymmetrie en residuele stroming hangt samen het patroon van eb- en vloedgeulen: ebgedomineerde stroming in de ebgeulen, vloedgedomineerde stroming in de vloedgeulen. Dit betekent een grootschalige residuele stroomcirculatie die gegenereerd wordt door de hoofdgeulen, met daarop gesuperponeerd enkele kleinschalige circulaties veroorzaakt door de kortsluitgeulen. Daarnaast bevestigen de vervalmetingen de hydrodynamische samenhang tussen het drempelgebied B1 en de kortsluitgeule Zuid-Everingen (CC, hypothese 2).

De kortsluitgeul BC4 (drempelgeul) is een vloedgeul: de drempel ligt aan de landwaartse zijde van de geul. De dieptegemiddelde stroming in de geul wordt gedomineerd door stroomversnellingen en -vertragingen die ter hoogte van de drempel gepaard gaan met stroomdivergentie en -convergentie. De ebstroom die de drempel in de geul nadert divergeert en versnelt (30-40%) op de bovenstroomse/landwaartse zijde van de drempel. Op de benedenstroomse/zeewaartse zijde van de drempel vertraagt de ebstroom. Van de drempel richting het centrale deel van de geul versnelt de ebstroom weer. De vloedstroom vertoont een vergelijkbaar maar tegengesteld gericht stroompatroon: versnelling (12-33%) in het centrale geulgedeelte, divergentie en vertraging richting drempel (10-20%), forse versnelling (10-40%) op de bovenstroomse/zeewaartse zijde van de drempel, gevolgd door vertraging (10-50%) op de benedenstroomse/landwaartse zijde van de drempel. Er zijn geen transversale secundaire circulaties in de geul waargenomen. De intensiteit van de stroomprocessen is het sterkst tijdens vloed. Daarnaast zijn de stroomasymmetrie en residuele stroming in de geul overwegend vloedgedomineerd. Beiden nemen toe met de getijslag. Het omslag punt tussen eb- en vloedgedomineerde stroming ligt boven op de drempel.

De kortsluitgeul BC3 (fig. 3.1) is qua morfologie een ebgeul. De primaire waterbeweging vertoont overeenkomsten met het stroompatroon in de vloedgedomineerde kortsluitgeul BC4. De ebstroom in BC3 versnelt in het centrale geulgedeelte (10-20%), divergeert en vertraagt (10-30%) richting drempel, versnelt enigszins (10%) bovenop de drempel en convergeert en vertraagt fors (20-50%) op de benedenstroomse zijde van de drempel. De vloedstroom divergeert en versnelt (10-25%) op de bovenstroomse/zeewaartse zijde van de drempel en vertraagt (5-30%) en convergeert enigszins op de benedenstroomse zijde van de drempel. De vloedstroom lijkt in het centrale geulgedeelte iets te versnellen. De grotere intensiteit van de processen tijdens eb en de stroomasymmetrie en residuele stroming duiden op een ebgedomineerde stroming in de geul. Ook in de ebgeul bevindt het omslagpunt tussen eb- en vloedgedomineerde stroming zich op de drempel en neemt de residuele stroming toe met de getijslag.

In tegenstelling tot de kortsluitgeul BC4 neemt de stroomasymmetrie af met de getijslag. Een tweede verschil tussen de waterbeweging in de ebgeul (BC3) en de vloedgeul (BC4) betreft de aanwezigheid van een transversale secundaire circulatie in centrale gekromde deel van de ebgeul BC3. Hierbij is de stroming in de onderste helft van de verticaal naar de binnenbocht gericht en in de bovenste helft naar de buitenbocht gericht. Deze circulaties worden gedurende nagenoeg het gehele getij waargenomen, waarbij de intensiteit het grootste is tijdens maximum ebstroom. Tijdens eb bereiken de secundaire stroomsnelheden nabij de bodem (op 0.5-1m boven de bodem) waarden tot 0.25m/s (17% van de hoofdstroom). De verschillen in stroomrichting tussen de dieptegemiddelde stroming en de stroming dicht bij de bodem variëren tussen de 10 en 16 graden. Tijdens vloed is de secundaire stroming beduidend zwakker (5-10% van de hoofdstroom). De richtingsverschillen in de verticaal bedragen dan 5 tot 10 graden. Deze zwakkere secundaire stroming gaat samen met een kleinere stroomlijnkromming<sup>2</sup>. De snelle geulmigratie en secundaire circulaties in de ebgedomineerde drempelgeul BC3 en de afwezigheid van deze processen in de vloedgedomineerde geul BC4, suggereert dat de secundaire stroming verantwoordelijk is voor de geulmigratie (hypothese 3).

In beide kortsluitgeulen (BC3 en BC4) duidt het patroon van stroomversnellingen en -vertragingen en de vorm van de stroomverticaal op de aanwezigheid van residuele longitudinale secundaire circulaties, met name in de drempelgebieden van de geulen. Als gevolg hiervan zal het residuele stroompatroon dicht bij de bodem sterker eb- of vloedgedomineerd zijn dan het dieptegemiddelde residuele stroompatroon.

Het globale residuele stroompatroon op de drempel B1 hangt nauw samen met de morfologie en het patroon van de drempelgeulen: ebgedomineerde stroming in de ebgeulen en vloedgedomineerde stroming in de vloedgeulen (ondersteuning hypothese 1). Als het stroompatroon indicatief is voor het residuele sediment transport betekent dit dat de kortsluitgeulen horizontale sedimentcirculaties op de drempel veroorzaken. De intensiteit en het netto effect van de circulatie zal hierbij toenemen met de doodtij-springtij cyclus.

De instantane en residuele stroompatronen suggereren dat de drempels getijgemiddeld (netto) sedimentatie gebeiden zijn waarbij gedurende een getij het sediment heen en weer wordt verplaatsts van de ene zijde van de drempel naar de andere zijde. Tijdens vloed erodeert de zeewaartse zijde van de drempels waarbij het sediment wordt afgezet op de landwaartse zijde van de drempel. Tijdens eb draait het patroon om: erosie op de landwaartse zijde en sedimentatie op de zeewaartse zijde. De uiteindelijke morfologische veranderingen en instandhouding van de drempels worden bepaald door de locatie van het omslagpunt tussen eb- en vloedgedomineerde residuele transporten en de grootte en richting van de gradiënten in het residuele sediment transport. Hierbij doen zich waarschijnlijk temporele variaties voor ten gevolge van de doodtij-springtij cyclus en het stadium van geulontwikkeling.

Op basis van modelberekeningen worden de implicaties van de hierboven geschetste processen voor het sediment transport en de meest elementaire aspecten van geulgedrag uitgewerkt voor het patroon van drempelgeulen in 1995. De vragen hierbij zijn:

- 4.1 Zijn de geulmorfologie en de residuele waterbeweging indicatief voor de residuele transportpatronen?
- 4.2 Komen de waargenomen secundaire stromingen overeen met de theorie (zoals die geïmplementeerd is in de model-software)
- 4.3 Wordt de migratie van de kortsluitgeul(en) veroorzaakt door de transversale secundaire circulaties of zijn er ook nog andere processen in het spel?
- 4.4 Zijn de drempels in de kortsluitgeulen BC3 en BC4 getijgemiddeld convergentiezones van sediment, waarbij gedurende het getij sediment heen en weer wordt verplaatst van de ene zijde van de drempel naar de andere zijde van de drempel? Hoe varieert dit proces met de doodtij-springtij cyclus en met het stadium van geulontwikkeling?

<sup>2</sup>Opmerking: de vergelijking tussen gemeten en theoretische secundaire stroming zoals weergegeven op blz. 111 is onjuist en onvolledig.

1.5 Modelberekeningen (hoofdstuk 5, in voorbereiding)

De modelberekeningen richten zich op het verklaren van de waargenomen samenhang in de geulontwikkeling en de meest elementaire aspecten van het geulgedrag van de drempelgeulen, aan de hand van de vragen 3.1 t/m 3.2 en 4.1 t/m 4.4 ( zie blz. 6 en deze bladzijde).

Hiervoor is op basis van de Delft2D-software en een bestaand kromlijnig Waqua-model van de totale Westerschelde een nieuw model voor het westelijk deel van de Westerschelde gemaakt. Het model beslaat het gebied van de voordelta tot en met de drempel van Hansweert. Het model wordt door waterstanden aangedreven waarbij de randvoorwaarden aan de landrand zijn gegenereerd met een groter model (tot de grens Nederland-België). Met het model kunnen zowel initiële als dynamische sommen van waterbeweging, sedimenttransport en bodemontwikkeling worden gemaakt.

Het stroommodel is geverifieerd aan de hand van de diverse metingen van waterstanden, vervallen

en debieten in de Terneuzen sectie. Hieruit blijkt dat de primaire waterbeweging in het onderzoeksgebied goed wordt gesimuleerd. De secundaire stroming zit niet goed in het model (eerste vraag blz. 7). Een evaluatie van de gemeten en berekende secundaire stroming in de drempelgeul BC3 laat zien dat het model de secundaire stroming onderschat tot een factor 4. Met name tijdens eb zijn de berekende secundaire stroomsnelheden beduidend kleiner dan de gemeten snelheden. De onderschatting wordt vermoedelijk veroorzaakt door een fout in de berekening van de kromtestraal van de stroomlijnen (te groot). Het is nog niet duidelijk of het hier gaat om een lokaal verschijnsel of dat de secundaire stroming systematisch wordt onderschat. Om hier meer inzicht in te krijgen zijn vergelijkingen met andere stroommetingen en resultaten van 3D-berekeningen nodig. Dat is binnen het huidige onderzoek helaas niet haalbaar. Waarschijnlijk wordt dit in de nabije toekomst door het WL uitgezocht in opdracht van RIKZ. Feit is wel dat modelformulering op basis van Kalkwijk en Booij (1986) is afgeleid voor geulen die niet zo sterk gekromd zijn als de geulen in de Westerschelde. Het gegeven dat de secundaire stroming in het model wordt onderschat betekent niet dat de migratiemechanismen van de geulen niet bestudeerd kunnen worden.

Een verificatie van de transportmodule is niet mogelijk door het ontbreken van betrouwbare sedimenttransportmetingen. Wel zal er een beperkte overall verificatie worden uitgevoerd. Hierbij zullen de berekende en gemeten geulontwikkeling in het drempelgebied B1 met elkaar worden vergeleken.

Om de rekentijden van dynamische sommen te reduceren is op basis van de methode van Latteux (1995) een morfologisch getij bepaald. Bij deze bepaling is er zo eenvoudig mogelijk gerekend. Dat wil zeggen evenwichts sediment transport zonder de effecten van secundaire stroming. Het blijkt dat het getij van 2 mei 1995 het lange-termijn residuele transport het best beschrijft. Dit getij is ongeveer 8 procent sterker dan het gemiddeld getij.

Bij het onderbouwen van de samenhang in de geulontwikkeling is in eerste instantie gekeken of het drempelgebied in de vloedgeul FC1 een sedimentbron kan zijn geweest voor de sedimenterende ebgeul EC2 (vraag 3.1 op blz. 6). Hiervoor zijn de initiële sedimenttransporten en bodemveranderingen voor de morfologische situatie van 1974 berekend en vergeleken met de waargenomen lange-termijn trends. De bodemtopografie van 1974 is gekozen omdat het midden in de periode 1964-1982 valt, die gekenmerkt wordt door nagenoeg lineaire trends van sedimentatie in de ebgeul EC2 en erosie van de vloedgeul FC2 en het drempelgebied B1 in de vloedgeul FC2.

Voordat de berekeningen voor 1974 werden uitgevoerd is nagegaan of het morfologisch getij van 1995 toegepast kon worden voor deze oudere situatie. De belangrijkste motivatie hiervoor is dat morfologische getijrandvoorwaarden voor oudere situaties niet eenvoudig te bepalen zijn. Met name de landwaartse rand van het model vormt hier een probleem omdat voor het aanmaken van de randvoorwaarden een model van het hele estuarium nodig is. Bovendien laten de waterstandsmetingen bij Westkapelle (zeerand van het model) en Hansweert (nabij landrand) slechts kleine veranderingen in het verticale getij gedurende de periode 1960-1995 zien. Op basis van dit gegeven zijn met de getijrandvoorwaarden van 1995 stroomberekeningen voor 1964, 1974, 1982 en 1994 uitgevoerd. De resultaten van de berekeningen zijn gebruikt om de ruimtelijke en temporele veranderingen in de verdeling van eb- en vloedvolumina in de Terneuzen sectie en de Hansweert sectie te vergelijken met de waarnemingen. Uit de vergelijking blijkt dat het model de herverdeling van de debieten in de Hansweert sectie en de niet noemenswaardig veranderde debietverdeling in de Terneuzen sectie goed reproduceert. Hieruit is geconcludeerd dat het gebruik van de randvoorwaarden van 1995 voor morfologische situaties vanaf 1960 geoorloofd is voor het westelijk deel van de Westerschelde.

De initiële berekeningen van de residuele sedimenttransporten en bodemveranderingen voor 1974 zijn opgeschaald naar jaarwaarden door de getijgemiddelde transporten en inhoudsveranderingen te vermenigvuldigen met het aantal getijden. De inhoudsveranderingen per volledige hoofdgeul zijn vervolgens vergeleken met de waargenomen erosie en sedimentatietendenzen waarbij de effecten van baggeren en storten zijn inbegrepen. De berekende en waargenomen inhoudsveranderingen van de hoofdgeulen in de Hansweert sectie komen aardig overeen. Voor de Terneuzen sectie is die overeenkomst beduidend minder goed. Het probleem doet zich voor in het drempelgebied van de vloedgeul. In plaats van erosie voorspelt het model sedimentatie. Er is een klein lichtpuntje als het gaat om het beantwoorden van de vraag of de drempel een sedimentbron kan zijn geweest voor de sedimenterende ebgeul in de Hansweert sectie. In tegenstelling tot de situatie (1995) wordt het sedimenttransportpatroon over de drempel van de vloedgeul in 1974 (en 1982) gekenmerkt door een kleine rechtstreekse sediment-'bypass' van de drempel naar de sedimenterende ebgeul. Om inzicht te krijgen in de oorzaak van het verschil tussen berekende en gemeten inhoudsveranderingen worden de processen in het drempelgebied meer in detail bestudeerd.

## 1.6 De rol van de kortsluitgeulen in de morfologische ontwikkeling van het geulsysteem

Opmerking: de in deze paragraaf voorgestelde rol van de kortsluitgeulen wordt nog verder onderbouwd op basis van modelberekeningen.

De kortsluitgeulen, de drempelgeulen in het bijzonder, beïnvloeden de morfologische ontwikkeling van de hoofdgeulen op de tijdsschaal van jaren tot enkele decennia. Met hun gedrag lijken ze zowel de flexibiliteit als de stabiliteit van de geulen in de estuariene sectie te vergroten en de ontwikkeling van het geulsysteem in aangrenzende secties te kunnen beïnvloeden. Met flexibiliteit wordt bedoeld dat de kortsluitgeulen extern opgelegde verstoringen opvangen (bufferen) waardoor het effect van de verstoringen op de overige delen van het geulsysteem zo klein mogelijk is. Dit resulteert in het handhaven van de geulstabiliteit. Kortsluitgeulen kunnen ook een nieuw dynamisch evenwicht van de hoofdgeulen initieren dat morfologisch stabieler (=minder veranderlijk) is dan het voorgaande. Deze functie van de kortsluitgeulen komt naar voren uit de waargenomen (nog te verklaren) geulontwikkeling in de Hansweert sectie en de Terneuzen sectie:

In de Hansweert sectie heeft het ontstaan van een ebgedomineerde drempelgeul in het drempelgebied van de grote vloedgeul (1951) uiteindelijk geresulteerd in een nieuw morfodynamisch evenwicht van de geulen. Het aanpassingsproces gedurende de periode 1951-1986 ging gepaard met aanzienlijke morfologische veranderingen van de hoofdgeulen en een netto sedimentatie in de estuariene sectie waarbij er een sedimentaanvoer vanuit de Terneuzen sectie moet zijn geweest.

Het huidige geulsysteem van de Hansweert sectie is vanuit morfologisch oogpunt stabieler dan het geulsysteem van voor 1950: de veranderingen in het patroon en de zandbalans van de geulen sinds 1986 zijn gering. Het geulsysteem ontleent haar huidige stabiliteit waarschijnlijk voor een belangrijk deel aan de dijken. De dijken fixeren de ligging van de hoofdgeulen en beperken daarmee de bewegingsvrijheid van de kortsluitgeul BC. De huidige stabiliteit heeft ook een keerzijde. Door de afwezigheid van meerdere kortsluitgeulen met een quasi-cyclisch gedrag lijkt het geulsysteem kwetsbaarder te zijn geworden voor opgelegde morfologische veranderingen. Hierbij moet vooral worden gedacht aan het baggeren en storten, gelet op het feit dat de huidige ingrepen in de grote vloedgeul van dezelfde orde zijn als de residuele transportcapaciteit van de geul. Een 'bufferende' werking van de kortsluitgeulen die ervoor kan zorgen dat opgelegde morfologische veranderingen zich niet of slechts gedempt door het hele geulsysteem verplaatsen, is nagenoeg verdwenen. Dat zo'n bufferende werking er kan zijn blijkt uit de morfologische ontwikkelingen in de Terneuzen sectie die waarschijnlijk zijn geïnitieerd door de veranderingen in de Hansweert sectie.

Het geulsysteem van de Terneuzen sectie verkeert sinds enkele decennia in een dynamisch evenwicht. De grote morfologische veranderingen in dit geulsysteem beperken zich (ruimtelijk) tot de erosie van het drempelgebied B1 in de grote vloedgeul FC1 gedurende de periode 1964-1988. De bufferende werking van de kortsluitgeulen blijkt uit het feit dat de forse erosie van het drempelgebied niet heeft geleid tot morfologische veranderingen elders in de hoofdgeulen van de Terneuzen sectie (=flexibiliteit gericht op handhaven stabiliteit). Dit kan alleen verklaard worden doordat de debieten over het drempelgebied niet of nauwelijks zijn veranderd ondanks de forse erosie. De veranderingen in het patroon en de afmetingen van de drempelgeulen moeten de vorm van de drempel zodanig hebben veranderd dat de totale debieten over de drempel nagenoeg hetzelfde zijn gebleven. Eventuele kleine veranderingen in de debieten over de drempel zullen zijn opgevangen door de dwarsgeul Zuid-Everingen en het landwaartse deel van de ebgeul Pas van Terneuzen (hoofdstukken 2 en 4, bijlage B). Een geringe erosie en toename van debieten op de drempel kunnen leiden tot een forse afname van de debieten en een sedimentatie in de dwarsgeul. Door deze morfologische aanpassing van de dwarsgeul worden de veranderingen van het drempelgebied slechts gedempt doorgegeven aan de zeewaarts gelegen delen van de hoofdgeulen. Dit impliceert dat de bufferende werking van de twee typen kortsluitgeulen in de Terneuzen-sectie een soort 'twee-traps-rakket' is. Zodra het dynamisch evenwicht van de geulen door een externe forcering wordt verstoord zullen morfologische aanpassingen in eerste instantie plaatsvinden in het drempelgebied van de grote vloedgeul. De veranderingen van de drempelgeulen gaan gepaard met veranderingen in de debieten over de drempel die zo klein mogelijk zijn. Zodra de drempelgeulen de verstoring niet volledig kunnen opvangen en de debietveranderingen over de drempel te groot worden, treedt de buffering door de dwarsgeulen in werking.

De voorgestelde functie van de kortsluitgeulen in de Terneuzen sectie zou in de nabije toekomst zichtbaar kunnen worden. In het kader van de verdieping van de Westerschelde worden sinds 1996 aanzienlijke hoeveelheden sediment (maximaal 8-9Mm³/jr wordt toegestaan, in de praktijk 5Mm³/jr) gestort in de vloedgeul Everingen (FC1). Onder invloed van het vloedgedomineerde sediment transport in de geul zal dit sediment naar het drempelgebied worden verplaatst. Op basis van het waargenomen geulgedrag is de verwachting dat een deel van het gestorte sediment geborgen wordt in het drempelgebied doordat het huidige 3/4-voudige patroon van drempelgeulen zal veranderen in een tweevoudig patroon van drempelgeulen (vergelijkbaar met 1955).

#### 1.7 Voorlopige conclusies

Terugkomend op het centrale onderzoeksthema en de geformuleerde hypothesen kunnen de volgende voorlopige conclusies worden getrokken (verdere uitwerking vindt momenteel plaats aan de hand van modelberekeningen):

- Hypothese 1: De kortsluitgeulen in het drempelgebied B1 (de drempelgeulen, BC#) zorgen door
  patroonveranderingen en geulmigraties voor de temporele variaties in het sedimentbudget en de
  geometrie van de drempel (B1) in de grote vloedgeul (FC1). Er zijn geen aanwijzingen dat de
  drempelgeulen zorgen voor de instandhouding van de drempel B1.
- 'Hypothese 2': Vanuit hydrodynamisch oogpunt is de waterbeweging in de kortsluitgeul Zuid-Everingen (CC) sterk gerelateerd aan de waterbeweging over de drempel (B1) in de vloedgeul (FC1). Deze samenhang blijkt niet uit de morfologische geulgedrag: de erosie van de drempel B1 ging niet gepaard met duidelijke morfologische veranderingen van de kortsluitgeul (sedimentatie). Mogelijke verklaringen hiervoor zijn: a) de erosie van de drempel B1 heeft niet geleid tot een toename van de debieten over de drempel, b) een sedimentatie in de kortsluitgeul is gecompenseerd door de zandwinning, c) een sedimentatie in de kortsluitgeul wordt compenseerd door een erosie ten gevolge van geulexpansie (stadium van geulontwikkeling).

- Hypothese 3: Het is nog niet duidelijk of de transversale secundaire circulaties ('spiraalstroming') bepalend zijn voor de migratie van de kortsluitgeulen. Het feit dat dergelijke circulaties wel zijn waargenomen in een snel migrerende (eb)geul en niet zijn waargenomen in een nauwelijks migrerende (vloed)geul geeft wel aan dat ze een rol spelen in het migratieproces.
- De (vermoedelijke) functie van kortsluitgeulen: de kortsluitgeulen lijken zowel de flexibiliteit als de stabiliteit van het geulenstelsel te vergroten en de ontwikkeling van de hoofdgeulen in de 'eigen' en aangrenzende estuariene secties te kunnen beïnvloeden. Met flexibiliteit wordt bedoeld dat de kortsluitgeulen extern opgelegde verstoringen opvangen (bufferen) waardoor het effect van de verstoringen op de overige delen van het geulsysteem zo klein mogelijk is. Dit resulteert in het handhaven van de geulstabiliteit. Dit lijkt het geval te zijn in de Terneuzen sectie. Kortsluitgeulen kunnen ook een nieuw dynamisch evenwicht van de hoofdgeulen initiëren dat morfologisch stabieler (=minder veranderlijk) is dan het voorgaande (Hansweert sectie). Wanneer dit het geval is kan de geulmorfologie in de aangrenzende estuariene secties als gevolg hiervan veranderen.
- Overeenkomsten in de waterbeweging tussen twee drempelgeulen: de instantane waterbeweging in de drempelgeulen BC3(=ebgeul) en BC4 (=vloedgeul) wordt gekenmerkt door de volgende processen: advectieve stroomversnellingen in het centrale geulgedeelte, stroomvertraging en divergentie richting de drempel, stroomversnelling op de bovenstroomse zijde en nabij de top van de drempel gevolgd door forse stroomvertragingen en -convergentie op de benedenstroomse zijde van de drempel. De stroomversnellingen en -vertragingen duiden op de aanwezigheid van residuele longitudinale secundaire circulaties, met name in het drempelgebied van de geulen. De intensiteit van deze processen lijkt toe te nemen met de getijslag.
- Verschillen in de waterbeweging tussen de drempelgeulen BC3 en BC4. De waterbeweging in de drempelgeulen BC3 en BC4 is in twee opzichten verschillend:
  - in tegenstelling tot de vloedgeul (BC4) zijn in de ebgeul sterke transversale secundaire circulaties waargenomen. Deze circulaties zijn sterker (tot een factor 4) dan op basis van de bestaande theorie (Kalkwijk en Booij, 1986) verwacht zou worden.
  - De stroomasymmetrie in de ebgeul neemt af met de getijslag, terwijl deze in de vloedgeul toeneemt.
- De instandhouding van drempels in de drempelgeulen BC3 en BC4: de instantane en residuele stroompatronen suggereren dat de drempels getijgemiddeld (netto) sedimentatie gebieden zijn waarbij gedurende het getij het sediment heen en weer wordt verplaatst van de ene zijde van de drempel naar de andere zijde. Het netto effect van deze processen op de morfologie van de drempels zal hierbij waarschijnlijk variëren met de doodtij-springtij cyclus en het stadium van geulontwikkeling.
- Sedimenttransportpatronen: de morfologie van de geulen is een goede indicator voor de globale residuele stroom- en sediment transportpatronen (richtingen). Dat betekent dat vloedgeulen gekenmerkt worden door een overwegend vloedgedomineerde stroming en residueel sediment transport. In ebgeulen zijn de stroom- en sedimenttransportpatronen overwegend ebgedomineerd. Hierbij kan er binnen het dwarsprofiel van een geul nog wel sprake zijn van eb- en vloedgedomineerde geuldelen.
- Aanbevelingen voor het beheer: gelet op de vermoedelijke functie van de kortsluitgeulen is het wenselijk om het fenomeen kortsluitgeulen, voor zo ver mogelijk, te handhaven. Dit betekent niet dat bijvoorbeeld het storten van sediment in de omgeving van kortsluitgeulen ten alle tijde vermeden moet worden. Wel verdient het aanbeveling om in geval van systematisch baggeren of

storten, de morfologische ontwikkeling en het globale stroompatroon (debietmetingen) in de nabije omgeving goed te monitoren. Bij de huidige stortingen in de Everingen, in het kader van de verdieping, zou gedacht kunnen worden aan twee peilingen van vak 4 per jaar aangevuld met één ADCP-debietmeting per jaar in zowel de kortsluitgeul Zuid-Everingen als het drempelgebied van de vloedgeul Everingen. Bij het bepalen van grote langdurige stortlokaties is het wenselijk om voor het omringende geulsysteem de morfologische geschiedenis per geul/geuldeel, in termen van sedimentbudgetten, te bepalen (dat is sinds kort eenvoudig en snel te doen). Daarnaast kunnen schattingen van de residuele transport capaciteit en -richting in de geulen, op basis van modelberekeningen, waardevol zijn bij kiezen van effectieve stortlokaties.

# 2 MORPHODYNAMICS OF TIDAL CHANNELS AND SHOALS IN THE WESTERSCHELDE

#### 2.1 Introduction

This chapter explains the research topic and the aims of research. For this purpose the system of tidal channels and shoals in the estuary is considered a morphodynamic system with coupling and feedback mechanisms between form and process. These interactions are simplified outlined in Figure 2.1. In the estuarine morphodynamic system the water motion is the driving force. This water motion, that is driven both by external energy inputs and internal steering, induces sediment transport. The sediment transport in turn controls the morphological evolution through the sediment balance. The morphodynamic cycle is closed when the morphological changes affect the water motion. These mutual adaptations of the hydrodynamics, sediment transport processes, the morphology and external energy inputs are called morphodynamics. The morphology observed in nature is the time integrated response of this morphodynamic cycle (Wright and Thom, 1977; De Vriend, 1990; Van de Meene, 1994).

Although schematizing the geomorphology is liable to subjectivity, it often is a first step in recognizing the complex morphodynamic behaviour that exists in morphodynamic systems. Therefore this chapter starts with a schematization and description of the estuary and the system of tidal channels and shoals from a geomorphological point of view.

## 2.2 Morphologic phenomena and behaviour

## 2.2.1 General geomorphologic characteristics of the Schelde estuary

The Schelde estuary has a funnel shaped geometry and covers an area of approximately 370 km² (Figure 2.2). The funnel shaped geometry of the estuary is marked by some sharp bends at Bath and between Hansweert and Terneuzen, that find expression in the embankments along the estuary. The land reclamation during the last two centuries partially imposed the geometry of the estuary. The averaged depth of the Westerschelde is approximately 10-11 meters with respect to NAP (= Dutch ordnance level). The length of the estuary from Vlissingen up to Gent amounts 160 km.

The estuary is marked by three morphologically distinct zones (Figure 2.2):

- 1) Seaward of Vlissingen a large outer delta exists. The delta is bisected by two major tidal channels;
- A multiple channel system exists between Vlissingen and approximately the border between The Netherlands and Belgium. Elongate tidal shoals separate the tidal channels. This part of the Schelde estuary is named Westerschelde;

- 3) Confining of the estuary is accompanied by a single tidal channel with alternate bank-attached bars landward from Doel. A similar channel morphology has been identified in other confining estuaries by Dalrymple et.al. (1992). This morphological zone extends beyond Heemiksem;
- 4) Landward from Heemiksem the estuarine channel is directly linked to the river channels. In this zone the tidal range diminishes rapidly due to frictional dissipation.

This subdivision in four morphological zones approximately resembles the morphological zones of macro-tidal estuaries as distinguished by Dalrymple et al. (1992).

## 2.2.2 Geomorphologic characteristics of the tidal channels in the Westerschelde

The multiple channel system in the Westerschelde (see previous section) is subject of this thesis. Although the channels and shoals are inextricably linked, it are the channels that provide patterns for visual recognition and for morphometry (Geyl, 1976). Therefore this section focuses on the tidal channels.

## Geomorphology of tidal channels - previous work

Based on earlier work (Van Veen, 1936), Van Veen (1950) described the geomorphology of the channels in the Westerschelde as a regular system of mutually evasive ebb and flood channels separated by intertidal shoals. The regularity of the system of channels and shoals is to a large extent determined by the geometry (embankments) of the estuary. Van Veen (1950) states that the regular two-fold channel pattern, consisting of an ebb and flood channel, develops when the width of estuary amounts three to five times the width of the main ebb channel. Allersma (1994) in addition concluded that the number of channels in the cross section increases with the tidal flood volume.

Separation of ebb and flood current resulting in mutually evasive ebb and flood channels and tidal shoals (Van Veen, 1936, 1950), is characteristic to many estuaries and tidal embayments (Geyl, 1976). Channel patterns related to the separation of ebb and flood current were studied by a.o. Van Veen (1950), Ahnert (1960), Robinson (1956, 1960), and Vertessy (1990, in Chappell and Woodroffe, 1994). Van Veen (1950) recognized three recurring arrangements of mutually evasive ebb and flood channels: the forked tongue pattern, the flanking attack pattern, and the wide estuary pattern (see Figure 2.3). From a navigational point of view an ideal system of ebb and flood channels consists of a sine-shaped (main) ebb channel with straight flood channels starting in each bend (Figure 2.3a, Van Veen, 1950). The channel pattern of the Westerschelde strongly resembles this ideal pattern (Van Veen, 1950). Ahnert (1960) independently identified a special form of tidal meander in Chesapeake Bay, which he termed "estuarine meander" (Figure 2.5b). Ahnert (1960) states that the estuarine meander is also characterised by the separation of ebb and flood flow. The

estuarine meanders are best developed in estuaries where maximum tidal ebb and flood flow occurs at approximately mean water level (Ahnert, 1960). Vertessy (1990, in Chappell and Woodroffe, 1994) studied estuarine meanders in the monsoonal South Alligator River (Australia), and showed that separation of ebb and flood flow occurs in some but not all estuarine meanders. When the estuarine meanders occur, midchannel shoals tend to be centred beneath large eddies which form in the lee of the cuspate inner bank (Figure 2.5c). Van Veen (1950) suggested the existence of sediment circulation cells that are related to the configuration of ebb and flood channels. The development of tidal shoals in relation to sediment circulation cells has been studied in Chesapeake Bay by Ludwick (1974) and Granat and Ludwick (1980). The mutual evasion of the ebb and flood current result in a similar pattern of net bedload transport that can be identified from the distribution of bed forms (Van Veen, 1936; Van Straaten, 1950, 1953; Harris and Collins 1985, 1988; Harris, 1988).

Mutual evasive ebb and flood dominated flows can result in similar ebb-dominated and flood-dominated channels. The configuration of the ebb and flood channels is indicative for sediment transport paths. Residual tidal flow and net sediment transport paths may be manifest in circulation cells (eddies), depending on the main channel configuration, which in turn may be partially imposed by the geometry (embankments) of the estuary.

Tidal channels in the Westerschelde - a schematization and classification

A closer look at the bathymetric maps of the Westerschelde reveals a systematic pattern of morphologic characteristics of the channels, that allow for a further division of tidal channels (see Figures 2.5, 2.6 and 2.7):

- main channels
- · secondary channels
- connecting channels:
  - bar channels
  - cross channels
  - margin channels

The morphology of these channels may be ebb dominated, flood dominated or indifferent. Ebb channels are bounded by bars at the seaward end of the channel, whereas flood channels are bounded by bars at the landward end (Figure 2.6). Indifferent channels have bars at both ends of the channel (Van Veen, 1936, 1950).

The main ebb and flood channels differ in their geomorphologic characteristics. The plan geometry of the main ebb channels is marked by clear bends and resembles a meandering river. The ebb channels form a more or less continuous meandering ebb channel due to their relatively deep bars. The curvature of this continuous meandering ebb channel shows a systematic variation (Figure 2.6): the ebb channels that are located to the north of the accompanying flood channel are sharply curved, whereas

the ebb channels that are located to the south of the flood channels are gently curved wide meanders. The main flood channels are straight channels parallel to the general alignment of the estuary. The flood channels tend to form a cut-off of the ebb channels and have relatively shallow and extensive bars at their landward margin. The bar of the flood channel and the upstream ebb channel are located side by side at several locations (Figure 2.6). The differences in plan geometry and the dimensions of the bars between the ebb and flood channel are persistent. Most main channels exhibit these morphological characteristics since approximately 1860/1890.

Several smaller secondary ebb and flood channels exist along the margins of the estuary (Figure 2.6). The secondary channels are separated from the main ebb and flood channels by tidal shoals. Although less important, the hydrodynamic function of the secondary channels is similar to the main channels. The channels have a 'transit function', i.e. the water volumes flowing through these channels add to the total tidal volume.

Connecting channels exist in the bar area of the main flood channel and in between an ebb and flood channel, bisecting the intertidal shoals. The channels form an connection between a larger ebb channel and a flood channel (Figure 2.6). The hydrodynamic function of the connecting channels differs from the main channels and secondary channels. The connecting channels do not primarily add in the total tidal discharge: they mainly influence the distribution of the tidal discharges between the main ebb and flood channel and between a main channel and a secondary channel. The life time of these channels is short compared to the main channels and usually comprises three successive stages: 1) formation, 2) expansion and migration and 3) degeneration. The connecting channels are striking phenomena that can be observed on the bathymetric maps from 1860 onwards. Generally these channels remain small. Nevertheless the connecting channels form the most dynamic elements of the channel and shoal system due to their relative fast migration. The division in bar channels, cross channels and margin channels is based on the geographical location of the connecting channels in the system of channels (Figure 2.7).

The bar channels are the most dynamic connecting channels and are located in the bar area of the flood channel. Together with the main flood channel these channels tend to form a short-cut of the main ebb channel (Figure 2.7). The bar channels have an orientation more or less parallel to the alignment of the flood channel. The bar channel and the meandering ebb channel meet at an angle. Ebb-dominated bar channels rapidly migrate in a seaward direction, with typical annual migration rates of hundred meters. Bar channels with a flood morphology display a complex migrational behaviour.

The cross channels are the second group of connecting channels. These channels form a cross connection between the main ebb and flood channel (Figure 2.7). The cross channels meet the main ebb and flood channel at angles. Ebb channels migrate in seaward direction, whereas a flood channel tends to migrate in landward direction. The

annual migration rates of approximately 40 meters are smaller than the migration rates of the bar channels.

Margin channels are connecting channels that occur near the margins of the estuary, where they form a connection between a secondary channel and a main channel (Figure 2.7). The margin channels resemble the cross channels. The margin channels meet both the main channel and the secondary channel at an angle. Ebb channels migrate in seaward direction, flood channels migrate in landward direction. The migration rates of the margin channels resemble the migration rates of the cross channels (40 m/year).

The geomorphological classification of the channels, as described above, has identified the existence of basically three different channel types. These types are: main channels, secondary channels and connecting channels. The channels occur in a regularly recurring channel pattern, that is indicated as the estuarine section. An estuarine section consists of an ebb meander and a straight flood channel, separated by tidal shoals and connected by one or more connecting channels. Six estuarine sections can be identified in the Westerschelde (Figure 2.8). The sections 2, 4, 5 and 6 can be identified on the maps since 1860. Section 3 exists since 1905, whereas section 1 is clearly developed since 1921. An estuarine stretch consists of a group of two or more estuarine sections. In the estuarine section bar channels and cross channels can occur. The secondary channels and the margin channels exist in between an estuarine section and the margins (embankments) of the estuary.

The morphological evolution of the estuarine sections differs and is marked by distinct interactions between the three types of channel. The next section outlines these morphological evolutions and interactions in each estuarine section.

## 2.2.3 Outline of the morphological behaviour of the tidal channels in the Westerschelde

Until approximately 1930 the morphological evolution of the channel and shoal system was dominated by the migration and meandering process of the ebb channels. Figure 2.9 shows the shifts of the thalwegs of the meandering ebb channels and the accompanied extension of the intertidal shoals and the flood channels. The annual migration rates of the main ebb channels varied between approximately 20 meters to almost 80 meters. Around 1930 most ebb channels had reached the embankments along the Westerschelde. Since then the main configuration of the major channels is fixed due to the presence of the embankments. An 'internal meandering' of the ebb channels, i.e. meandering of the ebb channel within the limits of the estuarine geometry, is however still going on. The changes in channel configuration since 1930 are relatively small and are related to the 'internal meandering' of the main ebb channels and human interference (dredging). The morphological evolutions up till 1930 were not entirely natural. Man interfered in the system by building two dams

that definitely separated the Westerschelde from the Oosterschelde in 1867 and 1871. The first regular dredging activities at the ebb channel bar in estuarine section 6 date from 1922 (Kleinjan, 1938).

## Estuarine section 1, the Vlissingen section

The expansion and migration of the main ebb channel lasted until approximately 1950 (e.g. De Looff and Van Malde, 1968). Due to this meandering and the westward migration of the ebb channel in the landward Terneuzen section (2, Figure 2.8), an ebb-dominated bar channel originated around 1960. Since then the morphologic evolutions of this estuarine section are dominated by the behaviour and development of this bar channel. The bar channel rapidly expanded and migrated with annual migration rates up to 100 meters since 1973. The expansion of the bar channel caused erosion of the flood channel bar (30\*10<sup>6</sup>m³) and sedimentation in the ebb channel (10\*10<sup>6</sup>m³, Jeuken, 1993). The bar channel is obliterating since approximately 1990, while small bar channels with a short life-time occur since 1986.

The gradual meandering of the main ebb channels caused an increase of the water surface slopes across the flood channel bar, that resulted in the formation of a migrating bar channel. The formation of the bar channel caused a deepening of the flood channel bar that opposed the increased water surface slopes. The ebb-dominated morphology of the bar channel suggests dominance of the ebb flow in the bar area of the flood channel.

### Estuarine section 2, the Terneuzen section

Apart from some small cyclic variations in the channel volume and a gradual migration of the outlet of the main ebb channel (20m/year since 1931), the morphology of the main channels is relatively stable. The channel volume and the averaged depth of the main channels remained approximately the same between 1960 and 1990. The both laterally and vertically expanding tidal shoals are bisected by several migrating cross channels (see Figures 2.8 and 2.9). Some of the cross channels probably originated as bar channels in the flood channel bar. (Kleinjan, 1933, Jansen and Volkers, 1939; De Looff and Van Malde, 1968). The life-time of the cross channels approximates several decades up to one century. The migrating cross channels rework the intertidal shoals. Ebb-dominated and flood dominated bar channels occur side by side in the flood channel bar. The flood-dominated bar channels display a complex migrational behaviour and can exist for several decades. The ebb-dominated bar channels migrate rapidly in seaward direction and have a lifetime of approximately one decade (Kleinjan, 1936; Anonymous, 1940; De looff and Van Malde, 1968). Degeneration of a bar channel is usually accompanied by the formation of a new bar channel.

The channels and shoals in this estuarine section seem to be in dynamic equilibrium since several decades. The gradual meandering of the main ebb channel is

accompanied by changes in the abundance of connecting channels. The behaviour of the connecting channels seems to dominate the morphological evolutions in this section. The ebb-dominated and flood-dominated bar channels that exist side by side, suggest that the flood channel bar is shaped by both the ebb and flood flow.

## Estuarine section 3, the Hansweert section

Up to 1950 the morphology of the main channels is typically an attacked flank pattern (Figure 2.3 and 2.9). The mutual evasion of the main channels induced the development of intertidal shoals between the ebb and flood channel. Jansen (1940) and Ringma (1950) describe the occurrence of migrating bar channels. In 1951 a small ebb-dominated bar channel was present. This bar channel rapidly expanded. Migration tendencies remained limited despite the strong flow curvature. The formation and subsequent expansion of the bar channel caused a sort of bend cut off of the meandering ebb channel and a considerable deepening of the flood channel bar. Before the formation of the bar channel, a larger part of the flood volume was transported through the ebb channel. The formation and expansion of the bar channel caused a redistribution of the tidal volumes. This redistribution was accompanied by a net sedimentation of  $40*10^6 \text{m}^3$  of sediment in the estuarine section (Jeuken, 1993; Van Kleef, 1995).

The formation and the expansion of the bar channel resulted in a deepening of the flood channel bar and a general shoaling of the ebb channel. The flood channel bar has become deeper than the ebb channel bar. The formation and expansion of the bar channel caused a new morphodynamic state in this section. The present channel morphology seems relatively stable. This stability is inherent to the limited freedom of movement of the bar channel.

#### Estuarine section 4, the Baalhoek section

Between 1860 and 1950 the morphology of this estuarine section strongly resembled the present morphology of section 2 (compare maps of 1905 and 1980 in Figure 2.9). Several migrating cross channels existed, that originated as bar channels. The averaged life time of these cross channels was 15 to 20 years (Kleinjan, 1933). Since 1950 only bar channels developed (De Looff and Van Malde, 1968). Between 1960 and 1973 extremely dynamic bar channels, with a life time of 7 years, were present (De Looff and Van Malde, 1976). Since 1970 the morphology became noticeably influenced by man. The artificial deepening (1970-1976) of the ebb channel bars induced a deepening of the entire ebb channel of 1.5m between 1970 and 1982 (Jeuken, 1993). Furthermore the intertidal shoal volume extended and the connecting channels disappeared. New ebb-dominated and flood-dominated bar channels did not originate until 1986. By then the flood channel had rotated in a clockwise direction over a distance of 900 meters since 1961. Since the formation of the bar channels, the depth of the flood channel increased by 20 percent. The depth and volume of the ebb channel remained constant (Jeuken, 1994).

Since 1931 the abundance of the connecting channels decreased suggesting changes in the hydrodynamic response of the main channels. A deepening of the ebb channel and the shoaling and rotation of the flood channel probably reduced the water level differences between the main channels, resulting in the (temporal) disappearance of the connecting channels. The occurrence of ebb-dominated and flood-dominated bar channels since 1986 suggests a nearly equal influence of the ebb and flood flow at the flood channel bar.

## Estuarine section 5, the Bath section

Between 1862 and 1935 several ebb-dominated bar channels existed in this section. The averaged life time of the bar channels was 5.5 years. Their migration rates added up to 250 m/year. Two migration cycles ended up in the main ebb channel. At the time that this happened the bar channel had expanded that much that a severe shoaling of the ebb channel bar in the upstream estuarine section occurred (Kleinjan, 1938). Dredging activities at this upstream bar probably obstruct the formation of large migrating bar channels since 1922 (Kleinjan, 1933, 1938; Sterling and Roovers, 1967). The estuarine section is eroding since at least 1955. Until 1967 this erosion was mainly due to sand mining (Uit den Bogaard, 1995). The artificial deepening of the ebb channel bar started in 1968 and caused a considerable erosion of the ebb channel. The intertidal shoals eroded, probably as a result of this artificially created sand deficit.

The ebb-dominated bar channels suggest ebb-dominated flow at the former flood channel bar. Human impact strongly affected the morphological evolutions of this section since 1930. Due to the disappearance of the intertidal shoals, the present morphology of estuarine section almost appears as a one channel system.

## Estuarine section 6, the border section

Man influences the morphological evolution of this section since 1920, when the first dredging activities were carried out at the ebb channel bar. Cross channels existed between 1920 and 1960. In the early seventies a guide wall was built to conduct the ebb flow. This resulted in the final disappearance of the cross channels, a slight sedimentation of the flood channel and probably a deepening of the ebb channel. Additional dredging activities were carried out between 1986 and 1987 to improve the ebb channel bend.

### Conclusions

Several interactions between the main channels, shoals and connecting channels mark the morphological evolution of the estuarine sections. The gradual meandering of the main ebb channels in the estuarine sections 1,2 and 3 caused the formation of new connecting channels. The increase of the ratio ebb channel length-flood channel length apparently favours the formation of bar channels and cross channels (sections 1,2,3 in

Figure 2.8). The abundance of connecting channels decreased in the eastern part of the Westerschelde. At least four morphological processes seem to induce the degeneration of connecting channels:

- a) deepening of the ebb channel (sections 4,5,6);
- b) shoaling of the flood channel (section 4);
- c) the extension of intertidal shoals (section 4);
- d) the formation of other connecting channels (sections 1,2).

The influence of the connecting channels on the morphological evolution of the main channels and shoals is two-fold:

- a) the formation and expansion of the bar channels in the Vlissingen section and the Hansweert section (1, 3, Figure 2.8), caused a sort of (temporal) bend cut-off of the main ebb channels. This 'bend cut off' induced a shoaling of the ebb channel and a deepening of the flood channel bar;
- b) The migration of the connecting channels causes a reworking of the tidal shoals. The rate of reworking depends on the migration rates of the connecting channels and the height of the shoals.

The life-time of connecting channels has three successive stages: 1) the formation, 2) expansion and usually migration, and eventually, 3) its degeneration. During all three stages a dynamically stable equilibrium seems to exist between the main channel and shoal system, and the connecting channels. The formation of the connecting channels appears as a feed back mechanism in the morphological evolution of the main channels and shoals. The largest or most abundant connecting channels exist near and at the flood channel bar. Apparently differences in channel length and channel depth between the main channel are important for the formation of connecting channels. Ebb-dominated bar channels exist(ed) in estuarine sections with a tight ebb meander (sections 1,3,5 in Figure 2.8, Figure 2.9), whereas ebb-dominated and flood-dominated bar channels exist side by side in estuarine section with a wide estuarine meander (sections 2,4 in Figure 2.8).

The classification of the tidal channels (section 2.2.3) and the preceding outline of the morphological behaviour arose several fundamental questions about the system of channels and shoals:

- Which process(es) causes the morphological differences in plan geometry and along channel morphometry (bar depth) between the main ebb and flood channel?
- What is the influence of the morphological differences between the main channels on the hydrodynamics and sediment transport in the channels? Are the morphological differences between the main channels maintained by specific processes or conditions?

- Which hydrodynamic process(es) or conditions cause the formation of bar and cross channels? What is the influence of the channel length and the bar depth on the flow pattern (water levels and velocities)?
- Which hydrodynamic processes determine the behaviour of the connecting channels? What is the influence of the primary and secondary water motion?
- In which way is the observed behaviour of the channels influenced by man?
   Despite the frequent dredging, disposal and mining of sediments, the system of channels and shoal seems to remain in dynamic equilibrium.

For a proper understanding and definition of the research theme a brief discussion on some important aspects of morphodynamic behaviour is desirable. This is the subject of the next section.

# 2.2.4 Some important aspects of morphodynamic behaviour

Time and space scales of the Westerschelde

The morphodynamic behaviour of the system of channels and shoals consists of mutual adjustments of morphology, hydrodynamics and sediment transport (Wright and Thom, 1977, see Figure 2.1). The sediment transport provides the time-dependent coupling mechanism by which the adjustments occur (Cowell and Thom, 1994). The 'chicken and egg' nature of morphodynamics (Wright and Thom, 1977), involves changes of morphological phenomena over a broad range of time and space scales that exist in morphodynamic systems (Cowell and Thom, 1994).

The geomorphological classification and description of the channel system of the Westerschelde, brings up the recognition of several spatial scales (Figure 2.10). Assuming that a primary scale relationship exists, a phenomenon (or process) is characterized by a specific temporal and spatial scale (De Vriend, 1991). Given a certain spatial scale of a morphodynamic system, a phenomenon may be noise, a component of the morphodynamic system, or an extrinsic condition (De Vriend, 1991). A phenomenon is noise when its time scale is much smaller than the time scale of the morphodynamic system. Dynamic scale interactions between the phenomenon and the morphodynamic system do not occur. When the time scale of the phenomenon is much larger than the time scale of the morphodynamic system and no feed back mechanisms exist, the phenomenon is an extrinsic condition (boundary condition). A phenomenon forms part of the morphodynamic system when the time scales are similar and feedback mechanisms occur.

The recurring channel pattern indicated as the estuarine section, appears as a prominent spatial scale in the Westerschelde (Figure 2.10). The main channels, the tidal shoals and the connecting channels form all components of this morphodynamic system. The embanked geometry of the Westerschelde and the infilling or deepening of the estuary, related to sea level fluctuations, are extrinsic conditions. The

morphodynamic behaviour of the ripples and dunes is noise on the scale of the estuarine section.

#### Feedback mechanisms

The feedback mechanisms are essential in the evolution of a morphodynamic system (Phillips, 1992). A feedback fundamentally occurs through the control that the solid boundary, i.e. the morphology, exerts over flows (Cowell and Thom, 1994). The control involves the fluid continuity and the bottom friction. Bottom friction affects the hydrodynamic response through the momentum equation, whereas the fluid continuity implies that changes in bed topography are accommodated by changes in flow velocity, water level (assuming hydrostatic pressure) and/or fluid density. A positive feedback amplifies instabilities causing an unstable system. A positive feedback is a form of self-organisation, which involves the evolution of the morphology towards a new equilibrium regime, i.e. a new morphodynamic state develops (Cowell and Thom, 1994). Negative feedbacks are stabilising processes that tend to oppose the instability and cause a state of dynamically stable equilibrium (Wright and Thom, 1977; Hardisty 1986 in Kroon, 1994; Cowell and Thom, 1994). Negative feedbacks cause self-regulation of the system. Adjustments of the morphodynamic processes occurs within a certain range of boundary condition in which the system is dynamically stable. Whether a feedback mechanism is positive or negative depends on the spatial scale of interest.

The formation of connecting channels is a negative feedback in the morphodynamic behaviour of most estuarine sections. The existence of steep water surface slopes between the main channels is reduced by the development of a connecting channel. In the Terneuzen section (2 in Figure 2.8) a dynamically stable equilibrium seems to exist, in which the behaviour of connecting channels might cause periodic fluctuations in the sediment budgets of the estuarine section. In the Hansweert section (3 in Figure 2.8) the formation and expansion of the bar channel acted as a positive feedback. The formation and expansion of the bar channel caused changes in the morphology of the channels and shoal and a redistribution of tidal volumes (see page 7). On the spatial scale of a single connecting channel positive and negative feedbacks occur. The expansion of the connecting channels after origination is a positive feedback. The expansion is however usually accompanied by the migration of the channel. Due to the migration, the connecting channel displaces towards a location of smaller water surface slopes eventually resulting in the degeneration of the channel. The migration of the connecting channels acts as a negative feedback in their morphodynamic behaviour.

## Morphological hysteresis and non-linearity

Phillips (1992) states that the existence of a long-term dynamic equilibrium is unlikely, due to the non-linear character of the system with complex and 'chaotic' behaviour. The systematic pattern and development of the tidal channels and shoals in

the Westerschelde partially contradicts this statement: a clear order exists in the apparent chaos, at least since the last hundred years.

In an estuarine morphodynamic system the hydrodynamic conditions (forces) are often changed before the morphology is fully adapted to the initial conditions. This is due to the relatively large reaction and relaxation times of the morphology, that cause a scale dependent morphological hysteresis (Kroon, 1994). The large time scales of the morphology and the non-linear character of the system complicate a morphodynamic analysis: many processes may be capable of transporting sediment, but they are not necessarily all relevant to the morphological behaviour of the morphodynamic system (Van de Meene, 1994). Therefore the problem is to isolate the processes and their interactions that determine the behaviour of the system of channels and shoals. This problem is similar to any study on medium and large scale phenomena (De Vriend, 1991; Terwindt and Wijnberg, 1991, Van de Meene, 1994).

## Approach used in this study

Studying the morphodynamics of the entire system of channels and shoals is not feasible for practical reasons. The recurring channel pattern indicated as the estuarine section offers however a possibility to study the morphodynamics of the channels and shoals in an inductive way: the correspondence of the estuarine sections suggests that some steering mechanisms present in one estuarine section might be present in the other sections as well. Therefore focusing on the spatial scale of one estuarine section and paying special attention to the formation and behaviour of connecting channels seems justified and well considered. The channel and shoal system of the Terneuzen section appears in dynamic equilibrium on the time scale of several decades (2, Figure 2.8). In addition abundant migrating connecting channels exist that interact with the main channels and shoals. For these reasons the Terneuzen section is chosen as the research area in the present study.

The analysis of the system of channels and shoal focusses on the net patterns of flow and sediment transport and the resulting morphological changes. The analysis is done on two different time scales. The processes responsible for the maintenance of the channel pattern are studied on the event time scale (i.e. hours to weeks). This analysis is based on field observations and numerical model calculations. The morphological behaviour of the channel and shoal system is studied on a historical time scale (months to decades), and will be based on available echosounding maps from 1955 (1931) onwards. By determining the relationship between the processes on the event time scale and their response (the morphology), and comparing this response with the observed morphological behaviour, it is attempted to identify the processes which dominate the evolution of the channel and shoal system in the Terneuzen section.

## 2.3 Hydrodynamics and sediment transport in the Terneuzen section

#### 2.3.1 Introduction

The previous section provided a framework for the definition of the research topic and the choice of the Terneuzen section as the study area. This section (2.3) presents a preliminary analysis (on the event time scale) of the primary flow pattern and sediment transports in the Terneuzen section. Purpose of this analysis is to explore and define the research problem more precisely.

Each sub section in this section (2.3) ends with a summary and preliminary conclusions that are relevant for the definition of the research problem. For the reader's convenience these summaries are cursively printed. The last section of this chapter (2.4) outlines the research problem and gives some hypothesis that may explain the problem, followed by the objectives and specific research questions of this thesis.

The water motion, that is driven both by external energy inputs and internal steering, is the driving force in the estuarine section. The main external energy inputs consist of the astronomical tide, the river inflow and the wind. The external energy inputs, especially the astronomical tide, are marked by more or less cyclic variations, i.e. characteristic time scales. The internal steering and the interactions between the different energy inputs result in a variety of hydrodynamic processes that manifests itself on different spatial scales of the morphology. These aspects of the water motion are schematically depicted in Figure 2.11. In the Terneuzen section the astronomical tide is the dominant energy input. The wind is a secondary energy input causing wind driven current and wind waves. The waves primarily affect the tidal shoals, whereas wind driven current can occur throughout the estuary. Due to the river inflow the water density is lower than at sea (approximately 1020 kg/m³). As the water column in the Terneuzen section is well mixed, the influence of the river inflow on the flow pattern can be negelected in the Terneuzen section. The gravitational circulation, indicated in Figure 2.11 exists between Bath and Antwerpen (Figure 2.2).

2.3.2 The general morphological differences between the main ebb and flood channels in relation to the deformation of the tidal wave

The main ebb channels in the estuarine sections are meander shaped and have relatively deep bars at the seaward end of the channel. The flood channels are straight and tend to cut-off the main ebb channels. The flood channels bars are relatively shallow (with respect to NAP, the Dutch Ordnance Level) and extensive.

Although giving a profound explanation of the fundamental morphological differences between the main channels is an interesting research topic, it is beyond the scope of this thesis. Nevertheless a provisional explanation is given below.

The persistent differences in channel shape and bar depth between the main ebb and flood channels exist(ed) in the entire Westerschelde. This suggests that these differences are due to an internal steering process that is manifest in each estuarine section of the Westerschelde. The deformation and propagation of the tidal wave is such a large scale process, that might explain the morphological differences between the main channels. This process and the way in which it might be related to the morphological differences between the main channels, is outlined below.

The distorted semi-diurnal tidal wave that enters the Westerschelde estuary is (further) modified by three distinct processes, that are related to the geometric characteristics of the estuary: 1) energy dissipation due to bottom friction; 2) landward convergence and shoaling, and 3) reflections at the shoals and estuary head, and due to sudden constrictions of the estuary.

The deformation of the vertical tide is illustrated in Figure 2.12. As the wave celerity is proportional to h<sup>0.5</sup>, the crest of the tidal wave propagates faster than the trough. The crest of the tidal wave (flood) tends to overtake the trough (ebb). The duration of the flood is shortened, whereas the duration of the ebb is prolonged. Energy losses due to bottom friction probably amplify this asymmetry. Generally the time asymmetry increases in landward direction due to decreasing water depth and increasing tidal range. The asymmetry of the vertical tide also appears from the time lags between the slack waters in Vlissingen and Antwerpen. High water slack at Antwerpen occurs approximately two hours later than at Vlissingen, whereas the time lag of the ebb amounts 2.5 hours. The tidal volumes are smaller than the basin storage due to this time lag. The mean tidal range increases from 4 meters at Vlissingen to 5.2 meters at Antwerpen (Figure 2.12). The convergence of the cross-section causes a concentration of energy and thus an amplification of the tidal range, that predominates the counteracting effect of frictional damping (energy ≈ H<sup>2</sup>L). The amplification of the vertical tide is characteristic to hypersynchronous estuaries. Some amplification due to reflection can be expected. Upstream of Heemiksem the tidal range diminishes due to frictional damping.

The deformation of the vertical tide is also apparent in the current velocities. The maximum flood velocities are larger than the maximum ebb velocities. The horizontal tide exhibits however an additional asymmetry that is related to the flooding of intertidal shoals and marshes (Parker, 1991; Aubrey et.al., 1991). The flood is an inundating current that is marked by a distinct peak in the velocity and discharge curve. Maximum velocities and discharges occur approximately one hour before high water slack, at the time that the intertidal shoals are completely inundated (NAP+1.7m). The simultaneous flooding of a large surface area of shoals causes is a sudden decrease of the averaged water depth and increase of the cross sectional area. This causes the "shoulder" in the velocity curve that precedes the period of maximum velocities. An inundation of the shoals that is distributed more evenly over the flood period would result in a smoother and more symmetrical velocity curve (Van der Spek, 1994). The extent of simultaneous flooding of intertidal shoals is primarily

controlled by the wave celerity (averaged channel depth). Maximum ebb velocities occur when the shoals have been partially drained (a water level near NAP).

It is the asymmetry of the horizontal tide that might partially explain the fundamental morphological differences between the main ebb and flood channel. Assume that some characteristic flood flow controls the morphology of the flood channels, and a characteristic ebb flow controls the morphology of the ebb channels. This characteristic flow is a long-term averaged velocity, like the significant velocity (see Chapter 4 for the definition). Then it is likely that the fundamental morphological differences between the main channels are partially related to the differences in water level at which the long-term characteristic velocities occur. Whatever the characteristic averaging period is, in the Westerschelde the characteristic ebb velocity occurs at a lower water level than the characteristic flood velocity. The meander shape of the ebb channel is probably due to effective secondary flows that accompany the concentrated ebb flow. Meandering of the flood channel does not occur due to the inundating character of the flood flow. The larger inertia and momentum (maximum velocity) of the flood flow reinforce the shooting through character of the flood channels. The limited freedom of movement may add to this. The estuarine meanders identified by Ahnert (1960, Figure 2.5b) consist of curved ebb and flood channels, and are best developed at places where the maximum ebb and flood velocities occur at approximately mean water level. The different bar depths can also be partially explained by the differences in water level at which the long-term characteristic velocity occurs: i.e. if these characteristic water levels are subtracted (ebb channel) or added (flood channel) to the depth of the bar with respect to NAP, the depth of the ebb and flood channel bars are less different.

# 2.3.3 The effect of channel dimensions on the primary flow pattern - a preliminary analysis

The formation of connecting channels is a negative feedback mechanism in the morphodynamic behaviour of the main channels and shoals in the Terneuzen section. The feedback involves the response of the tidal flow to the morphology of the main channels. This section presents a preliminary analysis of the flow pattern in the Terneuzen section. The objective of this analysis is three-fold:

- To obtain insight in which way the main channel morphology influences the flow pattern in the Terneuzen section;
- To obtain insight in the hydrodynamic processes and/or parameters that determine the water surface slopes across the bar channels and connecting channels, and;
- To obtain insight whether processes like flow acceleration and deceleration occur, which may affect the along-channel geometry of the main channels.

For these purposes a numerical simulation with Duflow was carried out. Duflow numerically solves the momentum and continuity equation for 1-dimensional unsteady flow in open channels (Spaans et.al., 1989). The Duflow model is calibrated with

water levels and verified with discharge measurements (Bollebakker, 1985). In each estuarine section one discharge measurement is available. The performance of Duflow at locations otherwise than the discharge measurements is not known (yet). The channel morphology is schematized in several channel sections. These Duflow sections are indicated in Figure 2.13. The along-channel morphometry of the channels, according to the Duflow schematization, is indicated in Figure 2.14, together with the channel axes and nodes in Duflow. In the ebb-channel the dimensionless depth  $(R/R_{mean})$ ) and the dimensionless cross-section  $(A/A_{mean})$  decrease towards the bar (seaward direction). The opposite applies to the flood channel.

A first estimate of the sediment transports revealed that the sediment transports near maximum tidal flow are several times larger than the sediment transports at other stages of the tide. Furthermore the spatial differences in transport capacity are largest near maximum flow. Therefore the preliminary analysis of the flow pattern is focused on these conditions.

The flow pattern in the main channels at maximum flow

Expected flow pattern: at the spatial scale of one estuarine the distortion of the progressive tidal wave is limited. The averaged depth and length of the main channels (11m) determine the time lags and water surface slopes in the estuarine section,

$$\frac{\delta h}{\delta x} \approx \frac{1}{c} \cdot \frac{\delta h}{\delta t}$$

where

h = water level (with respect to a reference level)

x = the along channel distance

t = time

 $c = propagation velocity of the tidal wave (=(gh)^{0.5})$ 

In the Terneuzen section time lags of approximately 20 minutes result in maximal water level differences across the estuarine section that vary between 20 and 50 cm during a neap spring cycle. The water surface slopes across the estuarine section generate tidal flows in the ebb channel and flood channel that approximately vary between 0.7m/s and 1.1 m/s during a neap spring cycle (when applying Chezy). The flow response in the main channels will be different, due to the morphological differences between these channels. The differences in the flow response will result in water surface slopes between the main ebb and flood channel, that in turn drive the water motion in the connecting channels. The spatial decrease of the cross-sectional areas towards the bars, suggests flow accelerations in the direction of the bars that are due to fluid continuity. As spatial differences in channel morphology are largest near the flood channel bar, the largest water surface slopes and flow accelerations are expected in this area.

Observed flow pattern: Figure 2.15 depicts the calculated flow response in the main channels at maximum ebb and flood flow, according to Duflow. The figures of the flow response in the flood channel (Fig. 2.15a en 2.15b) also contain information about the current velocities just landward of the flood channel bar (section 46 and 53 in Figure 2.14). The discharges (and cross-sections) of sections 52 and 45 are almost equal. To obtain a general picture of the flow pattern the current velocities of section 52 and 45 can be averaged. This averaged value is not indicated in Figure 2.15. The flow pattern in the flood hannel is on average marked by a slight flow acceleration towards the bar (Figure 2.15b and d). Near the flood channel bar the flow decelerates (between section 44 and 45, at flood), flow accelerates between 44 and 52. On average the flow slightly accelerates. This flow acceleration is observed during almost the entire tidal cycle, except at accelerating ebb flow. Just landward of the flood channel bar (section 53, Figure 2.13 and 2.15 b and d) the flow decelerates. This flow deceleration is observed during the entire tidal cycle. The flow strongly accelerates towards section 46. This acceleration, indicated in Figure 2.15b and d, seems however unrealistically large. The high current velocities in section 37 and 36 of the ebb channel yield a decelerating flow pattern towards the bar of the ebb channel (Figure 2.15 a and c). This flow pattern is present during the entire tidal cycle. The sudden decrease in current velocity between section 35 and 34 is due to the redistribution of the tidal discharge by the cross channel Zuid-Everingen (section 51, Figure 2.13). Between section 34 and 28 the flow pattern is rather uniform, despite the decrease in cross-sectional area of 20 percent (see Figure 2.15). The small fluctuations in current velocity in these sections are due to the redistribution of the discharge by other cross channels and margin channels. Seaward of ebb channel bar (sections 17 and 27, Figure 2.13), the flow pattern is complicated due to phase shifts of the maximum ebb. Maximum ebb occurs 50 minutes earlier in section 17 and more than one hour later in section 27 compared to section 28. At the considered time of maximum ebb the flow slighlty accelerates towards section 17 and strongly decellerates towards section 27 (not indicated in Figure 2.15) The water level pattern in the main channels reveals large water surface slopes near the flood channel bar both at maximum ebb and flood. The water level differences across the flood channel bar (section 45 and 52, Figure 2.13), that determine the primary flow in the bar channels, approximate 0.1m at maximum flood and 0.15m at maximum ebb (not explicitly indicated in Figure 2.15b and d). Small water level differences of 0.02m exist near the cross channel at maximum flood, whereas large water level differences of 0.09m are observed during ebb (not indicated in Figure 2.15, but in Figure 2.16, see next paragraph).

An analysis of the moment equation at maximum flow provides insight into the parameters that dominate the flow response in the large cross channel (section 51 in Figure 2.13). The simplest form of the moment equation reads as:

local acceleration+advective acceleration+water surface slope+bottom friction = 0

At maximum flow the water surface slope is primarily balanced by the bottom friction force, yielding the Chezy equation,

$$\frac{\Delta h}{\Delta L} = \frac{-Q|Q|}{C^2 A^2 R^2} = -\frac{\overline{U}|\overline{U}|}{C^2 R^2}$$

 $\Delta h$  = water level fall across a channel section

 $\Delta L$  = length of the considered channel section

Q = discharge in the channel section

C = Chezy coefficient of the channel section

R = hydraulic radius of the channel section

A = cross-sectional area of the channel section

 $\bar{u}$  = cross-sectional averaged velocity in the channel section

Figure 2.16 shows the values of the parameters in the bottom friction force, together with the water level differences across the main channel sections. The flow response in the channel sections A and C (Figure 2.16b) determine the flow pattern in the cross channel at maximum flood flow. At maximum flood flow the influence of the difference in channel length is largest (Fig 2.16b). The larger length of the ebb channel section results in a relatively small water surface slope, current velocity and cross-sectional area, compared to the flood channel section. The flow pattern in the channel sections B and D (Figure 2.16a) determine the flow response in the cross channel at maximum ebb. At maximum ebb flow the influence of the differences in channel depth is largest (Figure 2.16a). As the velocities in the main channel sections are of similar magnitude, the differences in discharge and cross-sectional area are due to the presence of the flood channel bar. The ebb-dominated water level differences across the cross channel Zuid-Everingen seem determined by the large water surface slopes across the flood channel bar at ebb.

The instantaneous flow response in the ebb and flood channel is different. The spatial changes in cross-sectional area cause small flow acceleration and steep water surface slopes near the flood channel bar (fluid continuity). The flow acceleration in the flood channel is smaller than suggested by the decrease of the cross-sectional area between section 42 and 45/52 of 50 % (Figures 2.15). Landward of the flood channel bar, the flow decelerates. The flow pattern in the ebb channel differs from the expected flow pattern: the flow tends to decelerate towards the ebb channel bar. The decrease of the cross-sectional area between section 34 and 28 by 20 %, is not accompanied by an acceleration of the flow. The small spatial fluctuations in current velocity are due the presence of severall small cross channels and margin channels (sections 25, 26, 49, 50, 51 in Figure 2.13).

Large water level differences across the flood channel bar (0.1m-0.15m over a distance of 2600m), generate strong tidal flows in the bar channels. The water level differences across the flood channel bar also determine the ebb-dominated tidal flow in the nearby cross channel (section 51 in Figure 2.13). A first analysis of the momentum equation at maximum flow suggests that the averaged depth of the flood channel bar determines the water level differences across the cross channel at

maximum ebb. The small water surface slopes at maximum flood seem determined by the differences in channel length between the main channels.

Channel morphology and the primary flow response: a sensitivity analysis

The large dimensions of the cross channel Zuid-Everingen (section 51, Figure 2.13), and the large discharges and water level differences at ebb suggest that the flow pattern in the main channels is influenced by the cross channel. I.e. the morphology is adjusted to the presence of the cross channel. A mutual hydrodynamic control between the main channels and the connecting channels can be expected, since the connecting channels appear as feedback phenomena in the morphological evolution of the main channels in the estuarine section(s) (section 2.2.3, p.10). To obtain some insight in the extent of mutual hydrodynamic control, a limited sensitivity analysis is carried out. Three morphologically distinct situations are considered (Figure 2.17):

- 1) a channel pattern without the large cross-channel;
- 2) a clockwise rotation of the cross channel of approximately 30°;
- 3) a deepening of the flood channel bar (sections 44,45 and 52, Figure 2.13) by 15%, due to e.g. the formation of bar channels.

Situation 1 is a hypothetical situation to estimate influence of the cross channel on the flow pattern, and thus the morphology of the main channel. Situations 2 and 3 are morphological changes that are manifest at a time scale of a few years to one decade.

The effect of the presence and orientation of the cross channel, and the depth of the flood channel bar on the initial flow response is illustrated in Figure 2.17a and 2.17b. Run 1 illustrates the influence of the large cross channel on the flow pattern in the estuarine section (Figure 2.17b). The cross channel clearly reduces the water level differences between the main channels and redistributes the tidal discharges between the main channel sections. The removal of the cross channel results in increased water surface slopes and current velocities in the bar area of the flood channel (section b, Figure 18b) and in the seaward reach of the ebb channel (section c, Figure 18b). A decrease in water surface slopes and velocities is observed in the inlet of the main channels (sections A and D, Figure 2.17b). Similar, but considerably less pronounced changes occur due to the clockwise rotation of the cross channel (Figure 18c). A deepening of the flood channel bar causes a reduction of water surface slopes and current velocities in the entire ebb channel, in the bar area of the flood channel and the cross channel. Current velocities and water surface slopes increase in the inlet of the flood channel. Given the along channel patterns in current velocity (Figure 2.15 and 2.17a), a deepening of the flood channel bar would reduce the spatial differences in current velocities.

The flow pattern and the morphology of the main channels in the Terneuzen section are adjusted to the presence of the large cross channel (section 51, in Figure 2.13). The cross channel clearly redistributes the tidal discharges. The sensitivity analysis suggests that a hydrodynamic control exists between the large cross channel and the bar channels (i.e. the flood channel bar). The presence of the cross channel seems to

reinforce the morphological differences between the main channels, especially near the flood channel bar.

## 2.3.4 Secondary flow phenomena

Thus far the discussion has focused on the cross-sectional averaged, primary flow pattern in the channels. A variety of mechanisms may however induce additional horizontal and vertical circulations that are superimposed on this primary flow. Although these circulations are secondary hydrodynamic phenomena they can affect the sediment transport patterns and thus the morphology (e.g. De Vriend, 1981; Kalkwijk and Booij, 1986).

The curvature of the primary flow in channels is responsible for the generation of water surface slopes and secondary circulations in a plane normal to the local axis of the primary flow (De Vriend, 1977; Heathershaw and Hammond, 1980). These secondary flows are typically one order of magnitude smaller than the primary flow (Thorne and Hey, 1979). The secondary current interacts with the primary flow resulting in a helical motion about the primary flow axis. This helical flow may be thought of as a streamwise vortex. In sharp channel bends, the development of secondary flows may be retarded. Wang et.al. (1991) define this relaxation as,

$$L_s = \frac{1-2\alpha}{2\alpha^2}h$$
  
 $L_s = \text{flow relaxation length (m)}$   
 $g = \text{gravity acceleration (m/s}^2)$   
 $C = \text{Chezy coefficient (m}^{0.5}/\text{s})$   
 $h = \text{water depth}$   
 $\alpha = g^{0.5}/\kappa C$   
 $\kappa = \text{von Kármàn constant (= 0.4)}$ 

Given a channel depth of 10 meters, and Chezy coefficient of 50, a relaxation length of approximately 140 meters exists.

Large water surface slopes normal to the local primary flow axis and large centrifugal accelerations may also exist near channel bifurcations (Ridderinkhof, 1990). The maximum secondary velocity can be approximated as (Jansen et.al., 1979, Van Rijn, 1990),

$$v_{fc} \approx 5.\frac{h}{R}.\overline{u}$$

where

v<sub>fc</sub> = secondary flow component due to flow curvature

h = water depth (m)

R = radius of flow curvature (m)

Given an averaged channel depth of 10 meters, R=1500m and u=1.5m/s, the maximum secondary velocity approximates 0.05m/s.

In wide systems (and channels) the rotation of the earth influences the flow pattern. The influence of the earth's rotation on a (quasi-)steady deep flow causes the current to veer progressively clockwise (in the northern hemisphere), with increasing distance from the bed (Soulsby, 1983). Due to this veering the near bed and near surface current directions deviate from the depth-averaged directions. The Coriolis force induces a secondary circulation normal to the primary flow, that is comparable with the secondary circulations due to the curvature of the primary flow in channel bends (Booij and Kalkwijk, 1983). The relative importance of secondary circulations due to the coriolis force and the centrifugal force can be approximated as (Booij and Kalkwijk, 1983),

$$\frac{v_{fc}}{v_{cf}} \approx \frac{1}{2} \cdot \frac{\Omega.R}{\overline{u}}$$

where

 $v_{cf}$  = secondary flow component due to the Coriolis force  $\Omega$  = coriolis parameter (± 2 $\omega$ sin  $\alpha$  $\approx$ 1.14\*10<sup>-4</sup>rad/s)

In the above example the secondary velocity due to the centrifugal force is 3.5 times larger than the secondary velocity due to the coriolis force. The secondary flow due to the Coriolis force behaves however differently under varying primary flow. The secondary flow velocity due to the Coriolis force is independent of the primary flow velocity, whereas the secondary velocity due to flow curvature is proportional to the square of the primary flow (Booij and Kalkwijk, 1983, Kalkwijk and Booij, 1986). In addition the secondary flow velocity changes sign with reversing tidal current directions, whereas the current direction due to flow curvature is constant through the tidal cycle. This last difference between the secondary flow velocities due to the Coriolis force and the centrifugal force, has been used to explain the differences in channel curvature of the main ebb channels in the Westerschelde (e.g. Allersma, 1992, 1994): assuming that the ebb channels are primarily formed by the ebb current, the sharply curved ebb meanders are due to the reinforcement of secondary ebb flows due to Coriolis force and flow curvature. In the wide meanders the secondary flow directions are opposite resulting in relatively small secondary flow velocities and limited bank erosion.

The above described vertical circulations perpendicular to the primary flow are due inertial effect in the vertical (=effect of bottom friction). These vertical circulations have net a zero net discharge. *Inertia of the primary flow in horizontal direction* (flow relaxation) may cause *cross streams* perpendicular to the channel axis (thalweg, Chang, 1987). Cross streams cause net discharges perpendicular to the local channel

axis. This phenomenon may be present in sharply curved channel bends. The relaxation length of the primary flow may be approximated by (De Vriend, 1990)

$$L_p = \frac{C^2.h}{2.g}$$

Vertical circulations parallel to the primary flow may originate due to accelerations and decelerations of the primary flow in downstream direction (Soulsby, 1983). The vertical distribution of the primary flow component becomes shoalter than the logarithmic distribution, when the primary flow accelerates and more oblique when the flow decelerates (De Vriend, 1977). The gravitational circulation due to the presence of fresh and salt water is a well-known vertical circulation in estuaries.

Flow curvature occurs at several locations in the estuary: near the transition of the Terneuzen section and the Hansweert section a sharp bend in the geometry of the Westerschelde exists. The two estuarine sections meet at an angle of almost 90 degrees. This bend in the estuarine geometry forces a strong curvature of the tidal flow and centrifugal accelerations that are probably accompanied by vertical circulations. The secondary circulations probably affect the near bed-flow near the flood channel bar of the Terneuzen section. Secondary circulations due to flow curvature are likely to occur in the meandering ebb channel, in most connecting channels, as the connecting channels meet at least one main channels at an angle, and probably near channel bifurcations. Secondary circulations due to the Coriolis acceleration are likely to occur. In curved channels these circulations are subordinate to the secondary circulations due to flow curvature. At flood these circulations reinforce the secondary circulations due to stream curvature in the main channels of the Terneuzen section. Given an averaged channel depth of 10m, and a Chezy coefficient of 50 m<sup>0.5</sup>/s, the flow relaxation length of the primary flow approximates 1274m. This suggests that cross streams might exist in the sharply curved entrances of connecting channels and near the flood channel bar in the Terneuzen section.

## 2.3.5 Sediment transport capacities in the main channels at maximum flow

The pattern of flow accelerations and decelerations suggest erosion of the flood channel bar at maximum ebb and flood. As the formation and behaviour of connecting channels seems inherently linked to the evolution of the bar, knowledge about the flow and sediment transport patterns near the bar is important. Therefore this section presents a preliminary analysis of the sediment transport pattern in the main channels of the Terneuzen section, using the calculated flow pattern according to Duflow (Figure 2.15). For this purpose the total sediment transport is defined as (Van Rijn, 1984, 1993)

$$q_{total} = q_{bedload} + q_{suspended}$$

$$q_{bedload} = 0.005.\overline{u}.h(\frac{\overline{u}-\overline{u}_{cr}}{((s-1)g.d_{50})^{0.5}})^{2.4}.(\frac{d_{50}}{h})^{1.2}$$

$$q_{suspended} = 0.012.\overline{u}.h(\frac{\overline{u}-\overline{u}_{cr}}{((s-1)g.d_{50})^{0.5}})^{2.4}.(\frac{d_{50}}{h}).(\frac{1}{D_{*}})^{0.6}$$

q = volumetric load transport (m<sup>2</sup>/s)

 $\bar{u}_{cr}$  = critical depth averaged velocity according to Shields

 $= 0.19.(d_{50})^{0.1} \log(12h/3d_{90})$ 

h = water depth (m)

ū = depth averaged velocity

D<sub>\*</sub> = dimensionless particle diameter (-)

s = relative density (-)

 $d_{50}$ ,  $d_{90}$  = particle diameters of the bed material

Assuming an uniform velocity distribution in the channel section(s), the cross-sectional averaged velocity and the hydraulic radius according to Duflow were used as input, instead of the depth averaged velocity and channel depth. It should be noted that the results do not significantly differ from sediment transport calculation based on the transport formula of Engelund-Hansen. The suspended sediment transports are approximately 9 times larger than the bed load transports. In reality this might be a factor 20 due to the practical definition of the bed load transport.

The results are given in Figure 2.18. Apart from the large transport capacity in the inlet of the ebb channel (section 37, Figure 2.13), the spatial differences in sediment transport in the ebb channel are small near the ebb channel bar. The ebb and flood patterns are similar. The small spatial differences in transport capacity near the ebb channel bar suggest an alternating pattern of relatively small erosion and sedimentation. A sediment input from the flood channel bar located in the seaward located Vlissingen section is likely (see below).

In the flood channel the flood transport capacity tends to increase towards the bar, indicating erosion of the top of the bar. As the high current velocity in the small channel section 46 is considered suspicious, a considerable decrease of the transport rates landward of the flood channel bar is likely, indicating sedimentation. At maximum ebb flow the largest transport rates also exist at the top of the flood channel bar. The decreasing transport capacity just seaward of the flood channel bar indicates sedimentation at ebb (section 44 and 45/52). The maximum flood transport is larger than the maximum ebb transport. The spatial differences in transport capacity just seaward of the flood channel bar are of similar magnitude at maximum ebb and flood. Landward of the flood channel bar the spatial differences in transport capacity are largest at maximum flood.

The tidal current sweeps the sediment to and fro from one side of the flood channel bar towards the other. Erosion of the flood channel bar is predicted both during ebb and flood. This suggests a deepening and lateral extension (flattening) of the flood channel bar under the considered tidal conditions. A clear deepening of the flood channel bar has however not been observed yet. The question is whether the flood channel bar is eroding, or whether there are other processes that balance this erosion.

This preliminary analysis in question neglects the following aspects and processes:

- the relaxation lengths of both water motion and the suspended sediment transport, that become important in non-uniform and non-steady flow condition where suspended sediment transport is dominant. In the bar area of the flood channel primary flow relaxation lengths of approximately 1000 meters occur. The adjustment of the suspended sediment transport to spatial changes in current velocity proceeds slow, because it takes time and therefore distance for the particles to settle out from suspension or to be mixed into the flow (Van Rijn, 1987, 1993). Fokking (in prep.) states that the adjustment length of the suspended sediment transport approximates 500 meters in small channels of the Westerschelde (water depth of 10m);
- Non-uniformity of the flow within the channel section(s) according to Duflow, especially the sections covering the flood channel bar.
- The sediment transport pattern at other stages of the tidal phase, and other tidal conditions.
- Secondary circulations near the flood channel bar, that are related to the strong curvature in the estuarine geometry;

# 2.4 Research questions

The study focuses on the connecting channels in the Terneuzen section (see Figure 2.8). The occurrence and the behaviour of the connecting channels are the central themes - What causes the presence of connecting channels, and what is the behaviour of the channels?

The occurrence of the connecting channels and the flow response in the connecting channels, is due to water surface slopes between the main ebb and flood channel in the estuarine section. These water surface slopes are in turn related to the morphological differences between the main ebb and flood channel (plan geometry  $\rightarrow$  channel length; depth and location of bars  $\rightarrow$  cross-sectional area and channel depth). A preliminary analysis of the flow pattern, based on the 1D-numerical model Duflow, yielded two important observations:

- Across the flood channel bar large water surface slopes exist, both at ebb and at flood, that determine the ebb-dominated flow in the nearby large cross channel.
   The flood channel bar appears to play a key role in the presence and flow response, and thus behaviour of the connecting channels.
- The tidal flow slightly accelerates towards the flood channel bar, both at maximum ebb and flood. The flow pattern suggests a flattening of the flood channel bar, due to erosion at the top of the bar and sedimentation just landward and seaward of the bar (see Figure 2.19). A preliminary analysis of the sediment transport capacity at maximum flow confirms this expected pattern of erosion and sedimentation. A clear deepening or flattening of the flood channel bar has however not been observed yet. Therefore a main research question is:

# Which processes maintain the flood channel bar?

Two mechanisms may explain why the flood channel bar is maintained. These mechanisms are outlined below and summarized as cursively printed hypothesis, followed by the approach necessary for testing the hypothesis.

**Mechanism 1:** A substantial part of the tidal discharge is conducted through the cross channel instead of across the flood channel bar. Without the large cross-channel the flow accelerations towards the flood channel bar would be much larger, causing substantial erosion and a deepening of the bar (see Figure 2.17 case B of the sensitivity analysis).

# Hypothesis 1: The large cross channel Zuid-Everingen maintains and controls the flood channel bar.

The verification of this hypothesis consists of two parts:

 Verification of the simulated global flow pattern in the Terneuzen section, based on measured discharges and water surface slopes (Chapter 4).

- A detailed and coherent analysis of the morphological evolution of the tidal channels and shoals in the Terneuzen section (Chapter 3). The maintenance of the flood channel bar by the cross channel should show up in the morphological behaviour of the flood channel bar and the cross channel during the last few decades. The analysis should address the following questions:
  - Is the morphological evolution of the flood channel bar marked by periods of erosion and sedimentation during the last decades?
  - If these periods occur, are they related to the morphology (location, size) and behaviour of the large cross channel?

Mechanism 2: The second mechanism that maintains the flood channel bar is provided by the bar channels. The preliminary analysis of the patterns of primary flow and sediment transport assumed uniformity of the flow at the flood channel bar. In reality these patterns will be highly non-uniform due to the presence of ebb-dominated and flood-dominated bar channels that occur side by side. The expected patterns of primary flow and sedimentation and erosion at ebb and flood are indicated in Figure 2.20b and c, together with the schematized bar morphology of 1982 and 1992. In the individual bar channels flow accelerations and decelerations occur. At ebb the flow accelerates towards the central part of the ebb-dominated bar channels and diverges and decelerates towards the small bar. The flow divergence towards the small bars is due to the increased width and cross-sectional area (note the shape of especially the ebb-dominated bar channel in Figure 2.20a). The ebb flow accelerates towards the small bars of the flood-dominated channels, and decelerates in the central part of the flood-dominated bar channel. At flood the opposite flow pattern exists, except that the flood flow probably accelerates towards the central part of the ebb-dominated channel. As a result the central parts of the bar channels tend to erode, whereas sedimentation is likely at the small bars of the bar channels. The simultaneous occurrence of ebbdominated and flood-dominated bar channels causes the formation of a zig-zag shaped subtidal shoal (Figure 2.21a), and a (eulerian) circulation of water and sediment at the flood channel bar (Figure 2.21b). The latter process keeps the sediment in the bar of the main flood channel.

# Hypothesis 2: The ebb-dominated and flood-dominated bar channels, that occur side by side, maintain the flood channel bar.

The verification of this hypothesis consists of analysing the patterns of primary flow and sediment transport in the bar channels - Does the expected pattern of flow and sediment transport occur and is it apparent under varying tidal conditions? The analysis will be based on:

- measured and calculated (2DH) current velocities in the bar channels;
- measured and calculated sediment transports in a bar channel. Purpose of the
  measurements is to verify whether flow deceleration towards the small bars is
  accompanied by decreasing sediment transports, and thus sedimentation (Figure
  2.20c). The sediment transport measurements also provide a means for quantifying
  the influence of the relaxation length of the suspended sediment on the patterns of

erosion and sedimentation. As an adjustment length of 500 meters is likely to occur, the erosion and sedimentation in the bar channels, and thus the morphology of the channels is expected to be influenced by this process.

The above described mechanisms and hypothesis state that the flood channel bar is maintained by both the large cross channel and the bar channels. This implies that the connecting channels maintain, and probably even reinforce, the causes of their own existence. Then a second relevant research question is:

# Is it possible to quantify the conditions, i.e. depth of the flood channel bar and water surface slopes, under which connecting channels are formed?

Two types of analyses are necessary to answer, i.e. explore, this question:

- A coherent analysis of the morphological behaviour of the connecting channels and the flood channel bar - is it possible to identify and quantify the morphological boundary conditions for the formation of connecting channels? The analysis should address the following questions:
  - Is the morphological evolution of the flood channel bar (depth and size) related to the presence (location, size) and the behaviour (expansion, migration, degeneration) of the large cross channel and the bar channels?
  - Does a coupling exist between the behaviour of the individual connecting channels?
  - Is the morphological behaviour of the flood channel bar and the connecting channels noticeably influenced by man (e.g. sand mining). If it is, in which way is the morphological behaviour influenced?
- Based on the results of the morphological analysis, calculations with a verified 2DH numerical model might offer a means for quantifying the hydrodynamic conditions (water surface slopes) under which bar channels are formed. A useful start might be the comparison of the water surface slopes and flow patterns in the present situation (1994/1995), in 1987 and in 1982. A shoaling of the flood channel bar, accompanied by the degeneration of former bar channels, occurred between 1982 and 1986. A new ebb-dominated bar channel originated in 1987, which expanded and migrated since then.

A striking aspect of the behaviour of the connecting channels is the migration of the (ebb-dominated) channels. Eventually this migration may result in the degeneration of the connecting channel due to their shift from the position with maximum water surface slopes to a less optimal location. An important compound question concerning the migration of the connecting channels is:

How exactly does the migrational behaviour of the connecting channels in the Terneuzen section look like, and which processes may explain this migrational behaviour?

The first part of the question addresses to the morphological evolution of the connecting channels on the time scale of years to decades, and involves the definition and quantification of morphometric channel parameters (Chapter 3). Special attention should be paid to the coupling between the migrational behaviour of individual connecting channels.

The second part of the question relates to the 3-dimensional flow structure and erosion and sedimentation patterns in the migrating channels. Horizontal and vertical circulations, superimposed on the primary flow, are likely to exist in the tidal channels (section 2.3.4). It are these secondary flow phenomena, together with the primary flow, that may cause the migration of the connecting channels. The expected patterns of flow, sediment transport and the locations of erosion and sedimentation, at ebb and flood are indicated in Figure 2.22 and 2.23, and outlined below.

Migration of the bar channel (mechanism 1): In the ebb-dominated bar channel two secondary flow mechanisms exist: 1) secondary vertical circulations due to flow curvature, and 2) cross streams, i.e. a flow component perpendicular to the thalweg due to inertia of the primary flow. The influence of the coriolis force on the secondary circulations is neglible in the connecting channel. The secondary circulations occur in the central part of the bar channel, primarily at ebb (Figure 2.22b). The effect of these circulations is a near-bed sediment transport directed toward the inner bend (see arrows in Figure 2.22c), causing erosion of the outer bend and sedimentation in the inner bend. At the entrance of the bar channel cross streams occur, both at ebb and flood. The cross streams cause erosion of the outer bend. This erosion is compensated for at flood in the inner bend: at flood sediment from the bar of the flood-dominated bar channel is deposited along the inner bend of the ebb-dominated bar channel. The erosion and sedimentation patterns at ebb and flood cause a southward shift (rotation) of the ebb-dominated channel, that is strongest at the entrance of the bar channel.

Hypothesis 3: The migration of the ebb-dominated bar channels is due to cross streams and flow deceleration at flood, and cross streams and secondary circulations at ebb.

Migration of the cross channel (mechanism 2): The primary flow response in the cross channel differs from the flow pattern in the bar channels. Due to the squared orientation of the cross channel with respect to the ebb and the flood channel, the flood flow concentrates in the eastern part of the channel, whereas the ebb flow concentrates in the western part of the channel (Figure 2.23b). In addition the maximum flood flow tends to shoot along the cross channel due to the larger inertia of the flood flow, compared to the ebb flow, and the higher water level at maximum flood flow. The secondary flow phenomena are similar to the ebb-dominated bar channels, i.e. secondary circulations in the central part of the channel and cross streams in the curved flow entrances (Figure 2.23b). The patterns of erosion and sedimentation at ebb and flood differ however due to the squared orientation of the cross channel (Figure 2.23c). In the cross channel the secondary flow patterns at flood

and ebb are oppositely directed, resulting in opposite erosion and sedimentation patterns, and relatively small migration rates (compared to the ebb-dominated bar channel).

Hypothesis 4: The ebb-dominated primary flow and accompanying secondary circulations and cross streams, cause the westward migration of the cross-channel Zuid-Everingen.

Testing of both hypotheses 3 and 4 consists of:

- Analysing the measured three-dimensional current structure is there field evidence for the presence of secondary circulations and cross streams (chapter 4)?
- Relating the observed three-dimensional flow structure to the morphology of the connecting channels (channel morphometry) and comparing the flow response with existing theories (chapter 4). By determining the relationship between the morphology and the response of the processes on the event time scale (chaper 4,5), and comparing this response with the observed morphological behaviour (chapter 3), it is attempted to identify the processes that dominate the behaviour of the connecting channels in the Terneuzen section (Chapter 6).

# 3 THE MORPHOLOGICAL BEHAVIOUR OF THE TIDAL CHANNELS

#### 3.1 Introduction

A quantitative description of the morphological developments of the channels is a prerequisite for a better understanding of the morphodynamic behaviour of channel systems. Previous studies on the channel evolution in the Westerschelde showed the large-scale erosional and depositional trends and the tendency towards a net landward sediment transport over the period 1955-1993. Furthermore, they qualitatively revealed the major changes in the plan-view channel configuration and the nature of the (quasi)-cyclic behaviour of the connecting channels. A coherent quantitative description of the morphological evolution of the channels is not yet available. This is particularly the case for the channel system of the Terneuzen section, the main focus of this study.

The Terneuzen section is located in the seaward part of the Westerschelde (Fig.3.1a). The channel system of this area consists of two main channels (FC1 and EC1, Fig.3.1b) and two types of connecting channels, viz. (Chapter 2): a large cross channel (CC, Fig.3.1b) and several bar channels (BC, Fig.3.1c,d). The channel system eroded with about 30 Mm<sup>3</sup> between 1955 and 1993 (Uit den Bogaard, 1995; Huijs, 1996; Vroon. et.al., 1997). Most of this erosion probably occurred in the main flood channel FC1 (Jeuken, 1993; Huijs, 1996). Whether and how this erosion was influenced by the other channels of the channel system is not known.

The map analyses of the Terneuzen section revealed an approximately stable configuration of the main channels EC1 and FC1 since about 1930. At the timescale of one to several decades the bar channels BC and cross channels CC tend to display a (quasi)-cyclic behaviour marked by channel expansion, transverse migration and eventually channel degeneration (Kleinjan, 1936; Janssen and Volkers,1939; Van Veen, 1950, De Looff and Van Malde, 1976). This behaviour of the connecting channels may be interrelated with the morphological evolution of the main channels (Chapter 2). In which way the connecting channels (BC, CC) and the main channels (FC1, EC1) developed and whether and how their evolution is interrelated is not known.

The budget studies indicate that the channel evolution of the Terneuzen section may also be related to the morphological developments in the Hansweert section. The Hansweert section borders on the landward side of the Terneuzen section. It essentially consists of a main ebb channel EC2 and a main flood channel FC2 (Fig. 3.1b). A bar channel BC is present in the bar area B3 of the flood channel FC2 (Fig. 3.1b). The formation of this bar channel in 1951, was accompanied by an erosion of the flood channel FC2, sedimentation in the ebb channel EC2 and a net sedimentation in the Hansweert section of about 40 Mm³ between 1955 and 1993 (e.g. Uit den Bogaard, 1995). The tendency towards a landward directed net sediment transport in the Westerschelde (Vroon et.al., 1997), suggests that most of the deposited sediment

came from the Terneuzen section. Hence, the morphological evolution of the channel systems in the Terneuzen and Hansweert section may be interrelated, although the nature of this relationship not known.

The quantitative descriptions of the channel evolution necessary to decribe the morphological behaviour of the channels and channel systems are lacking and cannot be adequately determined from the results of previous studies. Therefore, the objective of this chapter is to give such a a coherent quantitative description. More particularly it aims to determine:

- the temporal and spatial variations in the sediment budgets of the Terneuzen and the Hansweert section in order to identify the role of the various channels in the large-scale erosional and depositional trends;
- the morphological evolution of the main channels, the bar channels and the cross channel in the Terneuzen section and a possible morphological coherence.
- the morphological evolution of the main channels in the Hansweert section and to qualify the suggested morphological relationship between the channel evolution in this section and the Terneuzen section.

For this purpose the morphological data set, consisting of seventeen bathymetric maps covering the period 1955-1996 (section 3.2), was quantitatively analysed with a Geographical Information System (GIS). Sediment budgets were computed and the changes in the plan-view and cross-sectional channel geometry were determined to describe the channel evolution (section 3.3). Section 3.4 describes the changes in sediment budget and the morphological evolution of the main channels in the Terneuzen and Hansweert section. Sections 3.5 and 3.6 focus on the evolution of the bar channels and cross channel respectively. The major findings are summarised in section 3.7.

The results of this chapter and the current observations in chapter 4 form a basis for the morphological computations in Chapter 5. A comparison of the observed and computed channel evolution can give insight into the mechanisms that determine the behaviour of the channels and the channel system of the Terneuzen section. Besides the scientific relevance, the results may also support the design of the optimal dredging strategies.

3.2 Survey methods, accuracy, data sets and data processing

Survey methods

All depth measurements since 1955 have been carried out with electronic echosounders and a positioning system. The experimental set-up changed over time. Since 1992 a Simrad EA 500 echosounder has been used. The instrument has a frequency of 700 kHz and a bundle width of one to five degrees. A Differential Global Positioning System is the standard positioning equipment since 1994.

The echosounding surveys are carried out in straight lines, spaced 200 metres apart. Since 1986 all echosoundings are automatically stored in a digital format. However, the echosoundings of the period 1955 until 1985 were only available as hand-written maps. Since 1994 most of these maps were digitized. The along-transect sampling interval of the manually digitized maps is about 25 metres. For the automatically stored echosoundings this distance amounts about one metre. Thus the sampling density of the maps since 1986 is about 25 times larger compared to the older maps.

# Accuracy

Establishing the accuracy of the echosoundings is difficult as it depends on various factors that changed over time. For instance, the instrumental set-up and its accuracy changed. Both stochastic and systematic errors determine the accuracy of the echosoundings. These errors have different effects on the results of the morphological analyses.

Based on earlier work of Nanninga (1985, Wadden Sea data) and Jonkers (1991, Oosterschelde), Storm et. al. (1994) estimated the accuracy of the bathymetric maps of the Westerschelde. Accordingly, the stochastic error of each depth value on the maps is essentially determined by the following factors:

- the depth measurement has a stochastic error of ±0.05-0.15m;
- the accuracy of the positioning system introduces an inaccuracy of the depth measurement of  $\pm 0.1$ -0.35m
- the reduction to Dutch ordnance level has an estimated inaccuracy of  $\pm 0.05$ m.
- rounding errors introduce another inaccuracy of  $\pm 0.03$ m.

As a result, the total stochastic error of each measured depth value ranges between  $\pm 0.2m$  and  $\pm 0.4m$ . The error is smallest for intertidal areas and largest for steep channel banks.

The effect of the stochastic error on the results of the morphological analyses is small as it disappears after spatial averaging. This is concluded from the following: the connecting channels are the smallest channels in the present analysis. The channels have a length of about three kilometres and a width of about one kilometre. Based on the sampling characteristics of the digitized data set, this means that the channel geometry is based on 600 depth measurements. Suppose that the total stochastic error of each measurement is 0.4m and that it is normally distributed. Then the standard error of the overall mean channel depth approximates less than  $0.02m (0.4/\sqrt{600})$ .

Systematic errors may arise from various sources. A large systematic errors arises from the squat of the survey ships: the subsidence of a ship increases with ship speed and decreasing water depth. Squat causes an underestimation of the water depth of about 0.1m in the channels up to 0.2m above intertidal shoals (Storm et.al., 1994). The width of the echosounder bundle introduces systematically underestimated water depths (0.15m) at steep channel banks. These two systematic errors are more or less constant in time and therefore do not play an important role in the quantification of

the channel behaviour. However, more incidental systematic errors, caused by e.g. calibration or reduction errors, can significantly affect the results and interpretation of the morphological analyses. However, the presence magnitude and origin of these errors is often difficult to trace. An analysis of the erosion and sedimentation maps and an analysis of the trends of channel evolution can give insight into the net average magnitude of these systematic errors.

Only the large incidental systematic errors can be identified from the erosion-sedimentation maps. Based on an analysis of such maps, two (parts of the) echosoundings were excluded from the analysis, viz.: the bathymetric map of the Hansweert section of 1968 and a part of the bathymetric map of the Terneuzen section of 1984. The map of 1968 shows depths at the intertidal shoals and in parts of the two main channel (EC2, FC2 in Fig. 3.1) that are about 0.5m too large. The map of 1984 displays and area of 1.7 by 1.4km in the cross channel (cc in Fig. 3.1) that is about 3m too deep.

The net average magnitude of other the smaller systematic errors was estimated from the time-series of the budget computations. A trend analysis was carried out in which a linear and quadratic equation were fitted through the data. For each time-series the average spread of the observations around the regression models, i.e. the standard error, was computed. This standard error was then used as an estimate of the average systemeatic error in the observations. The analysis revealed the following results:

- the entire main channels EC1, FC1, EC2 and FC2 (Fig.3.1): the average standard error approximates 3Mm³ for the computed water volumes. This equals a standard error in the average water depth of 0.1-0.15m, and a relative error in the water volume of the channels of about 1%. The value of 3Mm³ for an individual budget computation implies a maximum systematic error in the computed budget changes of about 6Mm³ for the entire main channels.
- the individual channel sections (1-17 in Fig. 3.2): the average standard error is 1.2±0.5Mm³, equalling a depth error of 0.18±0.08m or a volume error of 1.4±0.6%. Thus, the maximum systematic error in the computed budget changes of each channel section is about 2.4Mm³.

#### Data sets

The data sets consist of 'standard' and 'specific' echosoundings. For the Terneuzen section seventeen digital data sets of 'standard' echosoundings are available, including the years: 1955, 1960, 1964, 1966, 1968, 1972, 1974, 1978, 1980, 1982, 1984, 1986, 1988, 1990, 1992, 1994 and 1996. More frequently surveyed echosoundings are available for specific areas of the Westerschelde. These are referred to as 'specific' echosoundings. One of the 'specific' echosoundings covers the bar B1 in the main flood channel FC1 of the Terneuzen section (Fig. 3.1). Although the size and survey frequency of this area are highly variable, about twenty five surveys are available since 1986.

#### Data processing

Data processing is the first general step in the analysis of the line-based data set. It consists of the reduction to Dutch ordnance level (NAP) and interpolation of the data. Reduction of the data set to NAP was generally done on the basis of water level observations along the estuary during the surveys. After this reduction an interpolation of the data set was conducted to obtain a continuous regular grid. For this purpose the DIGIPOL interpolation method was used (Van Munster et.al.(1995). This method is based on an image processing technology and follows an iterative approach. After a first rough interpolation, a straightforward triangulation, an estimate of the flow direction in each cell is made. Herein it is assumed that depth has less variation in the direction of water flow than perpendicular to this flow. Based on this direction estimate a direction sensitive interpolation is done. These last two steps are repeated until a stable result is obtained. The result consists of regular grids with a cellsize of 20 x 20 meters. These grids were then used for further analyses in the Geographical Information System ARC-INFO.

## 3.3 Methods for quantitative morphological analyses

#### 3.3.1 Introduction

The study focuses on the quantification of the morphological channel behaviour. For this purpose the following five analyses were carried out:

- The computation of the sediment budgets in the Terneuzen and Hanswert section.
  This analysis was made to identify the channels or channel parts that played a
  major role in the budget changes.
- The computation of the spatially averaged cross-sectional channel morphometry.
   The results of this analysis were used to identify the characteristic stages of channel evolution.
- The computation of the migration rates of the connecting channel. This analysis aims to characterise the morphological behaviour of these channels.
- The assessment of antropogenic activities in relation to channel change and channel size. This analysis was made to estimate the influence of dredging and dumping on the evolution of the connecting channels.
- The computation of the reworked sediment volumes at the bar in the main flood channel (B1 in Fig. 3.1). This analysis aims to characterise the total temporal variation in the morphological dynamics at the bar and to relate it to the behaviour of the bar channels (BC in Fig.3.1).

As already argued in section 3.1 the analyses focus on the channel behaviour in the Terneuzen and Hansweert section. The evolution of the channel system just seaward of the Terneuzen section is not considered here. Since 1960 the evolution of this seaward area is dominated by the behaviour of an ebb bar channel (Chapter 2). A significant influence of these developments on the evolution of the channels in the

Terneuzen section is not expected. This is concluded from the available discharge measurements at the seaward margin of the study area in 1958 and 1994. These measurements show only minor changes in relative distribution of the discharges between the main ebb and flood channel (EC1 amd FC1). This indicates that the general flow pattern hardly changed here. The behaviour of the channels landward of the Hansweert section are also not considered here. The channel evolution here is characterized by erosion of the main ebb channels and sedimentation in the main flood channels since 1970. This channel evolution has been largely attributed to the artificial deepening of the shipping lane between 1970 and 1975 (Chapter 2). However, previous budget studies did not show a significant influence of these developments on the evolution of the Terneuzen en Hansweert section.

## 3.3.2 The computation of sediment budgets

A schematisation of the channel system into channel sections (not cross-lines) formed the basis for the computations of sediment budgets (Fig. 3.2). The size of the sections ranges between 3km<sup>2</sup> and 12km<sup>2</sup>. The subdivision between main ebb and flood channels was based on the mean location of the watersheds over the intertidal shoals. The intertidal shoals were included in the main channel sections because they influence the current velocities in these channels. Channel sections 4 and 17 cover the bar areas B1 and B3 in the main flood channels FC1 and FC2 (Fig. 3.1). Channel section 10 defines the area of the cross channel CC (Fig. 3.1).

Hypsometric curves were computed for each channel section based on the schematisation and the available bathymetric maps. These curves describe the changes in surface area and water volume as a function of water depth, which were computed with standard commands in Arc-Info. They were then used to quantify the changes in the sediment budget of each channel section. Three volumes were determined, viz.:

- the total water volume below NAP+2.5m. Changes in this volume are due to alterations of the channels and the intertidal shoals;
- the water volume below NAP-2m, referred to as the channel volume.
- the sand volume above NAP-2m, referred to as the shoal volume. This is the sand volume stored in the inter-tidal shoals.

The evolution of the sediment budgets is influenced by dredging and dumping of sediment. To estimate this influence the dredged and dumped sediment volumes in each channel section were determined. This was done as follows:

- usually the dredged and dumped sediment volumes are measured in the dredging ships. For each dredging and dumping site the annually dredged or dumped sediment volumes were computed;
- these volumes were converted to in situ volumes by applying a bulking factor for fine sands of 10% (Bray et.al., 1997);

- the in situ volumes were assigned to the proper channel section. If the dredging or dumping sites intersected the channel sections, the assignment of the volumes was done in proportion to the surface area of these intersections;
- finally, the net volumes of dredging and dumping were computed. This was done by assigning a positive sign to the dredged volumes. The reason for this is that these activities potentially increase the water volume. The dumped sediment volumes were given a negavite sign, as dumping results in a potential decrease of the water volume. Then, the dumped and dredged sediment volumes were summed. This resulted in the net, annual volume of human impact in each channel section which were again summed over time. This yielded the net cumulative volume of human impact in each section.

Once the budget changes of each channel section were computed, the results of specific channel sections could be summed. In this way the budget changes of the entire main channels and estuarine sections were obtained as well.

## 3.3.3 The computation of the cross-sectional channel geometry

The cross-sectional channel geometry was decribed by the cross-sectional area and hydraulic radius of the channels at mean sea level. These parameters were chosen because of their hydrodynamic background, viz.:

- They are also used to describe the channel morphology in the one-dimensional momentum equation of flow;
- The cross-sectional area at mean sea level (NAP) is used in most empirical relationships which relate the cross-sectional area of the channels to the discharge through the channel (e.g. Gerritsen en De Jong, 1984; Bliek and Storm, 1995).

The cross-sectional area and hydraulic radius of the channels were computed as spatially averaged values. The input of the computations consisted of a hypsometric curve and an estimate of the length of each channel section. Details of the computation method are given in appendix 3.1. The obtained values are in fact average values based on more than hundred cross-sectional transects perpendicular to the channel axis.

The channels were schematised to compute the hypsometric curves and the average cross-sectional geometry. The schematisation of the main channels (EC#, FC#) and the two types of connecting channels (BC# and CC) differed.

For the main channels the same schematisation as to the budget computations was applied (Fig. 3.2). The length of the main channel sections was determined as the length of a flowing line through the deepest points. Only for channel section 4 (Fig. 3.2), the bar in the flood channel, this method was not feasible. This is due to the various bar channels that intersect the bar. Alternatively, a fixed channel length was defined based on the general alignment of the entire flood channel. As the length of

these channel axes hardly changed over time, the mean lengths over the period 1955-1996 were used in all computations.

The connecting channels are relatively small. Therefore, the schematisation of these channels was not further subdivided into smaller channel sections, as was done for the main channels. Instead, channel sections covering the entire channels were defined. Thus, the cross-sectional area and hydraulic radius were computed as spatially averaged values for the entire connecting channels. The lateral demarcation of the bar channels and cross channel slightly differed:

- The bar channels (bc in Fig. 3.1): similar to the main channels (see section 3.3.2) the schematisation of the bar channels was based on the pattern of watersheds which were computed with standard Arc-Info commands. The computed major watersheds follow the highest points between the various bar channels. In Chapter 4 it will be shown that these watersheds represent the transitions between the ebb-dominated flow in the ebb bar channel and the flood-dominated flow in the flood bar channel.
- The cross channel (cc in Fig. 3.1): the intertidal channel storage along the cross channel essentially influences the current patterns in the main channels, not in the cross channel. Therefore, these intertidal areas were excluded from the schematisation of the cross channel as much as possible. In practice the lateral boundary of the channel section approximately follows the NAP-2m depth contour. Near this depth the hypsometric curves shows an inflection point.

Both the bar channels and the cross channel migrate and the change their plan-view dimensions. Consequently, the schematisations of these channels changed for each bathymetric map. The changing length of the connecting channels was defined as the length of a connecting line through the deepest points of the channel.

### 3.3.4 The computation of the migration of the connecting channels

The quantification of the migration of the bar channels and the cross channel (bc and cc in Fig. 3.1) was based on the displacement of the channel banks. In this study channel banks were defined as those channel parts that have a slope value larger than 3%.

For both the accreting and eroding bank of a migrating channel the average slopes (S in %) and the mean erosion and sedimentation height (h) were computed in ArcInfo (Fig. 3.3). Based on these two parameters the horizontal displacement rate M (m/yr) of each channel bank was computed as,

$$M = \frac{h}{S*0.01*\Delta T} \tag{3.1}$$

where:

h = the mean erosion (-) or sedimentation height (+) of the eroding or accreting channel bank (m)

S = the average slope (%) of the eroding or accreting channel bank.

 $\Delta T$  = the time interval between two bathymetric maps (in years).

0.01 = factor to convert slopes in percent-rise to meters-rise;

Mean migration rates of a channel were determined by averaging the mean displacement rate of the goding and accreting channel bank. The average values of the eroded and deposited sediment volumes were computed as well, to compare them to the total sediment reworking at the bar area B1 of the main flood channel FC1 (Fig. 3.1).

# 3.3.5 The assessment of dredging and dumping on the evolution of the connecting channels

The morphologic evolution of the connecting channels (bc and cc in Fig. 3.1) may be sensibly influenced by dredging and dumping. Contrary to the main channels the length of these channels changed. This impedes a comparison of channel volumes and dredging volumes. Therefore, the dredged and dumped sediment volumes were converted to a potential change in the cross sectional area of the channels (in %). An additional advantage of this approach is that it directly relates the potential influence of human impact to channel size. The analysis was made as follows:

- for each period between two subsequent echosounding surveys the total volumes
  of dredged and dumped sediments were computed. Dredging potentially increases
  the channel cross section. Therefore these volumes were given a positive sign.
  Dumped sediment volumes obtained a negative sign.
- then the volume of human impact was divided by the average channel length during the considered period. This gives a potential change in the cross-sectional area of the channel in square meters  $(\Delta A_p)$ .
- The potential change in cross sectional area (ΔA<sub>p</sub>) was divided by the average cross-sectional area of the channel (A<sub>av</sub>) during the considered period. This value was then multiplied with 100%, resulting in the potential change in cross-sectional area expressed as a percentage of the average channel cross section.
- finally, the observed change in the cross-sectional area of the channel was also divided by the average cross-sectional area (A<sub>av</sub>) and expressed as a proportional change (%).

Thus, the result of this analysis consists of two time series. One which shows the potential change of the channel cross section (in %) due to dredging and dumping. The other displays the observed relative changes in the cross-sectional area of the channel. A positive value means an increase of the cross sectional area, whereas a negative value indicates a decrease (in %).

## 3.3.6 The computation of the sediment reworking

The temporal variation of the sediment budget of a certain area represents the net effect of erosional and depositional processes. However, small sediment budget changes do not necessarily imply a stable channel morphology. This may be particularly true for the bar area B1 in the main flood channel FC1 of the Terneuzen section (Fig. 3.1), where an abundance of migrating bar channels exists (bc in Fig. 3.1). Therefore, for this bar area the magnitude of the sediment reworking was determined as an additional indicator of the morphological dynamics. Herein, the sediment reworking (S) is defined as the average sum of the eroded ( $V_e$ ) and deposited sediment volumes ( $V_d$ ) in the bar area (section 4 in Fig. 3.2) over a time interval of two years:

$$S = 0.5 * (|V_e| + |V_d|)$$
 3.2

Generally the magnitude of the sediment reworking in a given area will depend on the time interval. However, the time interval between two successive echosoundings is seldomly the same. This difference in time interval was corrected for by determining and using the relationship between the magnitude of the sediment reworking and time interval for the bar area B1 (Fig 3.1). Figure 3.4 shows this relationship based on the standard and specific echosoundings. The exponential curves that were fitted through the data were used to index all observations with a time interval of approximately two years to exactly two years. This resulted in two time-series of the sediment reworking, viz.: one for the period 1955 to 1996 (based on standard echosoundings) and one for the period 1986-1996 (based on specific echousoundings).

Figure 3.4 shows a levelling off of the sediment reworking for time intervals larger than five to ten years: the reworking becomes independent of the time interval. It is believed that this time interval indicates the inherent morphological time scale of the considered phenomenom. Furthermore, Figure 3.4 depicts a large variation in the sediment reworking for a given time interval, indicating a temporal variation. It is this variation that is of interest in the present study as it indicates temporal changes in the morphological dynamics at the bar B1 that may be related to the behaviour of the bar channels.

- 3.4 The morphological evolution of the main channels in the Terneuzen and Hansweert section
- 3.4.1 The evolution of the planform channel geometry

The main changes in the planform channel geometry can be identified from Enclosure 2 and Figure 3.5. Enclosure 2 shows 6 bathymetric maps during the period 1955 to

1996 with an interval of about 9 years. Figure 3.5 displays the erosion-sedimentation patterns over the period 1955 to 1996.

In the Terneuzen section the major morphological changes occurred in the seaward part of the main ebb channel EC1 and the landward area of the main flood channel FC1 (Fig 3.5 and Enclosure 2). The seaward part of the ebb channel EC1 migrated in a seaward direction: the outer channel bank eroded while the inner bank accreted (Fig. 3.5). This proces has been going on since 1800 (Chapter 2). In the other areas of this channel alternating patterns of erosion and sedimentation are observed (Fig3.5). In the main flood channel FC1 various morphological changes occurred in the bar area B1 (sections 3 and 4, Fig 3.5, Enclosure 2). These are described in detail in section 3.5. The erosion-sedimentation map shows sedimentation along the northern channel bank and in section 1 of the channel (Fig. 3.5). The other deeper parts of the channel FC1 are dominated by erosion. The cross channel CC migrated in seaward direction (section 10 in Fig. 3.5, see also section 3.6).

In the Hansweert section the behaviour of a bar channel BC (Fig 3.1) dominated the evolution of the channels (Enclosure 2, Fig. 3.5). The bar channel BC originated in the bar area B3 of the flood channel FC2 in 1951. Since its formation the channel BC has had a small bar at its seaward end, i.e. the channel is an ebb channel (Van Veen, 1950). After its formation the ebb bar channel BC expanded and slightly rotated (Enclosure 2, Fig. 3.5). This channel evolution was accompanied by an extension of the intertidal shoals and sedimentation in the main ebb channel EC2 (Fig. 3.5, Enclosure 2). In 1980 the bar area B3 had eroded so much that the shipping lane was replaced from the ebb channel EC2 to the shorter flood channel FC2.

#### 3.4.2 Large-scale and small-scale variations in the sediment budgets

Large-scale variations in the sediment budgets

Figure 3.6 shows the main erosional and depositional trends in the Terneuzen and the Hansweert section between 1955 and 1996. The changes refer to alterations in the water volume below NAP+2.5m. Table 3.1 summarizes the changes in the sediment budgets over the period 1955 to 1996 in more detail.

The entire Terneuzen section is marked by a net erosion of about 34Mm³ and a net sediment dredging of 4Mm³ between 1955 and 1996 (Fig. 3.6, Table 3.1). Hence, the net erosion as a result of natural processes is about 30Mm³±12. Most of this erosion took place in the channels, especially in the flood channel FC1. Over the period 1955-1996 the net erosion in this channel induced by natural processes (24+20=44Mm³±6, Table 3.1) exceeded the net natural sedimentation in the main ebb channel EC1 (18-4=14Mm³±6, Table 3.1).

The Hansweert section is characterised by a net sediment deposition of about 39Mm<sup>3</sup> between 1955 and 1996 (Fig. 3.6, Table 3.1). The net dumping in this section is about 23 Mm<sup>3</sup>. Hence, the net deposition caused by natural processes is about  $16\text{Mm}^3 \pm 12$  between 1955 and 1996. This net deposition is due to a natural sedimentation in the main ebb channel EC2 ( $68+8=76\text{Mm}^3 \pm 6$ , Table 3.1) which exceeded the natural erosion in the main flood channelFC2 ( $29+31=60\text{Mm}^3 \pm 6$ , Table 3.1). The net deposition in the channels was larger than the sedimentation at the intertidal shoals (Table 3.1).

To conclude, including the effect of dredging and dumping, the Terneuzen section eroded with about  $30 \pm 12 \text{ Mm}^3$  between 1955 and 1996 (Table 3.1). In the Hansweert section a net natural sediment deposition of  $16 \pm 12 \text{Mm}^3$  occurred. During this period the flood channels FC1 and FC2 in both estuarine sections displayed a major net 'natural' erosion:  $44 \text{Mm}^3 \pm 6$  and  $60 \text{Mm}^3 \pm 6$  respectively. The ebb channels EC1 and EC2 showed a net natural sedimentation of  $14 \text{Mm}^3 \pm 6$  and  $76 \text{Mm}^3 \pm 6$  respectively.

Small-scale variations in the sediment budgets of the Terneuzen section

Tables 3.2 summarizes the overall sediment budget changes between 1955 and 1996 for each section of the main channels in the Terneuzen section in the same way as in Table 3.1. The net changes in the water volume below NAP+2.5 and the dredged sediment volumes in the Terneuzen and Hansweert section over the period 1955 and 1996 are depicted in Figure 3.7. Figures 3.8 and 3.9 show the temporal variation in the channel and shoal volumes of the main flood channel FC1 and the ebb channel EC1.

The net erosion of the main flood channel FC1 over the period 1955 to 1996 was essentially determined by the evolution of the channels and shoals in sections 3 and 4, the bar area B1 in the channel. This channel evolution does not show a steering human influence. This follows from Table 3.2 and Figures 3.7 and 3.8:

- Channel volume (Fig.3.8a): the general shape of the FC1-curve resembels the curve of section 4. The actual erosion process occurred between 1960 and 1990 (30 Mm³ in the entire channel). It was preceded and followed by short periods of minor sedimentation, which also marked the evolution of section 4. As a result of this sedimentation the net magnitude of the total channel erosion between 1955 and 1996 is largely determined by the erosion in section 3 and to a lesser extent by section 4 (Table 3.1).
- Shoal volume (Fig. 3.8b): the overall development of the intertidal shoals along the flood channel FC1 closely follows the evolution of the shoals in sections 3 and 4. The shoals along the channel (FC1-curve) display a net erosion of 2 Mm<sup>3</sup> over the period 1955 to 1996. Initially the shoals extended with about 3Mm<sup>3</sup> between 1960 and 1976. Since 1976 the intertidal shoal volume decreased with 4-5Mm<sup>3</sup>. This decrease almost entirely occurred in section 4.
- Dumping (Fig. 3.8c): net sediment dumpings were carried out in sections 1 and 4 since about 1970. These sediment dumping were not accompanied by a net

channel shoaling (cf. Fig. 3.8a). Hence, the erosion caused by 'natural processes' in section 4 is about twice as large as the net erosion (Table 3.2, Fig. 3.7).

The development of the ebb channel EC1 displays a spatially rather uniform picture. A possible steering human influence on the channel evolution is only observed in the most seaward part of the channel, section 5 (Fig. 3.7, 3.9, Table 3.2)

- Channel volume (Fig. 3.9a): Between 1955 and 1996 the channel volume remained approximately constant. Some minor fluctuations (± 4Mm³,1%) with a period of about five to ten years are superimposed on the average channel volume of about 340 Mm³. These fluctuations, which were also observed by Uit den Bogaard (1995), are ascribed to incidental systematic errors. Most individual channel sections also display an approximately constant channel volume. Only channel section 5 shows an increase in the channel volume (about 9 Mm³) which took place between 1970 and 1996.
- Shoal volume (Fig. 3.9b): over the period 1955 to 1996 the intertidal shoals along the channel extended with 3 Mm<sup>3</sup>. This increase essentially occurred in section 7 and to a lesser extent in section 5 (Fig. 3.9c) between 1955 and 1974.
- Dredging (Fig. 3.9c): in the ebb channel about 18 Mm<sup>3</sup> of sand has been dredged between 1955 and 1996. In channel section 5 the increase of the channel volume approximately coincides and equals the magnitude of the sediment dredging. This indicates that the erosion of this channel section was caused by dredging.

Small-scale variations in the sediment budgets of the Hansweert section

The results of the detailed budget computations for the Hansweert section are summarized in Figures 3.7, 3.10 and 3.11 and Table 3.3.

In the flood channel FC2 the net changes in the channel and shoal volume between 1955 and 1996 mainly occured in section 17 and to a lesser extent in section 16 (Fig. 3.7 and Table 3.3). In these areas the channel eroded whereas the intertidal shoals, bordering the channel FC2, were characterized by sedimentation. The substantial sediment dumpings in the channel did not steer this evolution:

- Channel volume (Fig. 3.10a): in channel sections 16 and 17 the total channel volume increased with about 20Mm<sup>3</sup> between 1955 and 1970. In section 17 the channel eroded with another 15Mm<sup>3</sup> between 1970 and 1996.
- Shoal volume (Fig.3.10b): the total shoal volume along the channel increased with 4Mm³ to almost 10Mm³ between 1955 and 1996. This extension largely occurred in sections 16 and 17 between 1955 and 1990 (Fig. 3.10b).
- Dumping/dredging (Fig. 3.10c): the net 'natural' erosion in the channel is considerable when the sediment dumpings in sections 15 and 16 are taken into account. Despite the sediment dumpings of about 40Mm3 between 1955 and 1996, the channel volumes did not decrease. In section 16 it even slightly increased. The dredging in section 17 (about 9 Mm3 between 1955 and 1996) was subordinate to these dumpings and is therefore not expected to have steered the erosion in this area.

The main ebb channel EC2 shows a spatially uniform picture of large channel sedimentation (Table 3.3) that essentially occurred between 1955 and 1986 (Fig. 3.7, 3.11). Man hardly influenced this evolution by dredging and dumping:

- Channel volume (Fig. 3.11a): all four channel sections display the same general trend of a decreasing channel volume that started around 1955 and stabilised around 1986.
- Shoal volume (Fig.3.11b): the small shoal volume along the channel slightly increased between 1955 and 1974. The evolution in the various sections differed: in section 11 the shoal volume decreased (1.5Mm³). Along channel section 12 it increased (3 Mm³), whereas in channel section 13 it remained more or less constant.
- Dredging/dumping: the long-term net effect of dredging and dumping over the period 1955 to 1996 is an erosion of approximately 8Mm³ (Table 3.2, Fig. 3.11c). Limited dredging has been carried out in sections 13 and 14 since 1955 (Fig. 3.11c). In section 11 man used to dredge to maintain the shipping lane. In 1980 the shipping lane was formally abandonned (section 3.4.1). Since then sediment dumpings were carried out in this area.

## 3.4.3 The evolution of the cross-sectional channel geometry

Figures 3.12 and 3.13 show the implications of the net budget changes for the cross-sectional area and hydraulic radius of the main channels in the Terneuzen and Hansweert section. Based on the results of the sediment budget analysis (section 3.4.2) some of the channel sections were merged.

The main channels EC1 and FC1 in the Terneuzen section (Fig. 3.12)

The major changes in the cross sectional geometry exist at and near the bar area B1 of the main flood channel FC1 (sections 3 and 4 in Fig. 3.12). In this area the average cross-sectional area and hydraulic radius increased in time with about 15 to 25% between 1955 and 1996 (Fig. 3.12a and b). In the other parts of the main channels the maximum temporal changes in the average cross-sectional geometry hardly exceeded 10%. In both the ebb channel EC1 and the flood channel FC1 the along-channel gradients in the depth and cross-sectional area decreased with time. Some details are given below.

The flood channel FC1 (Fig. 3.12a,b):

- Sections 1+2: the average cross-sectional area (34600m²) and depth (11.8m) hardly changed (order of 3 to 6%) between 1955 and 1996.
- Section 3 (bar area B1): the average cross-sectional area gradually increased with about 4400m<sup>2</sup> (24%) between 1955 and 1996. The hydraulic radius of this channel part increased with almost 3m (23%) between 1955 and 1978. After 1978 the depth levelled off.

• Section 4 (bar area B1): the cross-sectional area and depth increased with about 15% between 1955 and 1996. After an initial decrease of 12% between 1955 and 1960, the cross-sectional area increased with 5700m² (30%) between 1960 and 1988. The average depth increased with about 1.8m (32%) until 1982. Since 1990 the average bar depth and cross-sectional area slightly decreased.

## The ebb channel EC1 (Fig. 3.12c,d):

- Section 5: the average cross-sectional area and channel depth increased with about 2000m<sup>2</sup> and 1.3m respectively between 1955 and 1996 (10%).
- Sections 6+7: the average cross-sectional area remained approximately constant (24000 m²). However, the average depth of this channel part gradually increased with 1m (6%) over the period 1955 to 1996.
- Section 8: the cross-sectional area and depth remained approximately constant between 1955 and 1996. Only between 1955 and 1980 the cross-sectional dimensions temporarily increased and decreased with about 6%.
- Section 9: the average cross-sectional area and depth remained approximately constant over the period 1955 and 1996. The average depth (18.8m) varied with less than 1m (5%).

### The main channels EC2 and FC2 in the Hansweert section (Fig. 3.13)

In the Hansweert section the largest changes occurred in the entire main ebb channel EC2 and the bar area B3 of the main flood channel FC2 (section 17, Fig. 3.13). The evolution of the two channels tends to be opposite: in the bar area B3 of the flood channel FC2 the cross-sectional dimensions increased. As a result the along-channel depth gradients in this channel strongly decreased between 1955 and 1996. In the ebb channel EC2 the cross-sectional dimensions decreased (with 14-28%) and the along-channel gradients increased. The changes in the ebb channel EC2 essentially occurred between 1955 and 1986.

### The flood channel FC2 (Fig. 3.13a,b):

- Section 15: the cross-sectional area and channel depth slightly fluctuated (with less than 5%) around 21000m<sup>2</sup> and 16m respectively between 1955 and 1996.
- Section 16: the cross-sectional area fluctuated around 18000m<sup>2</sup> with about 500m<sup>2</sup> between 1955 and 1996. The average channel depth gradually increased with about 2m (16%) between 1955 and 1996.
- Section 17 (bar area B3) the average cross-sectional area and hydraulic radius increased with almost a factor two between 1955 and 1996. This increase was caused by the expansion of the large ebb bar channel BC (see section 3.4.1).

#### The ebb channel EC2 (Fig. 3.13c,d):

- Sections 11 and 14: the average channel depth decreased with almost 4m (27%) between 1955 and 1996.
- Sections 12 +13: the channel depth decreased with about 2m (14%) over the entire period 1955 to 1996.

#### 3.4.4 Discussion and conclusions

The objective of this section was to determine the morphological evolution of the main channels in the Terneuzen and Hansweert section and to asses the influence of dredging and dumping on this evolution. In addition it aimed to identify the coherence in the channel evolution. Below the characteristic aspects of the channel evolution are discussed and the coherence is inferred as far as possible. Herein, it is assumed that the morphology of the main ebb channels EC1 and EC2 is controlled by the ebb-dominated flow and that the flood flow largely determines the evolution of the main flood channels FC1 and FC2.

#### The Terneuzen section

In the Terneuzen section the major morphological changes occurred in the bar area B1 of the main flood channel FC1 (Fig. 3.1). The large-scale net erosion of the Terneuzen section, 34Mm³ between 1955 and 1996, is essentially explained by the erosion of this bar area (22 Mm³ in sections 3 and 4, Fig. 3.7, Table 3.2). The actual erosion proces took place between 1960 and about 1990, with the largest erosion rates occurring between 1960 and 1968. The sediment budgets of the ebb channel EC1 hardly changed. Apart from the most seaward part of this channel (section 5, Fig.3.7) dredging and dumping activities did not result in a net erosion or deposition. From this it is concluded that a general steering human influence on the channel evolution was absent in the Terneuzen section between 1955 and 1996.

In the eroding bar area B1 the cross-sectional area and channel depth increased with 15 to 25% between 1955 and 1996 (section 33, 4, Fig. 3.12). In the seaward part of the flood channel FC1 the channel dimensions changed with only 3-6% (sections 1+2, Fig. 3.12). The morphology of the ebb channel EC1 hardly changed. Only in the seaward part of this ebb channel the cross-sectional channel dimensions steadily increased in time with 6 to 10% (sections 5, 6+7, Fig. 3.12). This increase was probably the result of dredging. The landward part of the ebb channel EC1 did not display a clear trend of channel evolution: the cross-sectional channel dimensions varied with about 5%.

The preliminary model computations in Chapter 2 indicated that the observed erosion (15-25%) of the bar area B1 may have been accompanied by a minor and local redistribution of the discharges between the main channels: landward of the cross channel the discharges over the bar area B1 probably increased (5-10%) whereas they decreased in the ebb channel EC1 (5-10%) and the cross channel CC (20-25%). However, this part of the ebb channel EC1 did not show a steady decrease of the cross-sectional channel dimensions of 5-10% between 1955 and 1996. This indicates that either the pattern of ebb discharges hardly changed as a result of the bar erosion or the changes in channel morphology were to small to be identified. The pattern of

flood discharges probably changed without affecting the morphology of the ebb channel EC1.

Unfortunately, there are no standard discharge measurements available for the area just landward of the cross channel CC to confirm the expected changes in flow pattern. On the other hand these expected change are probably too small to be determined from such measurements. The available discharge measurements just seaward of the cross channel (Fig. 3.14a and b) do not show any significant changes in the distribution of the ebb and flood discharges between the main channels. This confirms the relatively stable channel morphology here. To conclude, the erosion of the bar area B1 in the flood channel FC1 largely explains the erosional trend in the Terneuzen section. This erosion probably did not significantly affect the morphology of the other parts in the main channels FC1 and EC1. Though, a relationship with the behaviour of the bar channels BC in the bar area B1 can be expected.

### The Hansweert section

In the Hansweert section the major morphological changes occurred in the bar area B3 of the main flood channel FC2 and the entire main ebb channel EC2. The evolution of the ebb bar channel BC in the bar area B3 since 1951, was accompanied by a net erosion of the flood channel FC2 (29 Mm³ between 1955 and 1996) and a net sedimentation in the ebb channel EC2 (68 Mm³ between 1955 and 1996), yielding a net sedimentation in the Hansweert section of about 37 m³ between 1955 and 1996. The sedimentation in the ebb channel EC2 lasted until approximately 1986, indicating that the channel system had reached a new equilibrium by then. The erosion of the flood channel FC2 occurred despite extensive sediment dumping (31 Mm³ between 1955 and 1996), whereas the net sedimentation in the ebb channel took place despite dredging activities (8 Mm³ between 1955 and 1996). From this it is concluded that man also did not steer the channel evolution in the Hansweert area.

The sedimentation in the ebb channel EC2 was accompanied by a large overall decrease in the cross-sectional area and channel depth (14-27% between 1955 and 1996, Fig. 3.13). In the bar area B3 flood channel FC2 the channel dimensions increased with almost a factor two. In the central part of the flood channel (section 16, Fig. 3.13) the depth increased with about 16% between 1955 and 1996.

The total tidal discharge in the estuary did not change significantly between 1955 and 1996 (Vroon et.al., 1997). Therefore, the large changes in the dimensions of the ebb channel EC2 indicate a considerable reduction of the ebb discharges in this channel and an increase of the discharges through the flood channel FC2. In other words, the observations indicate a redistribution of the discharges. The smaller increase of the cross-sectional dimensions of the flood channel FC2 imply a similar though smaller redistribution of the flood discharges.

The available discharge measurements in the middle of the estuarine section since 1932 confirm the inferred change in general flow pattern (see Fig. 3.14 c and d). Between 1955 and 1996 the ebb volumes in the flood channel increased with about 100Mm³ (60%) at the expense of the ebb volume in the ebb channel. The changes in the distribution of the flood volume are about twice as small. The largest changes in the flow pattern occurred between 1955 and 1970. To conclude, the formation of the bar channel BC and the subsequent erosion of the bar area B3 in the flood channel FC2 was accompanied by a redistribution of the discharges and an adaptation (shoaling) of the ebb channel EC2 that lasted until 1986.

The morphological changes in the Hansweert section and the Terneuzen section indeed seem to be related (section 3.1). More specifically, the observations suggest that the erosion in the bar area B1 in the Terneuzen section was induced by the morphological changes in the Hansweert section. This coherence is inferred from the following:

- The major erosion in the bar area B1 between 1960 and 1990 almost immediately followed the adataption of the ebb channel EC2 in eth Hansweert section between 1955 and 1986. Moreover, the erosion practically ceased as soon as the ebb channel EC2 had reached a new equilibrium.
- the bar area B1 in the flood channel FC1 determined the erosion of the Terneuzen section, not the ebb channel EC1. A flood channel is generally expected to induce a landward sediment transport, whereas an ebb channel tends to transport sediment in a seaward (ebb) direction (Van Veen, 1950). This suggests that the eroded sediments from the flood channel FC1 were transported in a landward direction to the Hansweert section. This confirms the general landward sediment transport in the Westerschelde between 1955 and 1993, as derived in previous budget studies. This relationship will be further elaborated in Chapter 5 using the model results.
- 3.5 The morphological evolution of the bar channels in the Terneuzen section
- 3.5.1 The evolution of the planform channel geometry

This section focusses on the morphological changes at the bar area B1 of the flood channel FC1 in more detail by considering the behaviour of the bar channels in this area.

During the period 1955 to 1996 the morphology of the bar channels changed twice, yielding three different channel patterns with specific morphological features. These patterns are depicted in Figure 3.15. Following Van Veen (1950) the bar channels can subdivided into ebb bar channels (bar at seaward end) and flood bar channels (bar at landward end).

Channel pattern 0 (Fig.3.15a):

This first pattern consisted of a large, probably migrating, ebb bar channel (BC -1) that was bordered by a flood bar channel (BC0) at the North. The channels had an

approximately east-west orientation. Old hydrographic maps reveal similar patterns during the period 1860-1935. The lifetime of the ebb bar channels between 1860 and 1935 approximated 12 years (Anonymous, 1940).

The period 1960 until 1964/1966 formed a transition period to pattern 1. It was marked by the absence of an ebb bar channel and the presence of a new flood bar channel (BC1, Fig.3.15b, Enclosure 3). During this phase the entire bar in the main flood channel (B1 in Fig.3.1) potruded in a landward direction over a distance of a few hundred metres.

## Channel pattern 1 (1966-1986, Fig. 3.15b):

This pattern also displayed one flood bar channel (BC1) and one ebb bar channel (BC2). However, the flood bar channel was located south of the ebb bar channel instead of north. Moreover, the channels met under an angle of about 45 degrees. The flood bar channel migrated to the South, whereas the ebb bar channel migrated to the East (see arrows in Fig. 3.15b). The migration of the channels induced an erosion of the intertidal shoals and a general widening of the bar area B1 in the main flood channel FC1. The main characteristics of this pattern can be observed until 1986 (Enclosure 3).

Between 1986 and 1988 the ebb bar channel BC2 and the flood bar channel B1 merged into one ebb bar channel (renamed as BC12) which rapidly migrated and degenerated (Enclosure 3). In 1994 this channel had disappeared. During the same time the third channel configuration (pattern 2) developed.

## Channel pattern 2 (1988-1996, Fig. 3.15c):

This pattern consisted of several smaller ebb and flood bar channels that were alligned more or less parallel. Two flood bar channels (BC4, BC5) and one to two ebb bar channels (BC12, BC3) marked the pattern during most of the time. The channels migrated to the South and eroded the remaining intertidal shoals (see arrows in Fig. 3.15c).

### 3.5.2 The evolution of the cross-sectional channel geometry

As no information on the evolution of channel pattern 0 is available, the description of the cross-sectional channel geometry is restricted to channel patterns 1 and 2.

### Channel pattern 1: 1966-1986

The flood bar channel BC1 displayed a cylic behaviour (Fig.3.16; Enclosure 3):

- Between 1964 and 1974 the channel expanded. The average cross channel area and water depth of the channel rapidly increased with about 40%.
- From 1974 onwards the channel migrated to the South with average annual migration rates ranging between 20 and 40 metres. This was followed the erosion

of the intertidal shoals and the degeneration of the channel which both started in 1976. Initially, only the cross-sectional area decreased whereas the channel depth continued to increase, i.e. the channel narrowed. Since 1984 the channel depth also declined.

Between 1984 and 1986 the former flood bar channel BC1 obtained an indifferent channel morphology, i.e. shallow bars developed at the landward and seaward end of the channel (Enclosure 3). The lifetime of the flood bar channel BC1 approximates 22 years.

The complex channel morphology of the ebb bar channel BC2 impeded an objective quantification of the cross-sectional channel geometry. The evolution of the ebb bar channel (BC2, Fig.3.16) does not show stages of major channel expansion and degeneration, like the flood bar channel BC1. The cross-sectional area of the channel probably increased from about 8000 m² in 1966 to 12000 m² in 1986. The channel depth at NAP fluctuated around 8m. During its evolution the channel transversely migrated in a landward (eastward) direction with annual migration rates of about 20 metres (Fig. 3.16c).

Dredging and dumping of sediment may have influenced the channel evolution. Figure 3.17 compares the evolution of the cross-sectional area of the two channels BC1 and BC2 with the potential changes as a result of dumping and dredging at the bar of the main flood channel.

- The flood bar channel BC1 (Fig. 3.17a): the maximum potential change in the
  cross sectional area are negatively or weakly positively correlated to the observed
  channel changes during most of the time. The increase of the channel cross
  section between 1964 and 1974 amply exceeded the potential decrease due to
  sediment dumping.
  - Between 1974 and 1984 dumping and channel evolution were slightly, positively correlated.
- The ebb bar channel BC2 (Fig. 3.17b): the net changes in the cross-sectional area of the channel are negatively correlated with the potential changes due to mining and dumping during most of the time.

## Channel pattern 2: 1988-1996

The flood bar channel BC1 and the ebb bar channel BC2 of channel pattern 1 had merged into the ebb bar channel BC12 between 1986 and 1988 (Enclosure 3). This merged channel wascharacterized channel pattern 2 during most of the time. Since its formation the channel BC12 rapidly migrated and degenerated and finally disappeared in 1994.

The ebb bar channel BC3 displayed a cyclic channel behaviour (Fig. 3.18):

• Between 1988 and 1993 the channel expanded. The cross-sectional area enlarged with about 65%. The average hydraulic radius of the channel increased with about

- 1.5m. During this stage of channel evolution the channel migrated to the South with average annual migration rates of 80m (Fig. 3.18c).
- The expansion and migration were followed by channel degeneration from 1993 onwards. A major channel curvature developed and the average annual migration rates increased from 80 to 115m.

In 1997 the channel had practically disappeared. The lifetime of the channel amounts nine years. The channel had migrated in a transverse direction over a distance of about 700 metres. A new ebb by channel had already originated just North of the channel in 1996.

Up until 1997 the two flood bar channels (BC4 and BC5) did not display a cyclic behaviour like the ebb bar channel (Fig. 3.18):

- The cross-sectional area of the two channels increased until 1995. The average depth of the channel BC4 gradually increased with about 1m. The depth of channel BC5 increased with 2.5m from 5m in 1991 to 7.5m in 1995.
- The increased migration and channel curvature of the ebb bar channel (BC3) was accompanied by a clockwise rotation of the northern flood bar channels (BC4, Fig. 3.18d). The latter tended to migrate to the South with average annual migration rates of 40m (Fig. 3.18c).

Since 1995 the cross-sectional area and depth of the two flood bar channels seem to decrease slightly.

Figure 3.19 compares the evolution of the cross-sectional area of the channels BC12, BC3, BC4 and BC5 with the maximum potential changes as a result of dumping and dredging of sediment. Sediment was dredged in the degenerating bar channel BC12. Incidental large dumpings were carried out in the entrance of the ebb bar channel BC3 in 1992/1993 and 1995. The evolution of the three bar channels is not clearly related to these antropogenic activities:

- The ebb bar channel BC12 (Fig. 3.19a): the decrease of the cross-sectional area between 1985 and 1990 predominates a potential channel shoaling induced by dumping.
- The ebb bar channel BC3 (Fig. 3.19b): the increase in the cross-sectional area between 1988 and 1992 amply exceeded a potential increase induced by dredging. During the degeneration of the channel the decrease of the cross-sectional area was positively correlated with the incidental dumpings.
- The flood bar channel BC4 (Fig. 3.19c): the observed alterations were larger or opposite to the potential effects of dumping and dredging during most of the time (Fig. 3.19b). Only in 1990, 1991 and 1992 the net and potential changes in cross-sectional area were positively correlated and of similar magnitude.
- The flood bar channel BC5 (Fig. 3.19d): during the stage of channel expansion between 1993 and 1995 large sediment dumping were carried out. Thus channel evolution and antropogenic activities were negatively correlated.

## 3.5.3 The reworking of sediment

Figure 3.20 shows the magnitude of the sediment reworking at the bar, i.e. the average volume of the eroded and deposited sediments within periods of two years (section 3.3.5). Indicated are the total sediment reworking at the bar and the reworking induced by the migration of the banks of the bar channels BC1 to BC4. Thus this figure describes the temporal variation in the morphological dynamics of the bar area B1 of the main flood channel Fig. 1 (Fig. 3.1) in relation to the migrational behaviour of the bar channels. The sediment reworking at the bar displays a distinct temporal variation that can be related to the pattern and the migration of the bar channels (Fig. 3.20):

## Channel pattern 1 (1968-1986, Fig. 3.20a):

The total sediment reworking gradually increased from about 4Mm<sup>3</sup> between 1968 and 1978 to 8Mm<sup>3</sup> in 1986. The increase in the total sediment reworking between 1980 and 1985 coincided with the increased migration rates and the sediment reworking at the channel banks of the flood bar channel (BC1 in Fig. 3.20a).

## Channel pattern 2 (1988-1996, Fig. 3.20b):

The total sediment reworking was in the order of 9Mm<sup>3</sup>. Between 1993 and 1995 the displacement of sediment temporarily increased from 8 to 10Mm<sup>3</sup>. This increase approximately coincided with a temporally enlarged sediment reworking induced by the migration of the ebb bar channel BC3.

In both Figures 3.20a and b the sum of the sediment reworking induced by the channel migration does not equal the total reworking. This is inherent to the definition of channel migration (see section 3.3.4, slope values > 3%).

#### 3.5.4 Discussion and conclusions

The purpose of the previous three sections was to identify the characteristic changes and stages in the evolution of the bar channels, and to asses the influence of dumping and dredging on this evolution. The remarkable aspects of the channel evolution, including the possible relationship with the behaviour of the main channels, are discussed in this section.

The evolution of both channel patterns 1 and 2 were dominated by the behaviour of one bar channel, viz.: the flood bar channel (BC1) of pattern 1 and the ebb bar channel (BC3) of pattern 2. Both bar channels displayed a clear stage of channel expansion, transverse migration followed by channel degeneration, i.e. a (quasi-) cyclic channel behaviour. The life-time of two channels and the channel patterns differed considerably: 20 years (BC1/pattern 1) versus 9 years (BC3/ pattern 2). The migration of the channels appears as a feedback in the channel evolution, as it is eventually followed by the degeneration of the channels. A possible explanation for this phenomenom may be the following: as a result of the migration the channel moves

from a location of optimum water surface slopes to a less optimal location. The water surface slopes decrease inducing a reduction of the currents in the channel. This in turn causes sedimentation in the channel and possibly increased migration rates as the channel depth often decreases. An increase in migration rate may then even reinforce the channel degeneration. This hypothesis and the migration mechanisms of the channels will be further elaborated in Chapter 5.

The (quasi-) cyclical behaviour of the bar channels, occuring at the time-scale of one to three decades, indicates that dumping and dredging did not steer this evolution. This was confirmed by the short-term changes in the cross-sectional area of the channels which appeared to be weakly or negatively correlated to the potential effects of dumping and dredging. Sediment transport computations (Chapter 5) should support this conclusion.

The pattern and migration of the bar channels are related to the reworking of sediment at the bar B1. During channel pattern 1 the average sediment reworking appeared to be almost twice as small as during pattern 2 (5Mm versus 9Mm). This difference is explained by the migration, number and size of the bar channels. The many small bar channels of pattern 2 are accompanied by a larger total length of moving channel banks (9km) than the few large bar channels of pattern 1 (6km). In addition to this, the migration rates of the smaller channels of pattern 2 exceeded the displacement rates of the channels of pattern 1 by a factor 2. Consequently, the sediment reworking was larger during pattern 2 than during pattern 1.

The pattern of bar channels can be related to the major changes in the sediment budgets and morphology of the main channels in the Terneuzen and Hansweert section:

- The formation and evolution of channel pattern 1 (1960-1986) approximately coincided in time with the erosion of the flood channel FC1 in the Terneuzen section (1960-1990) and the adaptation of the ebb channel EC2 in the Hansweert section (1955-1986). Particularly the formation and expansion of the channel pattern between 1960 and 1968 were accompanied by a rapid erosion of the bar area B1 in the flood channel FC1.
- Channel pattern 2 (1988-1996) followed the new equilibrium of the ebb channel EC2 around 1986 and approximately coincided with a stabilisation of the sediment budget of the bar area B1 (and the entire flood channel FC1) around 1990.

This relationship indicates that the net sediment transport patterns at the bar area B1 changed with the pattern of bar channels. It also supports the presumption that the erosion of the flood channel FC1 in the Terneuzen section was induced by the morphological changes in the Hansweert section (section 3.4.5). These hypotheses will be further elaborated in Chapter 5 using the model results.

## 3.6 The morphological evolution of the cross channel in the Terneuzen section

## 3.6.1 The evolution of the planform channel geometry

The changes in the planform geometry of the cross channel (CC in Fig. 3.1) concern its overall morphology and migration (Figure 3.21 and Enclosure 3).

In 1955 the cross channel had an indifferent channel morphology, i.e. the channel was neither an ebb channel or a flood channel (see Enclosure 3). Between 1955 and 1964 the erosion along landward channel bank decreased and the bar at the landward entrance of the channel disappeared. Since 1964 the channel has only a bar the seaward end of the channel, indicating that the channel had changed into an ebb channel (Van Veen, 1950).

Since 1955 the channel is transversely migrating in a seaward direction with average annual migration rates of about fifteen metres (Fig. 3.14a and b). The total displacement of the channel since 1955 amounts 800 metres. The transformation into an ebb channel was accompanied by a clock-wise rotation of the channel (15-20°) between 1955 and 1968, while the channel length remained the same. Between 1968 and 1988 the channel (thalweg) rotated in an anti-clockwise direction over 20°, and the channel length increased with about 900m (30%).

# 3.6.2 The evolution of the cross-sectional channel geometry

At the timescale of four decades the cross-sectional channel geometry does not display characteristics of a (quasi-) cyclic channel behaviour, i.e. channel expansion followed by degeneration (Fig. 3.21c):

- After the transformation into an ebb channel, the cross-sectional area and width of the channel decreased (20%) between 1966 and 1972. The bathymetric maps show that this decline is due to a continued reduction of the erosion along the landward channel bank (Enclosure 3).
- Between 1972 and 1980 the average cross-sectional dimensions of the channel enlarged again. The cross-sectional area increased with about almost 1000m<sup>2</sup> (13%). The hydraulic radius increased with more than one metre (15%).
- The variations in the cross-sectional channel geometry between 1980 and 1996 were smaller. The cross-sectional area declined with 6% between 1980 and 1988. Between 1988 and 1996 it enlarged with 15%. The bathymetric maps reveal a deepening of the ebb entrance of the channel in this same period (Enclosure 3).
   In 1996 the channel had approximately the same cross-sectional area as in 1955.

However, the shape of the channel had changed into a longer, narrower but deeper ebb channel.

In the channel about 6Mm<sup>3</sup> of sand has been dredged between 1955 and 1996. This may have influenced the channel evolution. The potential long-term net effect of this

dredging is an increase in the average channel cross-sectional area of about 20%, assumed that the sediment was not replenished by natural processes. Figure 3.14d compares the observed relative changes in cross-sectional area with the potential changes due to dredging in more temporal detail. Positive values indicate an increase in cross-sectional area. Negative values imply a decrease. The influence of the dredging on the short-term channel evolution is not evident:

- The relatively strong decrease of the channel cross section between 1966 and 1972 occurred despite an increased dredging. The smaller gradual decrease of the channel cross-section between 1980 and 1988 (6%) also took place despite the dredging.
- On the other hand, the potential increase as a result of dredging and the net channel evolution were positively correlated between 1960 and 1968, between 1976 and 1980 and since 1988.

#### 3.6.3 Discussion and conclusions

The most remarkable morphological change of the channel involved its transformation from an indifferent channel into an ebb channel between 1955 and 1964 (section 3.6.1). During this change the channel rotated in a clockwise orientation and migrated in a seaward direction. The preliminary model computations (Chapter 2) suggest that this was a logical concurrence of events: the displacement and rotation probably resulted in a reduction of especially the flood discharges and to a lesser extent the ebb discharges. In other words, the tidal flow and probably the sediment transports became more ebb-dominated. Following Van Veen (1950), this favours a tidal channel with an ebb morphology (bar at seaward end).

Apart from the change into an ebb channel, the cross channel did not display any particular stages of channel evolution that indicate a (quasi-) cyclic channel behaviour. Instead, the channel migrated in seaward direction with average annual migration rates of about 15m, while the cross-sectional area remained approximately constant. Only some short-term variations in the cross-sectional area of about 6 to 20% occurred. These observations imply that at the considered time-scale of 40 years the net channel evolution is marked by only one evolutionary stage. This is not unlikely as the channels' predecessor had a lifetime of over one hundred years.

The short-term fluctuations in channel dimensions may have been caused by small morphological and hydrodynamical changes (< 5%) of the main channels. The morphological observations of the main channels displayed a severe erosion (15-25%) of the bar area B1 in the flood channel FC1 between 1955 and 1996. As discussed in Chapter 2 and in section 3.4.5 this erosion was probably accompanied by a redistribution of the discharges between the main channels EC1 and FC1 and a major reduction (20-25%) of the discharges and velocities in the cross channel. Hence, a sedimentation and a steady decrease of the cross-sectional area (20-25%) of the cross channel could be expected. The observations revealed this relationship only for the

period 1964 to 1972: during this period the bar area B1 rapidly eroded and deepened (15-20%) while the bar channels of pattern 1 formed and expanded. These changes were almost immediately followed by a sedimentation and a decrease of the cross-sectional area (20%) of the cross channel between 1966 and 1972. Despite the continued erosion of the bar B1 between 1972 and 1990, the cross-sectional dimensions of the cross channel did not steadily decrease but remained approximately constant. The absence of this long-term relationship may be explained by the dredging (sand mining) in the cross-channel. Theoretically, the long-term effect of the dredging in the channel is an artificial increase of the cross-sectional area of the channel of about 20%. This might have blurred the expected channel shoaling. This will be further elaborated in Chapter 5 using the model results.

### 3.7 Conclusions

This chapter aimed to characterise the morphological behaviour of the different channel types in the Terneuzen and Hansweert section and to infer the coherence in the evolution of these channels as far as possible. The main findings are summarised in this section.

The major morphological changes of the *main channels* in the Terneuzen section were observed in the bar area B1 of the flood channel FC1, where an abundance of bar channels exists. The erosion of this area largely explains the generally observed erosion of the Terneuzen section between 1955 and 1996. It was accompanied by a local increase of the cross-sectional channel dimensions (hydraulic radius and cross-sectional area) of 15-25%. These changes of the bar area did not significantly affect the morphology of the other parts in the main channels FC1 and FC2.

In the Hansweert section the bar area B3 of the flood channel FC2 considerably eroded as a result of the evolving ebb bar channel BC. This erosion was accompanied by a shift in distribution of the discharges and a net deposition in the estuarine section. The discharges and cross-sectional dimensions of the ebb channel EC2 decreased. Especially in the bar area B3 of the flood channel FC2 they increased. The whole adaptation proces lasted from about 1955 to 1986.

The general evolution of the main channels (FC1, EC1, FC2 and EC2) in both the Terneuzen and Hansweert section was not steered by dredging or dumping. Only the erosion of the seaward part of the ebb channel EC1 (9Mm³ between 1955 and 1996) was probably induced by dredging.

The planform channel geometry of the *bar channels* displayed three different channel patterns between 1955 and 1996, viz.: pattern 0 (?-1955), pattern 1 (1966-1986) and pattern 2 (1988-1996). The evolution of both patterns 1 and 2 were dominated by one cyclically behaving bar channel (BC1 and BC3, Fig. 3.1). Although at different time scales (9 and 22 years), both channels displayed a clear stage of channel expansion

followed by channel degeneration. The transverse migration of the channels seems to play an important role in this channel evolution, as it is eventually followed by the degeneration of the channel and the disapperance of the channel pattern. Moreover, the channel migration largely determines the sediment reworking at the bar B1: during pattern 2 it was almost twice as large as during pattern 1. This channel behaviour was not sensibly influenced by dredging.

Apart from the change into an ebb channel, between 1955 and 1964, the *cross channel CC* did not display specific stages of channel evolution. Since 1955 the channel migrated in a seaward direction (15m/yr). The cross-sectional area remained approximately constant with some short-term fluctuations of about 6-20%. Thus, at the considered time-scale of 40 years the channel seems to be marked by only one evolutionary stage. The influence of dredging on this channel behaviour is not evident. Theoretically, the long-term effect is an artificial increase of the channel cross-section of about 20% between 1955 and 1996.

The concurrence of events indicates a morphological coherence in the evolution of the various channels in the Terneuzen and Hansweert section, viz.:

Firstly, the erosion of the bar area B1 in the flood channel FC1 was probably induced by the above-described changes of the main channels in the Hansweert section: the erosion of the bar B1 (1960-1990) almost coincided in time with the sedimentation in the ebb channel EC2 of the Hansweert section (1955 and 1986). In addition, the erosion of the bar B1 ceased around 1990 (and even restored), shortly after the ebb channel EC2 had reached a new equilibrium around 1986. The relationship might be explained by an increased net flood transport of sediment from the flood channel FC1 and the bar area B1 towards the Hansweert section.

Secondly, the budget changes of the bar B1 are interrelated with the evolution of the bar channels: the erosion of the bar area B1 between 1960 and 1990 approximately coincided with the formation and evolution of bar channel pattern 1 (1964-1986). Particularly, the rapid erosion of the bar B1 between 1960 and 1968 concurred with the formation and expansion of this channel pattern (1964-1972). Alternatively, channel pattern 2 (1988-1996) evolved while the erosion of the bar B1 ceased (1990). Thus, the net sediment transports and resulting budgets changes of the bar area B1 are strongly interrelated with the evolution of the bar channels.

Finally, the morphology of the cross channel partially followed the morphological evolution of the bar area B1 and the bar channels BC in an opposite way. The rapid erosion of the bar B1 (1960-1968) and the formation and expansion of bar channel pattern 1 (1964-1972) were almost immediately followed by a sedimentation and a reduction of the cross-sectional area (20%) of the cross channel CC (1966-1972). This relationship between bar area B1 and cross channel CC is explained by a redistribution of the discharges between the main channels (Chapter 2). Dredging in the cross

channel may explain the absence of this relationship during the entire period of the bar erosion (1960-1990).

To conclude, the bar channels BC and the bar areas B1 and B3 in the main flood channels FC1 and FC2 largely determined the net erosion of the Terneuzen section and the net sedimentation in the Hansweert section. More specifically, the results indicate that the erosion of the bar area B3 and the subsequent adaptation of the main channels EC2 and FC2 in the Hansweert section, induced the erosion of the bar area B1 and th change in the pattern of bar channels in the Terneuzen section. This relationship might be explained by a net flood-dominant flood transport in the bar area B1 that was larger during bar channel pattern 1 than during pattern 2. The erosion of the bar B1 hardly influenced the morphological evolution of the other channels or channel sections in the Terneuzen section. Only the initial erosion of the bar area B1 and the expansion of bar channel pattern 1, were followed by a temporal shoaling of the cross channel CC. This explained by an increase of the (flood) discharges over the bar area B1 at the expense of the discharge through the cross channel.

These preliminary relationships will be further elaborated in Chapter 5 using the model results. The influence of dredging and dumping on channel evolution and the migration of the bar channels and the cross channel will also be further analysed in Chapter 5. Chapter 6 gives a synthesis based on the results of Chapters 2, 3, 4 and 5.

## 4 HYDRODYNAMIC PROCESSES - FIELD OBSERVATIONS

#### 4.1 Introduction

This chapter gives an overview of the tidal and residual current patterns in the study area based on several current observations. This overview forms the basis for a preliminary discussion of two fundamental questions, underlying the research questions formulated in chapter 2:

- 1. What is the hydrodynamic function of the connecting channels in the system of main channels and shoals?
- 2. Is the distinction of different types of connecting channels reflected in the Hydrodynamics of these channels? Are the hydrodynamics in the channels marked by basic differences which justify the distinction in channel type?

These questions imply an analysis of the hydrodynamics at two spatial scales. The first question requires an analysis of the general hydrodynamics in the entire study area. The results of this analysis also serve as a frame of reference for the second question, which requires an analysis of the hydrodynamics of different connecting channels.

## General hydrodynamics in the study area

The general flow pattern in the study area may display influences of hydrodynamic processes acting in the entire estuary, referred as regional processes and processes which are specific for the system of channels and shoals in the study area, the local processes.

The most prominent regional process is the propagation and deformation of the tidal wave at sea and in the estuary (see also Chapter 2). The interaction between the oscillating tide and the estuarine morphology generally causes deformation of the tidal wave during propagation. The estuarine hypsometry, this is the vertical distribution of basin surface (Boon and Byrne, 1981), determines the character of the inundation and subsequent emergence of the intertidal shoals during a tidal cycle. As propagation of the tidal wave is depth-dependent, the hypsometry affects the range, phase differences and asymmetry of the tide. As a result the propagation of the tidal wave may be accompanied by:

- · changes in wave amplitude;
- development of asymmetries in the water levels. This means differences in the duration of fall and rise;
- development of asymmetries in the currents, meaning differences in the magnitude of (peak) ebb and flood velocities;
- phase differences between water levels and currents.

In most estuaries the deformation of the tidal wave and the development of tidal asymmetries tend to increase in landward direction and with tidal range (e.g. Friederichs and Aubrey, 1988; Lessa and Masselink, 1995).

Local processes which may influence the general flow pattern in the study area involve the presence of ebb and flood channels. Van Veen (1936;1950) recognized the existence of ebb and flood channels in estuaries by their morphologic characteristics and their net water transports. Well-established empirical relationsships between channel geometry and tidal flow parameters, most commonly cross sectional area and tidal volume (e.g. O' Brien, 1969; Van de Kreeke and Haring, 1979; De Jong and Gerritsen, 1984; Bliek and Storm, 1995; Friederichs, 1995), suggest major spatial variations of the water transports in the study area due to the presence and morphology of ebb and flood channels. The presence of ebb and flood channels may also result in spatial variations in current asymmetry and residual flow (e.g. Ridderinkhof, 1988; De Jonge, 1992; Fokkink et. al. in prep.).

Both tidal wave propagation and the presence of ebb and flood channels may cause asymmetries in the tidal flow, i.e. differences between ebb and flood flow, in the study area. Asymmetries of tidal currents control sediment transport and morphology to a significant degree (e.g. Postma, 1967; Aubrey, 1986; Speer et al. 1992; Van de Kreeke and Robaczewska, 1993). Therefore insight into the origin and magnitude of tidal asymmetries is important.

Tidal wave propagation is expected to impose boundary conditions on the general temporal variations of tidal flow in the study area. The morphology and configuration of the tidal channels are expected to determine the spatial distribution and asymmetry of the tidal flow in the study area. Therefore section 4.4 focus on the following questions:

- 1.1 To what extent are the temporal variations of tidal flow determined by the propagation of the tidal wave (section 4.4.2)?
  - do the water levels, hydraulic gradients and currents display general asymmetries which are characteristic for the tidal flow in the estuary?
  - is tidal flow marked by phase differences between water levels, falls and currents?
- 1.2 Are the spatial patterns of hydraulic gradients and water transports during ebb and flood related to the morphology and configuration of the tidal channels (4.4.3 and 4.4.4)?
- 1.3 Are current asymmetry and residual flow marked by specific temporal and spatial variations (section 4.4.5)?

The results are synthesized in section 4.4.6.

Hydrodynamics of connecting channels

From a morphological point of view, current observations were obtained in three different types of connecting channels (Figure 4.1):

- 1 an ebb bar channel:
- 2 a flood bar channel:
- 3 an ebb cross channel.

This distinction in channel type reflects differences in

- · overall channel morphology, this means an ebb channel or flood channel and
- the location of the connecting channel, i.e a cross channel or a bar channel. The ebb bar channel and ebb cross channel are marked by a bar at the seaward end of the channel. The bar in the channels is asymmetric in seaward direction. This means a steeper bed slope at the seaward side of the bar than at the landward side of the bar. The general alignment of the ebb channels is marked by channel curvature. The flood bar channel has a relatively straight channel alignment and a shallow bar at the landward end of the channel. The bar in the flood bar channel tends to be asymmetric in landward direction. The ebb bar channel and the flood bar channel are located in the bar of the main flood channel. The cross channel is located seaward of this bar and intersects the intertidal shoals between the main ebb and flood channel. Main question is whether there are basic differences in the hydrodynamics of these channels.

Tidal flow in the connecting channels may display advective flow accelerations and decelerations, flow convergence and divergence, differences between ebb and flood flow and differences in current asymmetry and residual flow, which in turn may affect sediment transports and the morphology of the channels. The curved alignment of the ebb channels indicates curvature of the tidal flow. Flow curvature affects the three dimensional current structure in the channels, resulting in secondary circulations. The vertical distribution of current vectors may display a progressive current veering as a result of the balance between pressure force and centrifugal force. As a result the near-bed current directions may differ from the depth-averaged current directions, thus affecting the direction of bed-shear stress and sediment transports in the channels. The present knowledge of the hydrodynamics and morphology in channels with a curved alignment refers primarily to river channels of constant width (e.g. Olesen, 1987, Ikeda and Parker, 1988, Mosselman, 1992, Seminara, 1995). Field observations of secondary flows in curved tidal channels is scarce (De Vriend, pers. comm.). The scarcity of such observations in larger tidal channels is probably due to the difficulty of measuring these processes with sufficient accuracy.

The hydrodynamics of connecting channels is an unexplored topic. To the authors knowledge information about the flow patterns in such channels is not available from literature. Field observations of the above described hydrodynamic processes in tidal channels in general is also scarce. Therefore the analysis of the current observations in the three channels focusses on the following two basic questions:

- 2.1 Which processes characterize the current patterns during ebb and flood?
  - Is the flow pattern marked by advective flow acceleration or deceleration?
  - Is the flow pattern marked by flow convergence or divergence?
  - Is the vertical current structure in the connecting channels marked by systematic patterns of secondary flows and current veering?
- 2.2 Are current asymmetry and the residual flow marked by specific temporal and spatial variations?

For each channel the results are discussed and synthesized at the end of sections 4.5 to 4.7.

Section 4.8 gives a prelimary discussion on the hydrodynamic function of the connecting channels and the distinction between different types of connecting channels.

#### 4.2 Measurement locations and methods

#### 4.2.1 Introduction

This section describes the experimental set-up of the field measurements. During the field-experiments a variety of techniques has been used, including routine measurements with standard, well tested instruments as well some specific less standard measurement methods. The measurement of tidal currents with impeller type current meters and floats belong to the routine field observations. The water motion close to the bed was measured with electromagnetic flow meters deployed in a frame. Detailed observations of the vertical current structure along several transects were obtained with a ship-borne Acoustic Doppler Current Profiler, which has been purchased by the Ministry of Transport and Public Works in 1995. A third specific experiment includes the measurement of water levels and falls in the study area.

The general hydrodynamics in the study area are discussed on the basis of water level measurements, discharge measurements and some long-term current observations. Figure 4.2 gives an overview of the measurement locations and discharge transects. Discharge measurements in transect 1,2,3,5 and 6 were carried out for the present study. To complete the spatial picture of tidal flow, results of discharge transect 4 are considered as well. This fourth discharge measurement was carried out in 1993. The computation of the discharges in transect 1 up to 4 is based on observations of the velocity profile with an Elmar impeller type current meter (see section 4.3). Discharges in transect 5 and 6 are based on current observations with an Acoustic Doppler Current Profiler. The discharge measurements covered 13 hours. The tidal conditions during the measurements ranged from mean tide to spring tide and are summarized in Table 4.1. At the water level stations water levels were registered for periods of two to four weeks. Due to instrument failure the data set at station 4 comprises two weeks, whereas the at other stations four weeks of reliable data were obtained.

The hydrodynamics of the three connecting channels are discussed on the basis of various current observations obtained during the period February 1994 until February 1996. The spatial and temporal resolution of the current observations in the three channels differs. Figures 4.3, 4.4 and 4.5 give overviews of the current measurements in 1994, 1995 and 1996. The numbers in these figures refer to measurement locations/numbers of each type of measurement. Relatively many current observations, in the entire channel, were obtained in the ebb bar channel. Relatively little information is available of the flow response in the cross channel. Current information in the ebb bar channel is essentially based on: a float measurement, several long-term

current meter deployments ('Flachsee') and detailed observation of the vertical current structure along three transects over 12.5 hours (ADCP). Current information in the flood bar channel consists of: several long-term current meter deployments and ADCP-observations. Measurements in the cross channel include: a discharge measurement based on Elmar point observations, float measurements and point-observations of the vertical current structure in the channel bend.

Appendix 4.1 gives details of the measurement locations and period.

### 4.2.2 Tidal water levels

Water levels were measured with new pressure sensors (Druck, ptx 630-1521). The pressure sensors were installed in gauging tubes that were mounted at injected measuring poles at a distance of 1 meter (Photo 4.1). The pressure sensors were fixed on a cap, that was screwed on the bottom of the gauging tube by a diver. Each cap contained a hole with a diameter of 0.012m to enable the entrance of water. Data sampling and storage was done with a Campbell data logger (model CR10 with a SM716 storage module). The data logger was programmed to sample in a burst mode, with a burst interval of 10 minutes, a sampling period of 1 minute and a sampling frequency of 2 Hz. The mean and standard deviation of each burst were stored in the data logger. The measured pressure was compensated for air pressure by using double ventilating wires.

The pressure sensors have a measurement range of 0 to 1 bar and an instrumental accuracy of  $\pm$  0.35%. In practice this instrumental accuracy is neglible as each stored pressure is the mean of 120 measured values. The measurements were not corrected for drift in offset, which varied between 0.001m and 0.017m for the different pressure sensors. The accuracy of the water level measurements is essentially determined by the unknown variations in water density during the measurements and the reduction of the measured pressure to Dutch Ordnance Level (NAP).

Water quality surveys carried out by the Ministry of Transport and Public works indicate that the maximum differences in water density along the study area amount 2 to 3 kg/m³, indicating a longitudinal density gradient of 0.25 kg/m³km. Under the assumption of a constant water density of 1019kg/m³, this density variation implies an uncertainty in the measured water level of 0.015m.

The height of the pressure sensors with respect to Dutch Ordnance Level was determined by the Geodetic Survey Department of Rijkswaterstaat. The height of the pressure sensors with respect to NAP was measured with a Global Positioning System using two local stations within a distance of 5 kilometer at land, in fact an accurate sort of DGPS. The measurements were carried out three times. The average accuracy of the measurements varies between  $\pm 0.015m$  and  $\pm 0.025m$ . This implies a maximum systematic inaccuracy in the computed water level differences of 0.05m. The overall accuracy of the water level measurements is summarized in Table 4.2

#### 4.2.3 Tidal currents

Current observations with floats and impeller-type current meters

Observations of langragian current patterns were obtained with float measurements over a period of 6 to 13 hours. At two or four different locations in a channel two floats with depths of 1 and 4 or 6 meters were simultaneously released from a survey ship. After each release a boat started to follow the floats, registrating the positions of the floats by GPS as often as possible, until the floats reached the end of the floating section or the channel. In this way several lagrangian current patterns were measured within a couple of hours. At the same time observations of the vertical velocity profile were obtained at one or two locations in the channel with an Elmar impeller-type current meter from an anchored ship. Generally the sampling period of the Elmar is 1 minute.

Simultaneous observations of the vertical velocity profile at several locations in a cross section of a channel, with an Elmar, formed the basis for the computation of discharges and tidal volumes. The number of Elmar observations per channel cross section ranged between 4 and 9. The number of measurement heights in each velocity profile depended on the water depth (6 to 7 points at water depth of 10 meters). Modernized 'Flachsee' impeller-type current meters registered current velocity and direction for periods of 30 days. The sampling interval of the 'Flachsee' current meters is 10 minutes, whereas as the sampling period lasts 1 minute.

Relatively little is known about the accuracy of impeller-type current meters. Arentsen (1986) gives a maximum overall error in the velocity measurement of 7.5%, whereas Adler (1993) concluded that the maximum accuracy of impeller-type current meters is 5%. The accuracy of the measured current direction is in the order of  $\pm$  4°.

A comparison of fourteen double deployed 'Flachsee' current meters revealed an average difference in speed of about 5%, whereas measured current directions differed by about 3 degrees on average. Neglecting the instrumental accuracy of the theoretical accuracy of computed discharges, based on Elmar current observations is in the order of 5% (Van Kerckhoven, 1995). In practice the accuracy of tidal volumes appears to be smaller, about 10% (De Jong and Gerritsen). The accuracy of individual discharges will be even smaller and is expected to be in the order of 15%.

Current observations with an Acoustic Doppler Current Profiler (ADCP)

In the summer of 1995 a ship-borne, broad-banded two-pulse Acoustic Doppler Current Profiler (ADCP) became operational. The ADCP, measuring eulerian velocity profiles at a high spatial resolution, was initially purchased for the execution of discharge measurements. The high resolution of the ADCP, both in vertical and horizontal direction, makes the ADCP a valuable instrument for studying the spatial structure of the velocity field in tidal environments (Van de Meene, 1994) In the

present study the ADCP was applied to study the three dimensional current structure and the tidal and spatial variation in discharges.

The measurement principle of the ADCP is that an acoustic signal emitted from a transducer, is being backscattered by small particles that are assumed to move with the current velocity. The transducers that register the backscattered signals experience a Doppler frequency shift, that is proportional to the component of the velocity parallel to the beam. The broad-band ADCP used in the present study has four narrow-beam transducers, looking downward and oriented 20° from the vertical (RDI, 1989, 1993). The use of four acoustic beams allows for the determination of three velocity components (u,v,w) plus a redundant (error) velocity estimate, all as a function of depth beneath the transducers. The ship's speed is determined by bottom tracking, i.e. by analyzing the Doppler shift of the bottom echo of an acoustic pulse.

The configuration of the ADCP has to be determined in advance, and determines the resolution in time and space and the theoretical accuracy. The system configurations during the two surveys are summarized in Table 4.3. The theoretical accuracy of an individual velocity measurement (ping) of the broad-band ADCP depends on, the frequency and length of the emitted pulse, the beam angle, and the profiling mode (RDI, 1993, 1994). For the configurations used in the present study this theoretical accuracy was ± 0.13m/s per ping. The average accuracy of the measured current velocity, the average of 5 and 20 pings, was 0.06m/s and 0.03m/s respectively. The horizontal resolution, the width of one velocity profile, was 13 meters during the first experiment and about 30 meters during the second experiment. The vertical resolution was set to 0.5m. The observations do not cover the entire water column. The data loss at the sea bed is due to side lobe effects and amounts 0.5m. At the water surface the data loss is determined by the depth of the transducers (1.74m). In practice it appeared that the first two current vectors near the surface were unreliable, yielding a near-surface data loss of 2.74m. The cause of this unreliability is unknown.

### Near-bed current current observations with a frame

A frame with six electromagnetic flow meters and an on-line connection to a ship, was used to study the near-bed currents in a channel bend. Photo 4.2 gives an overview of the instrumented frame. The frame is a three meter high tripod with relatively thin massive iron legs. The flow meters are suspended from the center of the frame, to minimize disturbance effects from the legs. Table 4.4 gives a summary of the measured variables and an overview of the sensors. Prior to deployment of the frame, a few echosoundings were carried out to determine the presence of bedforms. When megaripples and dunes were present, the frame was deployed just before the top of the bedform.

The EMF's are two-axis flow meters, with a spherical head with a diameter of 0.04m, produced by Delft Hydraulics. The flow meters have a range of  $\pm 2.50$  m/s, and an accuracy of  $\pm 1\%$ . Calibration of the EMF's was done by Delft Hydraulics in a towing

tank, just before the measurements. The zero-level of the EMF's was not stable over a period of 2 weeks. The drift in offset varied between 0 and 0.03m/s. The cause of this instability is not clear.

In the frame some supportive sensors were installed. A pressure sensor was used to register the tidal variation in water level. The orientation of the frame with respect to the magnetic north was determined with a Plessy fluxgate compas. The theoretical accuracy of the compass is  $\pm 1^{\circ}$ . Due to the proximity of the ship, the frame was deployed just next to the ship, deviations in compass direction were likely. To reduce this problem a Gyro compass of an Elmar was installed as well. The Gyro was used to determine the orientation of the frame just after deployment. Tiltmeters registered the position of the frame at the bed and movements of the frame under the influence of the tidal currents.

Unfortunately, the Gyro did not work properly during the measurements. This resulted in an unknown accuracy of the orientation of the frame and the direction of the current vectors with respect to the magnetic north. In addition one of the six EMF's did not work properly, resulting in a limited resolution of the near-bed velocity profile.

## 4.3 Data analysis

## 4.3.1 The analysis of water level measurements

The pressure field under long tidal waves is hydrostatic and can be converted to tidal water levels by the following equation:

$$h_{NAP} = \frac{p}{\rho \cdot g} + Z_{sensor} \tag{4.1}$$

where

 $h_{NAP}$  = water level with respect to Dutch Ordnance Level (=NAP) [m]

 $\rho$  = water density (1019) [kg/m<sup>3</sup>]

g = gravity acceleration (9.81)  $[m/s^2]$ 

 $Z_{\text{sensor}}$  = height of the pressure sensor with respect to NAP [m]

For the computation of water levels, according to equation 4.1, a constant water density was applied because no instantaneous information of the water density was available (see section 4.2.2). The time-series of the water levels formed the basis for the computation of water level differences and hydraulic gradients along six channel sections (see Figure 4.2 for locations):

- section 1 between station 1 and 3, the flood channel (length is 6116m).
- section 2 between station 3 and 2, the flood channel (length is 5881m).
- section 3 between station 1 and 4, the ebb channel (length is 9818m).
- section 4 between station 4 and 2, the ebb channel (length is 4810m).
- section 5 between station 3 and 4, the cross channel (length is 2847m).

• section 6 between station 1 and 2, the study area (length is about 12000m). Prior to further analysis the noise in the time-series of water level differences was reduced by applying a smoothing filter. For this purpose a quadratic equation was fitted by least squares to nine points of the time series (1.5 hours). The equation, written as a moving average, reads as (Davis, 1986),

$$\overline{D_i} = \frac{1}{231} [59D_i + 54(D_{i+1} + D_{i-1}) + 39(D_{i+2} + D_{i-2}) + 14(D_{i+3} + D_{i-3}) - 21(D_{i+4} + D_{i-4})]$$
(4.2)

As the window covers nine points (odd) of the time series, no phase shift is introduced. Filtering was done in the time domain because the interpretation focusses on the time-domain. Hydraulic gradients were computed as the ratio of the water level differences over the along-channel distance between two water level stations. The smoothed time-series enable the characterization of falls and hydraulic gradients at different locations and under different tidal conditions.

## 4.3.2 The analysis of current measurements

## Analysis of float measurements

The analysis of the float measurements focusses on the patterns of advective flow acceleration and deceleration of the near-surface currents (in %). Due to the duration of the individual float series (40-50 minutes), the measured flow patterns show velocity variations which are the result of both local and advective acelerations. To isolate the pattern of advective acelerations the following analysis procedure was applied:

- Based on simultaneously measured eulerian velocity profiles (Elmar observations), time-series of the depth average velocity were computed;
- 2 The time series of the computed depth-averaged currents were used to determine the relative changes in velocity over time, the local acceleration (%/minute);
- 3 For each float series a mean local acceleration (in % /minutes) was determined, by averaging the locale acceleration over the duration of the float measurement.
- 4 Measured lagrangian current patterns were screened for stretches of consistent acceleration, deceleration, or uniform flow along the flow path.
- Velocity variations along these stretches were converted to relative changes in current velocity by the taking the ratio of velocity values at the end of the stretch and the beginning of the selected stretch. (The computed relative changes in current velocity still include the effect of local acelerations);
- 6 The relative velocity variations along the selected stretches (5) were corrected for the effect of local acceleration as follows:
  - a) For each stretch the measurement duration in minutes was determined;
  - b) Then the measurement duration was multiplied by the computed mean local aceleration during the float series (3), resulting in a relative local aceleration (in %) for the considered stretch of the flow path.

c) The relative local acceleration was subtracted or added to the measured relative acceleration along the flow path (5), depending on the sign of the acceleration. This means that if along a specific stretch of the flow path, the measured flow accelerates with e.g. 20 %, while the velocity profiles indicate a local flow decelleration of 10%, the advective acceleration along the stretch amounts 30%.

In this way for each float measurement the patterns of advective flow acceleration were determined. The number and the accuracy of the individual flow paths is limited. Therefore mean flow paths and the spatial range of the flow paths, the envelope, were determined by making an overlay of all the float measurements. The mean flow and envelope were then drawn by eye.

Analysis of long-term current observations

The analysis of the long-term current observations focusses on three apects of the tidal flow:

- · the patterns of depth-averaged current vectors;
- the variations in current asymmetry, and;
- · the patterns of residual flow.

Prior to analysis, the noise in the data was reduced by applying the smoothing filter described in section 4.3.1, to the North and East carthesian velocity components.

The measured current velocities (not direction) were converted to depth-averaged values by assuming a logarithmic velocity profile, rough turbulent flow and an averaged roughness length based on bedform dimensions ( $z_o=0.033k_s$ ,  $k_s=0.4m$ ). The time-series of the depth-averaged velocity were used to make vector plots of flow pattern over ebb and flood and for a neap, mean and spring tide.

In literature maximum current velocities are usually used to characterize asymmetry of the flow. The asymmetry is then used as a first indicator for the direction of net bedload transport (e.g. Lessa and Masselink, 1995; Friederichs and Aubrey, 1988). Some people have suggested that this current asymmetry may also be used as a first indicator for the direction of net suspended sediment transport (Aubrey, 1986; Dronkers, 1986). In addition to the maximum velocity, a significant velocity was used in the present study. The significant velocity is defined as the mean of the 1/3 highest current velocities and represents the conditions near maximum flow over a period of about two hours. The advantage of the significant velocity is, that it gives a better weighting of the tidal variation in current velocities during the period in which most of the sediment transport occurs. Current asymmetry is then defined as the natural logarithm of the ratio of ebb velocity over flood velocity:

$$A_{u_s} = \ln \left( \frac{u_{ebb}}{u_{flood}} \right) \tag{4.3}$$

Where u indicates the considered flow parameter. A positive asymmetry ratio then indicates ebb-dominated currents, whereas a negative asymmetry indicates flood-

dominated flow. Mean significant current vectors and asymmetry ratios for neap, mean and spring tide where determined by applying a linear regression to the observation.

Residual currents are obtained by removing the tidal variation in the time series. This was done by applying the low-pass Godin-filter. The Godin-filter consists of three successive moving average procedures with periods of 25 hours (once) and 24 hours. The filter eliminates the  $M_2$  and  $S_2$  components entirely and all other components with periods shorter than 30 hours for more than 99 percent (Godin, 1972). The calculated residual currents may be topography induced currents, wind-driven currents and density-driven currents.

## The analysis of discharge measurements

The computation of discharges, based on point measurements of the vertical velocity profile, involves the computation and interpolation of the depth-averaged velocities perpendicular to the discharge transect (=channel cross section). Depth-averaged current velocities were computed by assuming a no slip-boundary condition and a water surface velocity equal to the velocity at one meter below the water surface. The depth-averaged current velocities were linear interpolated in time. Interpolation between two successive measurement locations was necessary because the distance between the measurement locations was not equidistant and too large to integrate the local discharges per metre channel width (q=u.h) as was e.g. done by De Jonge (1992). Interpolation of the depth-averaged velocities between two locations was done according to

$$u_{y} = (\frac{h_{y}}{h_{i}})^{0.5} u_{i} \tag{4.4}$$

where  $\bar{u}_y$  is the interpolated depth-averaged velocity [m/s] at position y in the cross section,  $h_i$  and  $u_i$  are the linearily interpolated water depth and current velocity [m and m/s], and  $h_y$  is the actual water depth at location y [m]. When no current infomation was available at the begin or end of the cross section a zero current velocity was assumed. Based on the interpolated depth-averaged current velocities the discharge Q [m<sup>3</sup>/s] was computed as

$$Q(t) = \int_{y=0}^{y=end} \overline{u}(y,t) \cdot h(y,t) \, dy \tag{4.5}$$

Integration of the total discharges over the ebb period and flood period results in the ebb and flood volumes, i.e. the total volume of water (V) flowing through the cross section at during ebb and flood [m<sup>3</sup>]. Residual transport velocities are calculated according to

$$V_{res} = \frac{V_{flood} - V_{ebb}}{A_{NAP} \cdot T} \tag{4.6}$$

where  $A_{NAP}$  is the cross-sectional area below NAP and T is the tidal period (44700 s). As long as processes of wind set up and set down are neglible,  $A_{NAP}$  corresponds with the tidally averaged variation in cross sectional area. Residual current velocities were computed as the mean cross-sectionally averaged velocity over a period of 12 hours and 25 minutes.

To obtain quasi-synoptic pictures of tidal flow in the study area, discharges, crosssectional velocities and tidal volumes were converted to similar tidal conditions. Usually conversion of tidal flow to specific tidal conditions is done by a assuming a linear proportional relationship between the parameter of interest and tidal range (e.g. De Jong and Gerritsen 1984; Pugh, 1987; Friederichs, 1995; Bliek and Storm, 1995). When considering tidal flow through entire estuarine cross section, this is a reasonable method of conversion. The conversion factor will be somewhat overestimated due to the phase lag between horizontal and vertical tide. In the case of tidal flow in individual ebb and flood channels this is not necessarily correct. In the present study long-term current observations, which were carried out during the discharge measurements, were used for the conversion of tidal flow. For each channel the longterm current meter data were used to compute depth-averaged currents (see above), local discharges and local ebb and flood volumes all as a function of tidal range. Then linear relationsships were fitted to the data to convert the tidal flow parameters of the discharge measurement to similar tidal conditions (mean, neap and spring tide). This way of conversion assumes that the observed tidal variation at one current meter location is representative for the entire cross-section of a channel.

Analysis of the vertical current structure measured with the ADCP

The analysis of the ADCP measurements focusses on:

- the distribution of the depth-averaged and cross-sectionally averaged flow along the transects
- the patterns of secondary flow and the veering of current vectors over the water column with respect to the depth-averaged flow direction.

Secondary flow is usually defined as the flow perpendicular to the depth-averaged flow direction, i.e. the primary flow. Figure 4.6 gives a definition sketch of the relevant coordinate systems used in the analysis.

The ADCP data were processed with the ADCP software package Transect. The software package resolves the velocity data into East and North components and combines the velocity data with the navigation. This results in data set consisting of two velocity components as a function of time, depth and distance along the transect:  $u_x, u_y = f(x, z, t)$ .  $U_x$  and  $u_y$  are the East and North components (i.e. carthesian velocity components).

Prior to further analysis and interpretation Kamminga (1995, 1996) removed the noise in the data set by applying an infinite impulse response filter. Detail of this filterering are given in appendix 4.2.

The computation of depth-averaged current velocities along the transects, requires extrapolation of the velocity profiles towards bottom and surface. One way to do this is fitting a parabolic profile through the velocity data, as was e.g. done by Simpson et.al. (1990). In the present study extrapolation of the velocity profile is based on the shape-function approach of Zittman (1992). The application of this approach is based on the work of Van de Meene (1994). The advantage of the shape-function approach, above e.g. a parabolic fit, is that it is possible to describe velocity profiles that deviate from the parabolic profile (Van de Meene, 1994). Details of the shape-function approach are summarized in appendix 4.3. It is emphasized that approach is used only as a statistical (curve-fitting) tool to compute the depth-averaged current vector in an objective way. For the computation of discharges and interpretation of depth-averaged flow patterns over the bars in the channel, the depth-averaged current vectors were decomposed in a velocity component parallel and perpendicular to the ADCP transects.

A second coordinate conversion was applied to quantify secondary flows and associated current veering. Based on the computed depth-averaged current direction, the measured and filtered velocity vectors in each profile were decomposed into a primary and secondary velocity component. In the new coordinate system the primary flood direction is positive and the ebb direction is negative (see Figure 4.6 for definition). For each current vector in the measured velocity profiles two parameters were computed:

- the magnitude of the secondary flow component relative to the depth averaged velocity, and;
- the veering of the current vector with respect to the depth-averaged current direction.

Contourplots of these two variables give insight into the presence, location and magnitude of secondary flow and circulations, due to e.g. flow curvature.

# 4.4 The general flow pattern in the study area

### 4.4.1 Introduction

This section discusses the temporal and spatial variations of the general flow pattern in the study area, based on water level measurements and current observations. Main question is which way the two main sources of tidal asymmetry, tidal wave propagation and topographically induced flow, dominate the general hydrodynamics in the study area. In section 4.1 it was postulated that tidal wave propagation controls the temporal variations of the flow pattern, whereas the pattern of ebb and flood channels determines the distributions and asymmetries of tidal flow in the study area. In this section results of the measurements are used to underpine these thesises.

The expected control of channel morphology on the distribution of tidal flow and current asymmetry is based on the well-known empirical relationships between tidal flow parameters and channel geometry (see section 4.1).

Figure 4.7a to 4.7c show the most commonly used relationship for the Westerschelde together with the observations for mean tidal conditions. In the study area tidal volumes and cross-sectional area range between 51 and 586\*10<sup>6</sup> m³ and about 7300 to 42000m² respectively. The measurements fit reasonably well to the existing relationships. Especially the relationship between the dominant tidal volume and cross-sectional area of Bliek and Storm (1995, Figure 4.7c) shows good agreement. In addition Figure 4.7d shows a less frequently used non-linear relationship between dominant tidal volume and an approximation of the stream power. The streampower is approximated by raising the depths along the transect to a power of 1.5 and integrating these values over the transect length. The advantage of the stream power is that differences in the shape of the cross-sectional profile are taken into account.

The spatial patterns of tidal flow in the study area are subject of section 4.4.3 to 4.4.5. Section 4.4.2 discusses the influence of tidal wave propagation on the temporal variations of tidal flow in the study area. A synthesis of the results is given in section 4.4.6.

## 4.4.2 Temporal variations of tidal flow

To evaluate the influence of the tidal wave propagation on the temporal variations of tidal flow in the study area, a comparison of these variations at different spatial scales, viz. the entire estuary and the study area, is required.

## Tidal flow in the estuary

The water levels at the seaward boundary of the estuary displays an asymmetry characterized by a shorter rise than fall. This asymmetry is related to the tidal wave propagating along the Dutch coast.

Figure 4.8 shows aspects of tidal wave propagation in the estuary based on the standard water level observations over the period 1980-1990 (data from Claessens and Meyvis, 1994). From Vlissingen to Antwerpen the tidal range increases with about 1.5 meter (Figure 4.8a). This amplification of the tidal range is due to landward convergence, shoaling and partial reflections. Landward of Antwerpen the tidal range decreases as a result of frictional damping. Figure 4.8b and c show the delays of high and low water with respect to Vlissingen for neap, mean and spring tide. Generally the delay of low water is larger than for high water due to the smaller water depth and larger friction under the through of the tidal wave. Figure 4.8d shows the difference in delay between high water and low water. This difference in delay increases in landward direction as a result of the decreasing water depth and the amplification of the tidal range. During spring tide the delay of low and high water is larger than during neap tide, probably as result of the larger currents velocities and smaller depth during low water. The duration of rising tide decreases in landward direction, whereas that of falling tide increases, resulting in the increase of the asymmetry in landward

direction (Figure 4.8e to g). The duration between two succesive high waters, one tidal period, is during spring tide 25 minutes shorter (12.4 hours) than during neap tide (12.7 hours, Figure 4.8h).

Discharge measurements in several cross sections along the estuary reveal phase differences between water level and discharge in the order of 2.5 to 3 hours (Figure 4.8i and j). Maximum flood discharges occur approximately 1.5 hours before the end of the flood and are preceded by a period of slowly increasing discharges. Maximum ebb discharges occur during the first four hours of the ebb period. The total maximum flood discharges over the entire estuarine cross section tend to exceed maximum ebb discharges.

To summarize tidal flow in the estuary shows a general asymmetry in the water levels characterized by a shorter rise than fall, which is imposed at the seaward boundary and amplified inside the estuary due to the interaction with the basin geometry. Water levels and currents are out of phase and display an asymmetry with respect to moments of maximum ebb and flood flow.

## Tidal flow in the study area

Figure 4.9 shows water levels at the seaward and landward boundary of the study area and the difference in water level, the fall, for a neap, a mean and a spring tide. Figure 4.10 shows the duration of falling tide and rising tide versus tidal range at Terneuzen, as occured during the water level measurements. Both figures confirm the general tidal asymmetry of the water levels and the increase of this asymmetry with tidal range. During neap tide the mean duration difference between rise and fall amounts 20 minutes, whereas during spring tide it approximates one hour (Figure 4.10). Figure 4.9 shows that the larger asymmetry during mean and spring tide is essentially due to the rapid rise in water level after mean water level is reached. The average time lag between the water level at the seaward (station 1) and the landward boundary (station 2) of the study area approximates 15-20 minutes (Figure 4.9). Given the distance of 12 kilometers between the two stations, this time lag indicates a wave celerity of about 10 m/s.

The above described phase difference between the landward and seaward margin of the study area and the neap-spring tidal variation in water levels result in general temporal variations of falls (Figure 4.9). The ebb is marked by gradually changing falls with maximum falls occurring during the first hours of the ebb period. On the other hand the flood is marked by smaller and almost constant falls between 8 and 10 hours and a short-lasting flood peak at about 11 hours after high water. The period of small and constant falls during flood coincides with the inundation of the intertidal shoals, the accompanying increase in basin storage and a slowing down of tidal rise. During this period the water level in the study area rises from about NAP-1.8m to approximately NAP-0.5m. Striking is the difference in falls between neap tide and spring tide. During neap tide the time-series of the falls has an almost symmetric appearance. During mean and spring tide the time series display a major asymmetry,

which is related to the development of a flood peak. In addition the time of maximum flood fall is retarded during spring tide. A linear regression of the moment of maximum flood falls versus tidal range indicates a retardation of about 25 minutes. Thus at spring tide maximum falls occur 25 minutes later, at a higher water level, than during neap tide. The development of the flood peak and the retardation of maximum flood are essentially due to the larger delay of high water and the faster rise of water levels during spring tide, compared to neap tide. The phase difference between zero falls and mean water level approximates 3.5-4 hours.

A comparison of the falls along the study area (Figure 4.9) with the falls along the five channel sections (Figure 4.11) reveals a similar general temporal variations in the main channels, sections 1 to 4. During flood temporal variations in falls along the cross channel, section 5, differ from the other channel section. Falls along the cross channel do not show a pronounced peak of maximum flood falls at about 11 hours after high water. In stead the end of the flood period is marked by short-lasting reversals in falls between 11 and 13 hours after high water, especially during mean tide and spring tide. The origin of these reversals is not yet clear. Neither is it known whether or not this reversal is a local phenomenom restricted to the area of the connecting channel. The large time lag between maximum flood falls in section 3 and 4 (the ebb channel), 0.5 hours compared to 10 minutes in the flood channel, indicates that the reversal in falls originates in or near the ebb channel.

Figure 4.12 shows the tidal variation of measured discharges and cross-sectional velocities in the individual channels. Zero discharges/currents occur about 2.5 hours before mean water level. Given the phase difference between falls and water levels of 3.5 to 4 hours, this means a time lag between falls and discharges of about 1-1.5 hours. As a result maximum flood discharges and currents occur after the inundation of the intertidal shoals at higher water level than maximum falls. Maximum ebb currents occur at a lower water level and smaller cross-sectional area during the emergence of the intertidal shoals. The characteristics of the temporal variations in falls are reflected in the discharges and currents. Tidal flow in the main channels and the bar channel display the pronounced flood peak and gently varying ebb discharges. Also the absence of a pronounced flood peak in the falls along the connecting channel is reflected in the time-series of the discharges. Tidal discharges and currents in the cross channel do not display a strongly developed flood peak between 11.5 and 12 hours. In stead weakly developed maximum discharges and velocities occur 0.5-1 hour earlier than in the main channels and the bar channels.

A closer look at Figure 4.12 reveals small spatial differences in ebb and flood duration and the moment of maximum flow. In the flood channel the flood flow lasts 0.5-1 hour longer than in the ebb channel. During ebb the opposite is true. In addition maximum ebb flow in the main flood channel tends to precede maximum ebb flow in the ebb channel by half an hour. Another aspect of maximum flow is the shift in time of maximum flood with increasing tidal range. To illustrate these latter aspects more clearly Figure 4.13 gives an overview of the moments of maximum velocities at

different locations in the study area, based on the discharge measurements and the long-term current observations. For the locations of the long-term current observations the mean time of maximum flood flow at neap, mean and spring tide is indicated.

Maximum ebb flow in the main flood channel occurs around 3.7 hours after high water, whereas maximum ebb flow in the ebb channel occurs around 4.2 hours after high water. Maximum ebb flow in the cross channel and the ebb bar channel coincide with maximum ebb in the main ebb channel. Maximum ebb in the flood bar channel and the main flood channel occur at 3 hours and 3.7 hours after high water respectively. Maximum flood flow in the main channels and the bar channels occurs around 11.6 hours after high water. During spring tide maximum flood generally occurs about 25 minutes later than during neap tide. This time shift of maximum currents confirms the similar time shift observed in the falls.

The long-term current observations in the cross channel (locations 5, 6 and 13), also display a pronounced spatial variation of the moment of maximum flow in the channel. Figure 4.14 shows some details of this variation. Maximum flood flow at the west side of the channel (location 5) occurs about one hour earlier than at the east side of the channel (location 6). At the east side of the channel, at location 6, a small flood peak is observed at the end of the flood period. This peak is absent at the west side of the channel (locations 5 and 13), where the short-lasting reversals in falls are observed. This phenomenom is also observed in the simultaneously measured current velocities at location 13, though with a time lag of about 1.5 hours. The time-scale of the reversal is about 3.5 hours. If this phenomenom is indicative for resonance in the channel, a length scale of about 30 kilometers is necessary to generate it. This might appear as additional generation of the overtide  $M_6$  in the time-series of the falls.

### Conclusions

The results sofar enable an evaluation of question 1.1 (section 4.1), regarding the influence of tidal wave propagation on the temporal variations of tidal flow in the study area.

Water levels in the study area display a general tidal asymmetry, charaterized by a faster rise than fall, which is related to tidal wave propgation. This asymmetry and the increase of this asymmetry with tidal range is is of particular importance, as it determines a major neap-spring tidal variation in the asymmetry of the falls and currents in the study area. Water levels and currents are generally out of phase by about 2.5 hours (70°). Zero falls precede zero water levels by about 3.5-4 hours, indicating a phase difference between falls and currents of about 1-1.5 hours.

The temporal variation of tidal flow revealed three local aspects, this means spatial variations within the study area: 1) the absence of a general flood peak in the falls, discharges and currents in the connecting channel, 2) maximum ebb currents in the flood channels, preceding maximum ebb currents in the eb channels by half an hour, and 3) a longer duration of the flood flow in the flood channel and longer duration of the ebb flow in the ebb channel.

Thus, basically it is the propagation and subsequent deformation of the tidal wave which determines the general temporal variations of tidal flow in the study area.

## 4.4.3 Current patterns during ebb

This section and the next section discuss the spatial patterns of water transports and hydraulic gradients. Main question is how tidal flood flow is distributed over the channels in the study area. The results focus on the conditions of mean and maximum tidal flow. The conditions of maximum currents are chosen because these periods are marked by the largest spatial gradients and sediment transport capacities which are important for channel morphology (chapter 2, Jeuken in prep.). Because the discharge measurements were not measured simultaneously, the velocity gradients are not considered here. An extensive treatment of the velocity gradients in channels over the entire tidal cycle is given in chapter 6 on the basis of validated flow computations.

## Falls and hydraulic gradients

Figure 4.15 depicts the spatial patterns of mean falls and hydraulic gradients and the values of these parameters during maximum ebb currents (4 hours after high water) for a neap, mean and spring tide. In the study area mean surface gradients range between  $0.8*10^{-5}$  and  $2.6*10^{-5}$  over the neap spring tidal cycle. The surface gradients during maximum flow vary between  $0.5*10^{-5}$  and  $3.2*10^{-5}$ . Largest falls and hydraulic gradients, both averaged over the ebb period and during maximum flow, occur along channel section 2, the bar area in the flood channel. Along this section mean surface gradients range between  $1.5*10^{-5}$  and  $2.55*10^{-5}$ , whereas maximum surface gradients range between 1.5 and  $3.2*10^{5}$ . Falls and surface slopes generally increase with tidal range. The magnitude of the increase differs for the five channel section, as is indicate by the slope of the relationsship fall versus tidal range.

During ebb, falls along the cross channel, section 5, are directly related to the falls along section 2, the bar in the flood channel and section 4, the ebb channel. The change of falls with tidal range shows that the increase of falls along the cross channel (section 5) is essentially determined by the increasing falls along section 2. From neap to spring tide mean and maximum falls along the cross channel increase from about 0.02m to 0.08m and from 0 to 0.12m respectively.

### Tidal volumes and discharges

Figure 4.16 and 4.17 depict the spatial patterns of ebb volumes and maximum discharges during the neap spring tidal cycle. For mean tidal conditions Figure 4.16 also shows estimates of the basin storage between successive discharge transects and the ebb volumes through the standard discharge transect 9, which is located seaward of the study area. The ebb volumes together with the estimates of the basin storage enable the arrangement of water budgets. The water budgets provide insight into the

reliability of the measurements and the lateral exchange of water between the main channels.

The water budgets during mean tidal conditions show discrepancies in the ebb and flood channel between discharge transect 2 and 4 (Figure 4.16). In the flood channel a surplus of about 44\*10<sup>6</sup>m<sup>3</sup> is observed, whereas a deficit of about 68\*10<sup>6</sup>m<sup>3</sup> exists in the ebb channel. The empirical relationship between cross-sectional area and dominant tidal volume suggests that the water deficit in the ebb channel may be due to an under-estimated ebb volume in transect 2 (about 50\*106m3 or 14% too small). The lateral water transport over the intertidal shoals towards the secondary channels of about 67\*106m3 seems realistic, given the eb volume in transect 9 of 107\*106m3 and the decrease in basin storage of about 32\*106m3. The cross sectional area over the shoals and connecting channels along the southern margin of the ebb channel is about 2.5 times larger than over the intertidal shoals along the northern margin of the ebb channel. This implies that the lateral water transport between the main ebb and flood channel of 66\*106m<sup>3</sup>, necessary to balance the budgets, is about 30-40\*106m<sup>3</sup> too large. If this overestimated lateral transport is attributed to a too large measured ebb volume in the flood channel of transect 4, the water budget in the flood channel is practically balanced.

Thus an underestimated ebb volume in the ebb channel of transect 2 of about 50\*10<sup>6</sup>m³ (14% error) and an overestimated ebb volume in the flood channel of transect 4 of about 35\*10<sup>6</sup>m³ (10% error) largely explain the discrepancies in the water budget. It is however noted that these over- and underestimations hardly exceed the incertainties in the discharge measurements.

Both the tidal volumes and the discharges during maximum flow display spatial variations in water transport along and between the main ebb and flood channel and a redistribution of the discharges by the connecting channels (Figure 4.16 and 4.17).

In the main ebb and flood channels, the ebb volume and discharge decrease with decreasing cross-sectional area towards the bars. For instance, during mean tide the ebb volume in the flood channel decreases in landward direction from 494 to  $260*10^6 \text{m}^3$ , indicating a decrease of about  $234*10^6 \text{m}^3$  (50%) in landward direction. About fifty percent of this decrease is due to a decrease in basin storage (117\*10<sup>6</sup>m³), whereas about 40% of the increase is related to the redistribution of the ebb volume by the cross channel. Under these conditions of mean tide, discharges in the flood channel during maximum flow decrease from 38228 to 16578 m³/s (55%). In the ebb channel the ebb volume decreases from 345 to 290\*10<sup>6</sup>m³ (20%) in seaward direction, despite the seaward increase in basin storage of  $105*10^6 \text{m}^3$ . This decrease in ebb volume is explained by the lateral water transport to the neighbouring channels. Maximum discharges reduces in seaward direction from 24252 to 20396m³/s (15-20%).

In both Figure 4.16 and 4.17 the approximate relative contribution of each channel to the total ebb volume and discharge through the transect is indicated between brackets (in %). The ebb volume is not equally distributed over the ebb channel and the flood channel. At the seaward margin of the study area (transect 1, Figure 4.4.11)

the distribution of ebb volumes is most unequal. The flood channel contributes about 65% of the total ebb volume, whereas the contribution of the ebb channel amounts only 32-35%. In the middle of the study area (transect 4) the ebb volumes are equally distributed over the ebb and flood channel. At the landward margin of the study area (transect 2) largest ebb volumes occur in the ebb channel, where the water transport through the ebb channel amounts 60% of the total ebb volume. The discharge during maximum ebb flow display a similar distribution of the ebb flow over the main channels.

The cross channel redistributes about 15% of the total ebb volume and the discharge during maximum ebb flow in transect 2. The redistribution of the ebb volume approximates the changes in the relative distribution of the water transports between the main channels: Landward of the cross channel the difference in relative ebb volume and discharge between ebb channel and flood channel amounts 15 to 20%. Just seaward of the cross channel (transect 4) this difference is 0 to 5%. The ebb bar channel and the flood bar channel also conduct about 12% of the total water transports during ebb. Together the three connecting channel account for almost 40% of the total ebb discharge in the study area, with largest ebb discharges occuring in the cross channel.

# Conclusions

To answer question 1.2 (section 4.1), regarding spatial variations in flow pattern. Spatial patterns of tidal flow in the study area are strongly related to the morphology and configuration of ebb and flood channels, as already suggested by the semi-empirical relationships between channel geometry and tidal flow (section 4.4.1).

The most prominent morphological feature is the bar in the main flood channel, as this bar is marked by largest falls and surface gradients which essentially determine the tidal variation in falls along the cross channel. The water transports display a pronounced spatial variation which relates well with the along channel changes in cross-sectional area and streampower. The cross channel redistributes about 15% of the total ebb discharge/volume. This indicates that part of the along-channel and 'between-channel' variation in water transports is related to the redistribution of water by the cross channel. The bar channels conduct a similar relative amount of the total water transport during ebb. The water budgets indicate that patterns of residual water transports (section 4.4.5) should be interpreted in a qualitative way.

## 4.4.4 Current patterns during flood

# Falls and hydraulic gradients

Figure 4.18 depicts the spatial patterns of falls and hydraulic gradients averaged over the flood and during maximum flood currents (11.6 hours), for a mean tide, a neap tide and a spring tide. The pattern of mean falls and surface slopes strongly resembles the mean ebb patterns (cf. Figure 4.15). Also during flood, largest mean surface

gradients, ranging between 1.5\*10<sup>-5</sup> and 2.4\*10<sup>-5</sup>, occur along the bar of the flood channel, section 2. From neap to spring tide mean falls and surface gradients generally increase with a factor 1.7-2. Falls and surface gradients during maximum flow display a general strong increase with increasing tidal range. This increase is related to the development of pronounced flood peaks (section 4.4.2). During maximum flood currents largest falls and surface gradients are observed in the ebb channel, along section 4. In this part of the ebb channel surface gradients range between 1.04\*10<sup>-5</sup> and 5.2\*10<sup>-5</sup> over the neap spring tidal cycle. These large surface gradients are related to the (locally?) small falls and short-lasting reversals in falls along the cross channel (section 4.4.2, Figure 4.11 & 4.14).

## Tidal volumes and discharges

Figures 4.19 and 4.20 show the pattern of flood volumes and discharges during maximum currents, for neap, mean and spring tide. In Figure 4.19 the estimates of the basin storage and the water deficits and surpluses, necessary to balance the mean tidal water budgets, are indicated as well.

Balancing the water budgets reveals discrepancies in especially the ebb channel between transect 4 and 2. In this part of the ebb channel a surplus of about 38\*10<sup>6</sup>m<sup>3</sup> exists. The flood volume of 111\*10<sup>6</sup>m<sup>3</sup> in transect 9 and the decrease in basin storage of about 30\*10<sup>6</sup>m<sup>3</sup>, indicate that the required lateral inflow of 126\*10<sup>6</sup>m<sup>3</sup> in the ebb channel between transect 1 and 4 is about 40 to 50\*10<sup>6</sup>m<sup>3</sup> too large. This large lateral inflow of 126\*10<sup>6</sup>m<sup>3</sup> and the consistent water budget between transect 9 and 1 suggest that the flood volume in the ebb channel of transect 4 is about 40\*10<sup>6</sup>m<sup>3</sup> (14%) too large. An overestimated flood volume in the ebb channel of transect 4 would also explain the water surplus in the ebb channel between transect 2 and 4.

Thus an overestimated flood volume in the ebb channel of transect 4 largely explains the discrepancies in the water budget. The discrepancies do however hardly exceed the accuracy of the discharge measurements.

Flow patterns during flood also display pronounced spatial variations in water transport along and between the channels (Figures 4.19 and 4.20).

Water transports in the main channels generally decrease with decreasing cross-sectional area towards the bars. As a result, tidal volumes in the flood channel strongly decrease in landward direction, whereas tidal volumes in the ebb channel tend to increase in landward direction. For instance, during mean tidal conditions the flood volume in the flood channel decreases towards the bar, with 340\*10<sup>6</sup>m³, from 585 to 344\*10<sup>6</sup>m³. About 117 million cubes (50%) of this decrease is due to the landward decrease in basin storage. The redistribution of the flood discharge by the cross channel accounts for about 20% of this decrease, whereas the remaining 30% decrease in flood volume must be due to lateral water transport over the intertidal shoals. In the ebb channel the mean flood volume increases in landward direction from 150 to about 253\*10<sup>6</sup>m³ (70%), despite the landward decrease in basin storage of about 105\*10<sup>6</sup>m³. This landward increase is partly due to the exchange of water from the main flood

channel to the ebb channel (about 130\*10<sup>6</sup>m³, including the cross channel). The remaining part of the flood volume, about 70\*10<sup>6</sup>m³ (instead of 126\*10<sup>6</sup>m³) is explained by the water transport over the intertidal shoals and through the connecting channels bordering the southern part of the main ebb channel. During mean tidal conditions the discharges during maximum flow reveal a similar decrease of discharges with decreasing cross-sectional area towards the bar (Figure 4.20).

Figures 4.19 and 4.20 also depict the relative distribution of volumes and discharges between the two main channels in each transect. The pattern of volumes and discharges display an unequal relative distribution over the main ebb and flood channel, with largest water transports occuring in the flood channel. The unequal distribution is most pronounced at the seaward boundary of the study area, where about 80% of the water transport takes place through the flood channel. This unequal distribution gradually decreases in landward direction. At the landward boundary of the study area the flood channel accounts for about 58% of the water transport.

The cross channel redistributes about 8 percent of the total water transport between the main ebb channel and flood channel. The water transports in the bar channels, especially the flood bar channel (transect 6), are larger than in the cross channel. During mean tide the water transport through the flood bar channel amounts almost 20% of the total water transport.

### Conclusions

The foregoing results enable an evaluation of question 1.2 and a comparison of the flow patterns during ebb and flood. Similar to the flow pattern during ebb, the flow pattern during flood is marked by major spatial variations. In some respects the distribution of tidal flow during flood differs from the flow pattern during ebb.

Also during flood largest mean falls and surface gradients occur over the bar in the flood channel. Largest surface gradients during maximum flow are however not observed along this bar, but along channel section 4, the entrance of the ebb channel. These large surface gradients are related to the reversals and small falls along the cross channel and are probably a local phenomen. The water transports in the channels during flood also decrease with decreasing cross-sectional area towards the bars, the relative distribution of water differs from ebb. During flood water transports in the flood channel generally exceed water transports in the ebb channel by a factor 1.4 to 4. During ebb largest water transports are not generally related to one channel, but depends on the location along the study area. Compared to the ebb, relatively much water is transported over the intertidal shoals during flood and relatively small water transports are observed in the cross channel (8% during flood against 14% during ebb). The smaller water transports in the cross channel during flood are accompanied by larger water transports in the two bar channels, when compared to the flow pattern during ebb (29% of the total water transport in stead of 25%).

## 4.4.5 Tidal current asymmetry and residual flow

In section 4.4.2 it was shown that the water levels in the study area display a asymmetry characterized by a faster rise than fall, which largerly determines the general determines the general temporal variations of tidal flow. The previous section showed that the distribution of tidal flow over the channels in the study area is strongly related to channel morphology. Then the question rises to what extent differences in the absolute magnitude between ebb and flood flow at a specific location are related to channel morphology. Are current asymmetry and residual flow marked by specific spatial and temporal variations (Question 1.3, section 4.1)?

### Current asymmetry

The tidal volumes, the maximum discharges and the maximum cross-sectional velocities in each discharge transect were used to compute current assymetry. The maximum values do not refer to one point of time which is exactly the same for all locations. To compute current asymmetry the actual maximum values as occurred during the measurement were used. The conversion of these values to neap mean and spring tide is based on a linear regression of maximum currents, measured with the long-term current meters, versus tidal range (section 4.3). Asymmetry between ebb and flood flow is defined as the natural logarithm of the ratio ebb flow over flood flow. Thus a positive asymmetry ratio indicates stronger ebb flow than flood flow, this mean ebb-dominance. Negative ratio's indicate flood-dominance of the flow.

Figures 4.21a to c show the patterns of current asymmetry in the tidal volumes, discharges and current velocities. Current asymmetry displays a pronounced spatial variation which can be related to channel morphology, i.e. the morphological distinction between ebb and flood channels.

General ebb-dominance of the tidal flow is observed in the main ebb channel and the (ebb) cross channel. In these channels the ebb volumes are 1.2 to 2 times larger than the flood volumes. This means that the residual water transports (see below) amply exceed the uncertainty in the measurements. Maximum ebb discharges in these channels are 1.03 to 1.45 times larger than the maximum flood discharges, despite the generally smaller cross-sectional area during ebb. This indicates stronger ebb velocities as is confirmed by Figure 4.21c. The asymmetry ratio's of 0.08 to 0.49 indicate that the ebb currents are about 10 to 60 % stronger than the maximum flood currents. In the bar channel with an ebb morphology (transect 5) water transport are slightly ebb-dominated. Maximum discharges and current velocities are flood-dominated.

Flood-dominance of the flow is observed in the main flood channel and in the bar channel with a flood morphology (transect 6). On average flood volumes are 20 to 40% larger than the ebb volumes. Maximum flood discharges are 3 to almost 70% larger than maximum ebb discharge, whereas maximum flood velocities exceed the ebb velocities up to 30%. Stricking is the tendency towards ebb-dominance of maximum flow during neap tide.

In the main flood channel, the cross channel (transect 3), the flood bar channel (transect 6) and the bar area of the main ebb channel (transect 1) current asymmetry

increases with tidal range. In the more landward part of the ebb channel (transect 2, 4) and the ebb bar channel flow asymmetry decreases with tidal range.

Figure 4.21c shows an aspect of current asymmetry between the main ebb and flood channel. Maximum ebb currents in the ebb channel exceed maximum ebb currents in the flood channel by 9-30%. On the other hand maximum flood velocities in the flood channel exceed maximum flood currents in the ebb channel by 12-52%.

## Residual flow

Residual flow is defined on the basis of cross-sectional velocity, water transports, and transport velocity. Integration of the cross-sectional velocity over the tidal period gives the residual velocity. The residual velocity is computed for the day and conditions of the measurements. Residual water transports are defined as the flood volume minus the ebb volume. The ratio of this residual watertransport and the mean cross-sectional area multiplied with the tidal period yields the residual transport velocity. Residual water transports and transport velocities are given for neap, mean and spring tide based on, the converted tidal volumes, the cross sectional area with respect to the ordnance level, and the duration of the tidal period between two successive high waters.

Figure 4.22 shows residual cross-sectional velocities as occurred during the discharge measurements. The residual velocities values only indicate the order of magnitude and direction of residual currents, as the values are based on current observations over a period of only 12.5 hours. In the main flood channel and the flood bar channel (transect 6) residual flood velocities, ranging between 0.02 and 0.06 m/s are observed. In the ebb channel and the cross channel (transect 3) ebb-dominated residual current velocities in the order of 0.06 to 0.20 m/s exist. Thus the direction of residual currents is related to the presence of ebb and flood channels.

Figure 4.23 shows the patterns of residual water transports and transport velocities in the study area. The pattern of residual flow displays residual water transports in seaward direction in the main ebb channel and the cross channel, i.e. an ebb-dominated residual water transport. In the main flood channel and in the flood bar channel a landward residual water transport is observed. The pattern of residual water transport in the main ebb and flood channel indicate the presence of a large scale circulation of net water transports which is related to the overall morphology of the main channels. The connecting channels, especially the cross channel, induce small-scale circulations of water transport within this large scale circulation. The magnitude of the transport velocities in these large and small-scale circulations varies between 0m/s and 0.21m/s and is largest near the bars in the main ebb and flood channel. Residual water transports in the individual channels tend to increase with tidal range indicating that the intensity of the circulation is not constant. During spring tide an enhanced circulation exists. The large scale circulation is not closed. The seaward water transports in the ebb channel are not completely balanced by the landward water

transports in the flood channel, especially during neap tide and in transect 1. Strictly speaking a small net seaward directed water transport should exist due to the generally small river discharge of about  $5*10^6$  m³ per tide on average. The imbalances may have several causes e.g.: 1) uncertainty in the measurement of tidal volumes (about 10%), 2) unknown errors in the conversion of tidal volumes, 3) inequal effects of meteorological forcings (set-up or set-down) during the four discharge measurements, which are not accounted for. This means that patterns of residual flow should be interpreted in a qualitative way.

Thus, in the study large and small-scale circulations of net water transports exit which are related to the presence of main ebb and flood channels and connecting channels. The intensity of the circulation is likely to increase with tidal range.

#### Conclusion

Current asymmetry and the direction of residual flow are related to the morphology of the channels (i.e. ebb channel or flood channel). This spatial variation indicates that the ebb and flood channels tend to form cells in which tidal flow circulates. The temporal variations of current asymmetry and residual flow suggest an increase of the intensity of this circulation with tidal range.

#### 4.4.6 Discussion and conclusion

Tidal flow in the study area is influenced by two different scources of tidal asymmetry:

- 1) the propagation and subsequent deformation of the tidal wave in the estuary;
- 2) the presence ebb and flood-dominated channels;

This section summarizes the influence of both mechanisms and evaluates the relative importance for the general flow pattern in a qualitative way.

The propagation and deformation of tidal wave in the estuary causes a general tidal asymmetry in the water levels characterized by a faster rise than fall. One part of this asymmetry is imposed at the seaward boundary, the other part is generated in the estuary due to the interaction of the tidal wave with the basin hypsometry. This results in a flood marked by a short-lasting event (0.5 hours) of maximum falls and currents at about one hour before the end of the flood period. Maximum flood is preceded by a period of small and gradually changing falls and currents. This latter feature can be related to a slowing down of tidal rise during the inundation of the intertidal shoals and the sudden increase in basin storage. The ebb is marked by a relatively long period (2 hours) of strong and almost constant falls and velocities, with maximum ebb currents occurring about halfway the ebb period.

As tidal range increases the asymmetry of the water levels increases and the delay of high and low water with respect to seaward boundary increases. This increase of the tidal asymmetry is of particular importance as it determines a major neap-spring tidal variation of the tidal flow in the study area. As tidal range increases tidal flow

becomes progressively asymmetric. The increased asymmetry of the tidal flow finds expression in:

- 1) the development of a pronounced flood peak in the falls and currents, and;
- 2) a retardation of maximum flood flow with respect to high water.

The most important change in water levels which induces these features, is the faster rise of the water levels above mean water level as tidal range increases. This phenomenom is considered a boundary condition for the tidal flow in the study area, as the faster rise is observed in both the seaward boundary conditions and the more landward water level stations. It is however not known to what extent the tidal propagation in the estuary influences the boundary conditions at sea.

Friction and probably partial reflection, induces a phase differences between water levels and currents of about 2.5 hours. Falls and currents are out of phase by 1 to 1.5 hours. Due to these phase differences maximum flood currents occur after the inundation of the shoals at a higher water level and larger cross sectional area than maximum ebb flow. Maximum ebb currents occur at about mean water level, whereas maximum flood currents occur at about 2 meters above mean water level.

The smaller cross-sectional area during maximum ebb favours ebb-dominance of the currents (e.g. Friederichs and Aubrey, 1988). The faster rise and smaller friction during flood favour a general flood dominance of the currents (e.g, Lamb, 1932; Dronkers, 1986). In the study area the net balance of these processes related to tidal wave propagation, is however overruled by the presence of ebb and flood-dominated channels. Although maximum falls and the total maximum discharges during flood are larger than during ebb, the patterns of net water transports, current asymmetries and residual currents display ebb-dominated flow in the ebb channels and flood-dominated flow in the flood channels. This pattern indicates that the main ebb and flood channel tend to form a cell in which tidal flow circulates. However, the intensity of the circulation is not constant over the neap spring tidal cycle and is largely determined by the neap-spring tidal changes in the asymmetry of the water levels imposed by tidal wave propgation. The neap-spring tidal variations of current asymmetry and residual flow suggest an enhancement of the circulation with tidal range. The presence of connecting channels in the study area causes small-scale circulations of flow within the large-scale circulation induced by the main ebb and flood channel. The connecting channels account for 8 to 20% of the total cross-sectional water transports in the study area. Especially the large cross channel is important as it redistributes the tidal discharge between the main channels, thus affecting the along-channel and betweenchannel variation in water transports and currents in the main ebb and flood channel. The influence of the cross channel on the general flow pattern is largest during ebb. This is confirmed by the ebb-dominated flow and the larger falls in cross channel during ebb compared to flood. The larger falls during ebb are in turn essentially determined by the large falls and surface gradients along the bar in the main flood channel.

To conclude, tidal wave propagation largely determines the general temporal variations of tidal flow and the temporal variation in the magnitude of current asymmetry and

residual currents over the neap-spring tidal cycle. The direction of current asymmetry and residual flow is controlled by ebb and flood-dominated channels. These ebb and flood channels tend to form cells in which tidal flow circulates. The implications of these conclusions for the sediment transport patterns in the study area are subject of chapter 6 (computations).

# 4.5 Hydrodynamics of the cross channel

### 4.5.1 Introduction

The observations of the general flow pattern in the study area (section 4.4), showed that the cross channel transports 8 and 14 percent of the total water transports during flood and ebb respectively. The cross-sectional averaged currents are in the order of 0.5m/s during flood and 1m/s during ebb, indicating strongly ebb-dominated flow. Another remarkable aspect concerns the moment of maximum flow in the cross channel. Contrary to the tidal flow in the main channels and the bar channels, maximum flood in the cross channel is not marked by the characteristic peak at the end of the flood period. In stead weakly developed maximum flood currents were observed which occur about 0.5 to 1 hours earlier than in the other channels of the study area. A related aspect is the short-lasting reversal in hydraulic gradients along the channel. The current patterns during flood, described in section 4.5.3 give additional information of what happens in the channel.

The flow patterns characterizing the ebb and flood flow in the channel are subject of this section. Question is to what extent the flow pattern is marked by processes like, advective flow accelerations and decelerations, convergence and divergence of the flow and current veering in the water column due to flow curvature. In addition variations in current asymmetry and residual flow are briefly described. It is noted that the flow observations are less complete than the current observations in the two bar channels (for locations see Figure 4.3). As a result it is not possible to give firm answers to the questions formulated in section 5.1.

## 4.5.2 Current patterns during ebb

#### Lagrangian tidal current patterns

This section describes lagrangian current patterns in the cross channel, based on float measurements in 1994. In the cross channel current patterns were measured twice: during extreme spring tidal conditions and during mean tidal conditions.

The results are focused on the patterns of advective acceleration and deceleration of the near-surface currents, i.e. the currents at one meter below the water surface. Figure 4.5.24 shows the mean flow paths and their envelopes during mean tidal conditions together with the locations and relative magnitude of advective accelerations and decelerations (see section 4.3 for methods and defionitions). Negative values indicate advective deceleration of the flow along the flow path, whereas positive changes indicate acceleration. Time-series of depth-averaged eulerian current velocities, measured at locations A and B are shown in the inset. The flow paths during spring tide fall within the envelopes of the flow paths during mean tide and display qualitatively similar patterns. Due to instrument malfunctioning of the Elmar it was not possible to determine the magnitude of advective flow accelerations and decellerations (du/dx) during spring tide.

The lagrangian current patterns in the cross channel during ebb show patterns of minor flow acceleration or deceleration (Figure 4.5.24):

- In the curved entrance of the ebb channel a tendency of limited flow acceleration (13%) along flow path 1 is observed;
- Along flow path 3 the flow decelerates just seaward of the bar by about 17%. This flow deceleration is not observed along flow path 4;
- At the bar flow acceleration of about 17% is observed during only two float series along flow path 3;
- The envelope of the mean flow paths in the curved channel entrance indicate a large spatial range.
- Current velocities along flow path 3 are 10 to 50 percent stronger than the
  velocities along flow path 4. This indicates that the centre of maximum ebb flow is
  located along the west side of the channel.

### Eulerian tidal current pattern

Figure 4.25 shows depth-averaged current vectors based on the five long-term current meter deployments in April 1994 (5 and 6) and November 1994 (locations 11, 12, 13), during mean tidal conditions. In the curved channel entrance (11, 12, 13) velocity gradients are generally small and do not exceed the measurement uncertainty, confirming the float measurements. The current velocities at location 5 and 6 are about 25-30% smaller than at locations 11, 12 and 13 in the curved channel entrance. This suggests deceleration of the ebb. It is however noted that the current velocities were not measured simultaneously. The current velocities at 2 hours after high water are remarkably small, when compared to the currents in the bar channels at the same time. Maximum ebb velocities range from about 0.8 to 1.1 m/s during the neap-spring tidal cycle.

#### Observations of the vertical current structure

This section describes observations of the vertical current structure in the curved entrance of the channel. The measurements consist of long-term current observations

of near-bed and near-surface currents at two locations (11 and 13 in Fig. 4.3), and near-bed current observations at five locations in the outer bend of the channel (1 to 5, Fig.4.3) over a period of 12.5 hours. Question is whether the vertical distribution of current vectors is marked by current veering.

Table 4.5 summarizes current veering in the water column based on the long-term mean significant current vectors at current meter locations 11 and 13. At location 12 only near-bed current observations were obtained, due to instrument malfunctioning. For the same reason no information of depth-averaged current vectors was obtained at location 12. The long-term mean ebb currents display a clock-wise veering of the near-bed currents with respect to the near-surface currents. Near the bed currents are directed more towards the inner bend and channel axis than near the surface. The depth-averaged and near-bed current vectors at location 11 are clockwise inclined with respect to the near-surface currents by about 10°. At this location the outer bank of the channel is relatively deep (5 meters). As a result near-surface currents are influenced more by the ebb current in the main ebb channel than the near-bed and depth-averaged currents. At location 13 the near-bed currents are clockwise (inward) inclined to the near-surface currents by about 16° The near-bed currents at location 13 show an inclination with respect to the local depth contours of about 14°. At location 12 near-bed currents are aligned parallel to the depth contours.

Figure 4.26 shows the difference between near-bed and near-surface current directions, the current veering, versus near-bed current velocity and versus the velocity difference between near-bed and near-surface current vectors. At location 11 no correlation exists between current veering and current velocity and between current veering and velocity difference. Although marked by considerable scatter, current veering at location 3 tends to increase with decreasing near-bed current velocities. Current veering is not correlated with velocity difference. Averaging the current vectors measured during neap tide and during spring tide reveals a small variation in near-bed current direction with tidal range. During neap tide near-bed currents are slightly stronger inclined to the local depth contour (by 15°) than during spring tide (12°). This difference is responsible for the weak correlation between near-bed current velocity and vertical current veering.

Table 4.6 gives an overview of the conditions and observations during the near-bed current measurements. Indicated are the near-bed and depth-averaged velocity vectors during accelerating, maximum and decelerating ebb. Unfortunately the orientation of the near-bed current directions with respect to the local channel axis is highly uncertain. This uncertainty is due to:

- an unknown and variable influence of the presence of the ship on the magnetic fluxgate compass;
- uncertainty in the orientation of the local channel axis ( $\pm$  4°).

In addition to these uncertainties it is not known to what extent the near-bed currents are influenced by the presence of the ship, as the frame had to be deployed just next to the ship. Table 4.6 reveals the following observations of the vertical current structure:

- during maximum ebb depth-averaged currents flow approximately paralel to the local depth countours at all locations except at location 5, where the depthaveraged currents are inclined to the depth contours by 17°.
- velocity differences between 0.3 and 2 meters above the bed are generally small and do not exceed 0.2m/s (maximum ebb, location 1, Table 4.6). Both vertical velocity profiles obtained with an Elmar and the long-term observations of nearbed and near-surface currents reveal small differences in current velocity over the water column;
- the near-bed currents do not display a systematic veering of the current vectors over the water depth;
- current velocities at 2 meters above the bed are 0.05-0.13m/s smaller than the currents at 1 and 1.5 meters above the bed. Current directions at 1.5 meters above the bed tend to differ by -15° to +62° from current directions at 1 and 2 meters above the bed. These differences are observed during maximum ebb at location 3 and 4, during accelerating ebb at locations 2, 3,4 and 5, and during decelerating ebb at location 2.

To summarize, only at current meter location 13 the vertical current structure is marked by a systematic veering of the current vectors.

#### Conclusion

Based on the relatively few current observations in the channel the flow pattern during ebb may be charcterized as follows (question 1, section 4.5.1): As the ebb flow enters the channel bend, current velocities slightly increase (13%). The depth-averaged currents display flow curvature and an alignment approximately parallel to the depth contours and channel allignment. Just downstream of channel bend, near the outer bank of the channel, the vertical current structure displays a veering of the current vectors which might be due to flow curvature. At this location of long-term current observations (13 in Fig. 4.25) near-surface current directions differ from the near-bed current directions by 16°. The near-bed and near-surface current velocities differ by about 0.25m/s. The float measurements indicate a tendency towards small flow acceleration (17%) at the upstream side of the bar and flow deceleration at the downstream side of the bar (17%).

### 4.5.3 Current patterns during flood

#### Lagrangian tidal current patterns

Figure 4.27 shows mean flow paths and their envelopes in the cross channel obtained during mean tidal conditions in November 1994. Abundant flow paths were only obtained in the bar area of the channel (locations 1 and 2 Figure 4.27). This fact is

related to the generally small current velocities in the cross channel during flood, as is illustrated by the time series of the eulerian currents at location A and B (inset in Fig. 4.27). Flow paths 1 and 2 display the following characteristics:

- Near-surface currents reveal a general pattern of large advective flow deceleration in the order of 40% over the bar of the channel;
- The flow paths gradually move towards the east side of the channel with increasing current velocity, resulting in a large spatial variation of flow paths as indicated by the envelopes (I).
- During maximum flow in the main channels the floats pass with maximum velocity along the entrance of cross channel and end in the shoal area (II in Figure 4.27). During this period current velocities along the flow path II are in the order of 1.2 to 1.3 m/s (not shown). At the same time current velocity at Elmar locations A amounts only 0.18m/s. This indicates seperation of the flood flow at the entrance of the channel. This phenomenom coincides with resonance-like peak observed in the falls along the cross channel (section 4.4.2, Figure 4.5 and 4.8);
- The mean velocity along the flow path at location 2 exceed the velocity along flow path 1 by about 10% (not shown).
- The flow paths at 4m and 1 meter below the water surface reveal a consistent difference in location (not shown). The larger near-surface currents are shifted towards the outer bend of the channel (east side) compared to the currents at 4 meter below the water surface. This difference indicates a tendency towards decreasing streamline curvature with increasing velocity.

## Eulerian tidal current pattern

Figure 4.28 shows current patterns in cross channel during flood, based on the current observations in April 1994 (locations 5 and 6) and November 1994. During flood current velocities in the channel are small, about 0.5-0.7 m/s during maximum flow. Flood currents at the east side of the channel (location 6) are stronger than at the west side of the channel, indicating that the centre of maximum flow is located at the east side of the channel. This confirms the float measurements. Current velocities at location 6 are 30 to 230% stronger than at the other measurement locations. In the channel bend, between location 11 and 13, the current vectors display advective acceleration of the weak flood flow in the order of 10 to 60% (0.15-0.23m/s). This increase is probably related to an influence of the stronger flood flow in the main ebb channel. Striking are the large velocity gradients between the east and west side of the channel during decelerating flood (12.5 hours).

#### Observations of the vertical current structure

Observations of the vertical current structure are restricted to outer channel bend where the current velocities during flood are very weak. Due to these generally small current velocities it is difficult to obtain reliable estimates of a posible veering of the current vectors over the water column. To illustrate this table 4.7 summarizes near-bed and near-surface current vectors at the three locations of long-term current

observations. Current velocities are small and hardly exceed 0.6m/s (location 11). In this part of the channel (location 12 and 13) depth-averaged significant flood currents are in the order of 0.3-0.4m/s. The observed current vectors are aligned parallel to the depth contours. Differences in current direction over the water depth do not exceed the uncertainty in the measurements ( $\pm$  4°).

### Conclusion

In the cross channel the current pattern during flood is dominated by strong advective flow deceleration (40-50%) over the bar of the channel and generally small current velocities in the central part of the channel. The centre of maximum flood currents gradually moves from the middle of the channel towards the east side of the channel as current velocities increase. At the moment of maximum flow in the main channels the flood flow tends to pass along the cross channel, causing the small currents in the channel. Observations of the vertical current structure did not reveal major and reliable veering of the current vectors over the water column.

# 4.5.4 Tidal current asymmetry and residual flow.

Sofar the tidal current patterns have been discussed without considering the differences in velocity magnitude between ebb and flood, i.e the current asymmetry and the residual flow. Both parameters give a first indication of net sediment transport direction in the channel. Question is whether both parameters display the specific spatial and temporal variations (for definition see section 4.3.3, long-term observations).

Figure 4.29 shows significant current vectors and asymmetry ratios during mean. Figure 4.29c shows current asymmetries for neap and spring tide. Positive asymmetry ratios indicate ebb-dominated flow, whereas negative ratios indicate flood-dominated flow. At the measurement locations ebb currents are about 16 to 120 % stronger than the ebb currents. Current asymmetry is smallest at east side of the channel where the centre of maximum flood flow is observed. The asymmetry ratios at neap and spring tide indicate an increase in asymmetry with tidal range. The magnitude of this increase is smallest at the east side of the channel (location 6) and largest at the west side of the channel (location 5 and 13).

The pattern of depth-averaged residual flow shows largest ebb-dominated residual currents in the order of 0.15m/s along the west side of the channel, where the centre of maximum ebb currents is located (Fig. 4.30). A smaller, ebb-dominated residual current directed towards the channel axis is observed along the east side of the channel (location 6).

To conclude current asymmetry and residual flow show ebb-dominated flow at the measurement locations. This confirms the discharge measurements (section 4.4).

#### 4.5.5 Discussion and conclusion

So far the current patterns during ebb and flood have been considered seperately. Question is whether these patterns show fundamental differences. Answering this question for the cross channel is not easy, as only a few current observation are available which cover primarily the channel bend.

One fundamental difference between ebb and flood involves the proces of advective flow acceleration and deceleration over the bar of the channel. During flood nearsurface current strongly decelerate over the bar in the channel (40%), whereas the ebb current displays a minor flow acceleration (17%). Another difference involves the centre of maximum flow. During flood the centre of maximum flow is located at the east side of the channel, whereas during ebb largest current velocities tend to occur at the west side of the channel. During maximum flood in the main channels, the flood tends to pass along the cross channel, resulting in generally small flood currents. During maximum ebb the flow does not pass along the entrance of the channels, but enters the channel where the current velocities reach maximum values. Reliable observations of a veering of current vectors over the water column in the cross channel are scarce. Only at one location near the bend in the channel alignment (13 in Figure 4.3) a systematic veering (16°) of the near-bed currents with respect to the near-surface currents was observed during ebb. During flood such a veering was not observed. The absence of this veering during flood makes sense, as the flood near this location does not display curvature of the tidal flow, wheras the ebb does. This also indicates that the observed current veering during ebb might be due to the flow curvature and the formation of a secondary circulation. Unfortunately it is not possible to give any firm conclusions on the presence of secondary circulations as the result is based on only two current meters in the water column at one location.

The observed current patterns and current asymmetry indicate that it is essentially ebb flow which controls channel morphology. The float measurements and the simultaneous elmar observations at the bar and in the entrance of the channel suggest however that the ebb-dominance is likely to decrease towards the bar and the northeast side of the channel where the flood flow enters the channel. To verify this hypothesis additional flow computations are necessary. These computations also give more insight into advective flow processes over the bar and the origin of the flow seperation during maximum flood flow.

# 4.6 Hydrodynamics of the ebb bar channel

### 4.6.1 Introduction

This section discusses the current observations in the ebb bar channel which were collected between April 1994 and June 1995. Basically the observations are based on

float measurements, ADCP measurements and several long-term current meter deployments. For an overview of the data set, the reader is referred to Figures 4.3 and 4.4 in section 4.3.

The discharge measurements described, in section 4.4, showed that the maximum discharges in the channel are in the order of 5000m³/s and that the channel conducts about 13% of the total water transports during ebb and flood. Maximum cross-sectional averaged velocities during ebb and flood are in the order of 1.2m/s. The residual flow in the channel appeared to be slightly ebb-dominated.

The results presented in this section focusses on the processes characterizing the current patterns in the channel during ebb and flood (questions 2.1 and 2.2, section 4.1). A synthesis of the hydrodynamics in the ebb bar channel is given in section 4.6.5.

# 4.6.2 Current patterns during ebb

## Lagrangian current patterns

This section describes lagrangian current pattern based on float measurements during a spring tide in November 1994. The results focus on the patterns of advective flow acceleration and deceleration of the currents at one meter below the water surface, i.e. the near-surface currents. Figures 4.31 and 4.32 show mean flow paths and their envelopes together with the locations and the order of magnitude of consistent, relative advective accelerations. Negative relative changes in current velocity indicate flow deceleration of the flow in flow direction, whereas positive changes indicate acceleration. Thus an relative velocity change of -20% means that current velocities at the end of the stretch along the flow path are 20% smaller than at the begin of the indicated stretch. The indicated time-series of depth-averaged eulerian current velocities, are based on simultaneous Elmar-measurements from an achored ship in the middle of the channel (see inset).

The lagrangian flow patterns display the following features (Fig. 4.31 and 4.32):

- General flow acceleration in the relatively deep and narrow central part of the channel in the order of 10-20%. During the period of accelerating ebb flow on 4 November (Figure 4.31), the advective acceleration approximated 10%. During maximum and decelerating ebb on 8 November (Figure 4.32) accelerations of 20 percent were observed;
- General divergence and deceleration (25-30%) of the flow from the central part of the channel towards the bar. During accelerating ebb on 4 november, relatively large flow decelerations of 48% are observed along flow path 2 (Figure 4.31).
- On 8 November the ebb flow in the entrance of the channel showed a tendency towards small flow deceleration;
- The envelopes of the mean flow paths display a relatively large spatial range

in the bar area of the channel. This variation is caused by a gradual displacement of the ebb flow from the southern bank of the channel towards the northern bank. Especially along flow path 1, the decelerating ebb flow bends towards the north. Thus in the ebb bar channel the ebb flow accelerates in the central part of the channel and diverges and decelerates with decreasing channel depth towards the bar.

# Eulerian tidal current patterns

This section describes the general features of the depth-averaged flow pattern based on the long-term current observations in November 1994 and June 1995. The current patterns are illustrated for the conditions of mean tide. Major variations in current pattern during neap tide and spring tide are described.

Figure 4.33 shows current vectors in the ebb bar channel during maximum ebb for a neap tide and spring tide in November 1994. This figure illustrates the general tendency towards flow acceleration in the central part of the channel, between location 15 and 17. In this part of the channel current velocities accelerate with about 15% (0.1-0.2m/s). Current velocities at location 17 are on average 25% larger than at location 14, the entrance of the ebb channel. The flow acceleration is observed during almost the entire ebb period and the neap-spring tidal cycle. Maximum ebb velocities in the channel range between 1 and 1.4 m/s during the neap-spring tidal cycle and occur at location 17.

Figure 4.34 shows depth-averaged current patterns over the bar in the ebb bar channel measured in the summer of 1995. At the upstream side of the bar the flow diverges, whereas the flow converges at the downstream side of the bar. Thus the ebb flow tends to flow around the bar. Flow divergence at the upstream side of the bar is accompanied by minor spatial velocity differences. Advective flow decelerations in the order of 15% (0.1-0.2m/s) are only observed between location 18 and 21/22 during decelerating ebb (4-6 hours after high water). The flow convergence at the downstream side of the bar is accompanied by strong flow deceleration between locations 21 and 24. The magnitude of flow deceleration tends to increase with time and ranges between 20 and 48% (0.2-0.48m/s). The above described flow features are observed during the entire neap-spring tidal cycle. Over the neap-spring tidal cycle maximum current velocities approximate 0.7 to 0.9 m/s at the downstream side of the bar and 1 to 1.1 at the upstream side of the bar.

Thus the eulerian current patterns during ebb display flow acceleration in the central part of the channel, flow around the bar and a tendency towards flow decelleration over the bar. These observations largely confirm the float measurements.

### Detailed current patterns

Detailed current patterns in the channel and over the bar were obtained along three straight transects with the ADCP during mean tidal conditions. Table 4.1 (transect 5)

summarizes the hydrodynamic and meteorological conditions during the measurements. The locations of the three transects are indicated in Figure 4.35a (transect numbers 5\_1, 5\_2 and 5\_3).

Figure 4.35b shows time-series of the cross-sectionally averaged current velocities perpendicular to the two cross-sections 5\_2 and 5\_3. The spatial distributions of the magnitude and the direction of the depth-averaged current vectors over the cross-sections are indicated in Figures c to f. Figure a shows the location and orientation of the transects.

The cross-sectionally averaged current velocities in the central part of the channel (transect 5\_2) are 10-35% (0.1-0.2 m/s) larger than near the bar, indicating flow deceleration. During maximum flow cross-sectionally averaged current velocities reduce with 15% (0.15 m/s) in seaward direction. The largest reduction in current velocity is observed during decelerating ebb (0.2 m/s, 35%).

The depth-averaged flow is not equally distributed over the cross-section. Near the bar (transect 5\_3) the location of maximum flow gradually shifts from the outer bank of the channel towards the inner bank (zero distance) with time. The direction of the depth-averaged current vector progressively increases with time and from the outer bend towards the inner bend. The spatial increase amounts 10 to 15° and indicates divergence of the tidal flow. In the central part of the channel (transect 5\_2) maximum depth-averaged flow occur in the deepest part of the cross section. The depth-averaged current direction slightly change over time and along the transect. Along the transect depth-averaged current directions differ by about 10°. This variation is primarily observed near the channel banks, in the middle of the cross-section the current direction varies only a few degrees.

Figure 4.36 shows the spatial variation in depth-averaged along-channel and cross channel velocity components during accelerating, maximum and decelerating ebb. The along-channel velocity component is defined as the velocity component parallel to the ADCP-transect. The cross-channel velocity component is the velocity perpendicular to the ADCP transect.

The small cross-channel velocities indicate that the ebb current flows approximately parallel (within 5°) to the ADCP transect during the entire ebb period. The current patterns display strong flow decelleration at the downstream (seaward) side of the bar and minor flow acceleration at the upstream side of the bar (Figure 4.36). At the downstream side of the bar, at a distance between 300 and 500 meters along the transect, the depth-averaged flow reduces with about 28% (0.3m/s) on average, confirming the above-described lagrangian and eulerian current patterns. This flow reduction is not equally distributed over the ebb period. The absolute and relative reduction of the flow tends to increase with time. Largest flow reductions of 30-37% (0.4-0.5 m/s) are observed during maximum and decelerating ebb. At the upstream side of the bar current velocities slightly increase towards the top of the bar during maximum and decelerating ebb flow. The trendline indicates an increase in velocity of about 7% (0.05-0.1m/s) on average. These small flow accelerations are related to

divergence of the ebb flow at the upstream side of the bar. The ebb current flows around the bar of the channel.

The depth-averaged current patterns obtained with the ADCP are marked by second-order fluctuations. The amplitude and length scale of these fluctuations increase with time and decreasing water level. The cause of these fluctuations is not clear. Turbulence and depth variations may cause such fluctuations. For instance, the increase in velocity of 0.3 m/s between 750 and 850m in the ebb bar channel during decelerating ebb (Figure 4.36), coincides with a sudden decrease in water depth. The increase in amplitude and length scale of the fluctuations suggests an influence of turbulence.

# Observations of the vertical current structure

This section describes the three dimensional current patterns along the two ADCP transects 5\_2 and 5\_3 (see Fig. 4.35a for locations). Main question is whether the direction of the near-bed current vectors systematically deviates from the depth-averaged current vector due to e.g. flow curvature and the formation of secondary circulations (question 2.1, section 4.1).

As a result of flow curvature and coriolis acceleration the vertical current structure may display secondary circulations. Secondary flow is generally defined as the flow perpendicular to the depth-averaged current direction, the primary flow. Secondary circulations consist of near-bed flow directed towards the inner bend of the channel and a near-surface flow directed towards the outer bend. By definition, the outward and inward secondary flow balance, yielding a zero depth-averaged secondary current.

In the previous paragraph it was shown that the direction of the depth-averaged current vector changes along the cross-section (Figure 4.35). This means that the plane in which the secondary flow is defined also changes along the transect. A contourplot of the secondary flow component may yield eroneous results, as it suggests flow in one plane where it is not. To overcome this problem contourplots were made of two variables, which are independent of the changing direction of the depth-averaged current (see also section 4.3.3, ADCP):

- a contourplot of the magnitude of current veering in the water column. For all
  current vectors in each velocity profile the veering of the current vector with
  respect to the depth-averaged current direction was determined. This plot gives
  direct information of the magnitude and location where the current direction
  deviates from the depth-averaged current.
- 2) a contourplot of the relative magnitude of the secondary currents. For all current vectors in each velocity profile the ratio of the secondary flow component over the depth-averaged current velocity was computed. This plot gives information about the relative strength and location of the secondary flow. This definition of the secondary flow also enables a comparison of the secondary flow pattern at different points in time.

In the above described contourplots secondary circulations and systematic current veering, related to flow curvature, are marked by a current veering which gradually

changes sign and magnitude over the water column. The convention for the sign of current veering and secondary flow is shown in Figure 4.6 (section 4.3.3). The direction of the primary flow during flood is the positive x and the direction of the primary ebb flow is the negative x. Then a negative secondary flow and current veering during ebb indicate that the current vector is deflected to the left with respect to the depth-averaged flow. Negative values during flood indicate a veering of the current vectors to the right.

Figure 4.5.37 shows contourplots of the secondary flow and accompanying current veering in the central part of the channel, cross-section 5\_2. The figures a to e represent the conditions from accelerating towards decelerating ebb flow. The left side of the cross section (zero distance) is the inner bend of the channel. The right side of the cross section (maximum distance) is the outer bend. Positive values indicate current vectors flows directed towards the inner bend (inward flow). Negative values imply flow towards the outer bend (outward flow), whereas zero means flow parallel to the depth-averaged current. The values of secondary flow and current veering near the banks of the channel, the first and last 50-100m of the transect, should not be taken into account, as in these regions the vertical coverage of the ADCP was less than 50% of the water column due to the small water depth. The computation of the depth-averaged current direction in these regions is essentially based on extrapolation of the measured values yielding relative large uncertainties.

Figure 4.37 shows a major pattern of secondary flows and a systematic current veering, consisting of inward directed near-bed currents up to about 4 meters above the bed and slightly outward directed currents at elevations above 4 meters. These patterns are characteristic for a secondary circulation related to flow curvature. Well-developed circulations are observed in the middle part of the cross-section (200-400m), during almost the entire ebb period (between 2 and 5 hours). Strongest secondary currents occur near the bed and during maximum flow. The magnitude of the secondary near-bed currents amounts 5 to 17% of the depth-averaged current velocity. The near-bed current directions, at about 0.7m above the bed, differ from the depth-averaged current directions by about 10-16° (Figure 4.36 b,d and e). For these conditions, the near-bed and depth-averaged current velocities differ by about 0.6-0.7 m/s (not shown).

In the straight channel section just landward of the bar (transect 5\_3) the above described patterns of secondary flow and current veering are not observed, indicating that secondary circulations are absent. Figure 4.38 illustrates this for the conditions of maximum flow. The coverage of the water column by the ADCP is limited. This means that the magnitude of the veering and secondary flow of an individual current vector may differ from (the unknown) reality. Neverthless the changes of these parameters over the water column are a usefull indicator of current veering. Compared to transect 5\_2 (Figure 4.37) tidal flow near the bar does not display a systematic veering of the current vectors from the water surface towards the bed. If the computed depth-averaged current directions are correct, there are no major differences in current direction between the near-bed and the depth-averaged flow. Tidal flow near the bar

seems to be dominated by flow divergence and advective flow accelerations and decellerations.

#### Conclusions

If it assumed that the characteristics of the flow pattern were not significantly affected by the morphological changes of the channel (migration) between November 1994 and June 1995, the current observations may be synthesized (answering question 2.1 in section 4.1).

The ebb flow, entering the ebb channel, accelerates towards the narrow and deep central part of the channel. Advective flow accelerations are typically in the order of 10-20%. In this central part of the channel the vertical current structure displays strong secondary circulations with near-bed secondary currents up to 0.25m/s, directed towards the inner bend of the channel. The difference in current direction between near-bed and depth-averaged currents amounts 10-16°, whereas the difference in current velocity approximates 0.6m/s. As channel depth decreases and channel width increases towards the bar in the channel, the ebb flow diverges. This flow divergence is accompanied by flow decellerations (10-30%) at the upstream side of the bar and a tendency towards small flow acceleration (10%) near the top of the bar. Downstream of the bar the ebb flow converges and strongly decelerates (20-50%) as the water depth abruptly increases.

## 4.6.3 Current patterns during flood

### Lagrangian tidal current patterns

Figure 4.39 shows mean flow paths and their envelopes in the ebb bar channel based on the float measurements during spring tide in November 1994. Figure 4.38 indicates the magnitude and locations of consistent advective flow accelerations and decellerations. Positive values indicate advective acceleration of the flow, negative values mean deceleration. The lagrangian flow patterns display the following features:

- Near-surface currents show a advective flow deceleration at the downstream side of the bar. Until maximum flow (I, in Figure 4.38) relatively large flow decelerations of about 25-30% exist. Considerable smaller decelerations are observed after 11.5 hours after high water, near maximum flow (II);
- Advective flow acceleration from the downstream side of the bar towards the
  central part of the channel during the entire flood period. Large advective flow
  accelerations, in the order 40 to 50 %, mark the flow pattern until approximately
  11.5 hours after high water (II in Figure 4.38). Considerably smaller accelerations
  exist during the last 1.5 hours of the flood (5-15%, I in Figure 4.38);
- The flood flow is aligned parallel to the southern bank of the channel. In the curved part of the ebb channel the near-surface flow is deflected away from the channel axis;

• The envelope of the mean flow paths indicates a small spatial variation in the channel, especially along flow path 1. At the end of flow path 2 a relatively large spatial variation is observed.

Thus, as water depth increases at the downstream side of the bar the near-surface currrents initially decelerates. As water depth increases and channel width decreases towards the central part of the channel, the flood flow accelerates.

## Eulerian tidal current patterns

Figure 4.40 shows depth-averaged current patterns in the channel, based on the long-term current measurements in November 1994. During most of the time depth-averaged velocity gradients in the central part of the channel do not exceed the uncertainty in the observations (10%). Only at 9 hours after high water, during steady flood a tendency towards flow acceleration of about 10-15% is observed in the central part of the channel between location 17 and 16. During decelerating flood, at 12.5 hours after high water, the flood tends to decelerate with 15 to 20% in this part of the channel. Landward of the ebb channel (location 14) current velocities are on average 30 percent (0.1-0.35m/s) smaller than in the channel, indicating deceleration of the flood flow. This flow deceleration is observed during the entire neap-spring tidal. Maximum flood currents in the channel range between 1.1 and about 1.5 m/s during the neap-spring tidal cycle.

Current patterns across the bar of the ebb bar channel, measured in the summer of 1995, are indicated in Figure 4.41. At upstream side of the bar the flood flow slightly diverges and accelerates towards the top of the bar. The magnitude of this acceleration amounts 10% to 25% (0.05-0.2m/s). At the downstream side of the bar spatial velocity differences are small and hardly exceed the uncertainty in the measurements (±10%). The current vector at the downstream (landward) side of the bar show a more or less parallel alignment. These flow features are observed during the entire neap-spring tidal cycle. Maximum flood currents range between 0.9 and 1.3 m/s during the neap-spring tidal cycle. Largest velocities are observed at location 23, at the steeply sloping upstream (seaward) side of the bar.

## Detailed tidal current patterns

Figure 4.42a shows time-series of the averaged current velocities perpendicular to the two cross-sections 5\_2 and 5\_3. The distributions of the magnitude and the direction of the depth-averaged current vectors over the cross-sections are indicated in Figures b to e.

Cross-sectionally averaged currents near the bar and in the central part of the channel are of similar magnitude (Figure 4.5.16). The differences in cross-sectionally averaged current velocity between bar and central part of the channel hardly exceed 6% (0.06m/s). Only between 8 and 9 hours after high water the flood flow accelerates with about 13-23% (0.1m/s) towards the central part of the channel.

The depth-averaged current velocity is not equally distributed over the cross-section. Near the bar (transect 3) largest current velocities occur at the left bank of the channel, between 0 and 300 meters along the transect. The direction of the depth-averaged current vectors shows a progressive decrease 10 to 15° from the inner bend to the outer bend. Especially near the outer bend current directions show an influence of the decreasing water on current direction. At this side of the cross-section currents are deflected towards the channel axis. In the central part of the channel (transect 2) largest current velocities tend to occur in the deepest part of the cross-section. Depth-averaged current directions display minor variations (a few degrees) in the central part of the channel. In this part of the channel depth-averaged currents are deflected away from the channel axis by about 10°. Largest variations in current direction (10-20°) are observed near the channel banks.

Figure 4.43 shows the spatial variation in depth-averaged currents over the bar along ADCP-transect 5\_1 (see Figure 4.5.3 for location), at different points of time during flood. Indicated are the velocity components parallel and perpendicular to the ADCP transect, i.e. the along-channel and cross-channel velocity components.

The flood flows approximately parallel to the ADCP transect (within 5°). The flow pattern over the bar is marked by small flow accelerations at the upstream side of the bar and minor flow decelerations and accelerations at the downstream side. Advective accelerations at the upstream side of the bar approximate 10% (0.1m/s). This increase in current velocity is observed during almost the entire flood period. The increase in current velocity is small, given the sudden decrease in water depth of about 5 meters. This may be explained by the flow divergence at the upstream side of the bar, as revealed by the long-term current observations (Fig. 4.40). At the downstream side of the bar small reductions in current velocity, of about 10% (0.1m/s), mark the depth-averaged flow pattern between 500 and 1200m. This reduction is observed during maximum and decelerating flood. The along channel current pattern indicates a tendency towards advective flow acceleration between 1200 and 2000 meters. During steady and decelerating flood rather sudden changes in current velocity of 0.25 m/s occur above the top of the bar (at a distance between 400 and 500m along the transect). The origin of these velocity variations is not known.

# Observations of the vertical current structure

Figure 4.44 shows contour plots of the relative magnitude of secondary flow and current veering in the curved part of the ebb channel during flood (for definition see section 4.5.2). Question is whether the vertical distribution of the current vectors displays a systematic current veering.

Near-bed currents in the central part of the channel show a tendency of positive secondary flows and current veering near the bed, indicating flow towards the inner bend with respect to the depth-averaged current direction. This near-bed flow is balanced by a flow directed towards the outer bend in the upper layer of the water column. These patterns of current veering and secondary flow indicate the presence of

(weak) secondary circulations. During most of the time near-bed secondary flows amount 5 to 10 % of the primary flow velocity. The near-bed current directions differ from the depth-averaged current directions by 6-11°. The near-bed current vectors are 50% (0.35-0.6m/s) smaller than the depth-averaged current vectors (not shown).

Near the bar of the ebb channel (transect 3) systematic patterns of current veering and secondary flow, as observed in the central part of the channel, are absent. This is illustrated for the conditions of maximum flow in Figure 4.45.

#### Conclusions

As the flood approaches the bar in the ebb channel from the upstream side (=seaward side), the tidal flow diverges and accelerates (10-25%) towards the top of the bar. At the downstream side of the bar the flood slightly converges and decelerates (5-30%). Cross-sectionally averaged currents (ADCP) and the depth-averaged currents indicate a minor flow acceleration towards the central part of the channel, whereas the near-surface currents (float) display flow accelerations of 10-40%. From sediment transport considerations the depth-averaged and cross-sectionally averaged currents are more important than the near-surface currents. The vertical current structure in the central part of the channel displays secondary flows and current veering, which indicate the presence of a (weak) secondary circulation related to flow curvature. The near-bed and depth-averaged currents differ 6-11° in direction and 0.35-0.6m/s (50%) in magnitude. Just landward of the channel, where the water depth suddenly increases, the flood flow strongly decelerates (30% velocity reduction on average).

# 4.6.4 Current asymmetry and residual flow

Sofar the tidal current patterns have been discussed without considering the differences in velocity magnitude between ebb and flood, i.e the current asymmetry and the residual flow (for a definition see section 4.3 or 4.5.4). Both parameters give a first indication of net sediment transport direction in the channel. Question is whether both parameters display specific spatial and temporal variation (for definitions see section 4.3.3 and equation 4.3.

Figure 4.46 shows the spatial pattern of significant current vectors during mean tide. The asymmetry ratio for neap and spring tide are indicated seperately in the two bottom figures. During mean tide current asymmetry in the channel is positive and ranges between 0 and 0.11 This means that the ebb flow is on average 0 to 12 percent stronger than the flood flow. The bar in the channel forms the transition zone between ebb-dominated and flood-dominated flow. At the landward side of the channel tidal flow tends to be ebb-dominated, whereas the seaward side is clearly flood-dominated. At the seaward side flood currents are about 15 to 25% stronger than the ebb currents.

Current asymmetry changes over the neap-spring tidal cycle. The asymmetry ratios during neap and spring tide show a decrease of the ebb-dominated current asymmetry

with tidal range in the channel. The changes in current asymmetry are in the order of 7-20%. At the seaward side of the bar flood-dominated current asymmetry increases with 0.13 to 0.29 (=16-34%).

Figure 4.47 shows long-term mean residual current vectors based on the application of the low pass Godin filter (see section 4.3). Residual currents in the ebb bar channel tend to be ebb-dominated. The magnitude of the residual currents ranges between 0.02 and 0.16m/s and is smallest near the top of the bar. Similar to the pattern of current asymmetry, residual currents at the seaward side of the bar are flood-dominated.

#### 4.6.5 Discussion and conclusion

The current observations during ebb and flood rises the question to what extent these the flow patterns are different and which tidal conditions control channel morphology. A second point of discussion is the observed secondary flow and current veering in the central part of the channel. Question is to what extent the observed secondary flow agrees with theory.

The current patterns during ebb and during flood display similar flow features in the central part of the channel and over the bar, however the intensity and location of these features is not the same. The alignment of the flow with respect to the channel morphology also differs.

In the central part of the channel largest velocity gradients are observed during ebb. The depth-averaged and near-surface currents during ebb display a consistent flow acceleration in the central part of the ebb channel of about 15%. Cross-sectionally averaged currents in this part of the channel are 10-30% larger than near the bar. During flood the cross-sectionally averaged and depth-averaged currents show only a minor acceleration of flood flow in the central part of the channel. Thus largest accelerations in the central part occur during ebb. The ebb flow is aligned parallel to the channel axis. The flood flow is deflected away from the channel axis towards the outer bend of the channel. This implies a stronger flow curvature during ebb than during flood. Both during ebb and during flood this flow curvature is accompanied by secondary circulations and systematic veering of the current vectors over the water depth. The magnitude of the current veering and secondary flow is however largest during ebb, probably as a result of the stronger flow curvature.

Tidal flow over the bar in the channel is marked by flow accelerations and decelerations and flow convergence and divergence. Velocity gradients and differences in current direction over the bar are largest during ebb. During ebb the flow diverges and slightly accelerates (about 10%) at the landward side of the bar. The flood flow decelerates at this landward side of the bar with about 10%. Current vectors during flood show an almost parallel alignment. At the seaward side of the bar, the ebb flow converges and decelerates with 28% on average. Under similar tidal conditions the flood flow displays flow divergence and small flow acceleration (10%).

Current asymmetry and residual flow are ebb-dominated in the channel and at the landward side of the bar. This indicates that the currents and transport capacity of the flow are stronger during ebb than during flood. The neap-spring variation in current asymmetry suggests a larger net ebb-transport of water and sediment during neap tide than during spring tide. Combining these observations with the larger velocity gradients and secondary circulations during ebb, yields the conclusion that the morphology of the ebb bar channel is essentially controlled by the ebb flow.

To observations of secondary flow may be compared with the theory underlying the secondary flow model of Kalkwijk and Booij (1986). According to their formulation the intensity of the fullly developed secondary flow may be approximated as (Wang et.al. 1991):

$$I = \frac{2.\overline{u}.h}{\kappa^2 R} + \frac{f.h}{\kappa^2} \tag{4.7}$$

where

I = intensity of secondary circulation [m/s];

 $\bar{u}$  = the depth averaged current velocity [m/s];

R = the radius of stream line curvature [m];

h = the water depth [m/s]

f = coefficient for geostrophic acceleration [rad/s];

 $\kappa$  = von Karman constant [0.4];

The radius of stream-line curvature (R) is determined from a bathymetric map. The lagrangian and eulerian tidal current patterns described in section 4.6.2 and 4.6.3 showed ebb flow paths approximately parallel to the inner bend of the channel. The flood flow paths approximately followed the outer bend of the channel. This yields a radius of curvature of about 1400m for the ebb flow and 2000m for the flood flow during the ADCP measurements.

Table 4.8 compares the measured maximum and mean near-bed secondary flow in the central part of the channel (between 200 and 400 m) with the computed magnitude of secondary flow, based on equation 4.7. Measurement and theory show a fairly good agreement. The comparison of the mean values of secondary flow during ebb is good during the periods of maximum ebb flow. For the conditions of accelerating and decelerating ebb flow (1.8 and 5.5 hours) the computed secondary flow is larger than the measured secondary flow. For these conditions the comparison of maximum values shows better agreement. The flood shows good agreement for both maximum and mean values. Only the at the end of the steady flood phase mean computed secondary flow are almost two times larger than the measured secondary flow. The differences between theory and measurement might be due to the fixed value of stream line curvature. Nevertheless, the comparison shows a consistent picture.

# 4.7 Hydrodynamics of the flood bar channel

#### 4.7.1 Introduction

The flood bar channel is the last channel where abundant current measurements were carried out. The current observations consist of ADCP measurements and several long-term current meter deployments (for an overview of the measurement locations see Figures 4.3 to 4.5).

From the results presented in section 4.4 it appeared that the flood bar channel transports about 13% of the total water transports during and up to 20% of the water transports during flood. This difference is related to flood velocities which are almost 40% larger than the ebb velocities. Main questions to be answered in this section are:

- are the flow patterns during ebb and flood marked by processes of advective flow acceleration, flow divergence or convergence?
- does the vertical distribution of current vectors display patterns of systematic veering, which can be related to flow curvature and the formation of secondary circulations?
- are current asymmetry and residual flow in the channel marked by specific variations?

Answers to these questions enables a comparison of the flow response during ebb and flood and an evaluation of the conditions which are likely to control the flood morphology of the channel (section 4.7.5).

## 4.7.2 Current patterns during ebb

## Eulerian tidal current patterns

Figure 4.48 shows depth-averaged current vectors in the channel during ebb for mean tidal conditions, based on the current measurements in August 1995. The ebb currents at locations 30, 31 and 32 display deflection of the ebb flow by the topography of the bar. The deflection increases with decreasing water level. At water levels beneath NAP (after 4 hours) ebb currents at location 31 flow approximately parallel to the depth contours of the bar. Unfortunately simultaneous current information at the top of the bar is not avalailable due to instrument malfunctioning. Advective flow acceleration is observed in the channel between location 28 and 29, where the ebb flow tends to accelerate with 20-45% (0.18m/s). This acceleration is observed during the period of maximum flow (2-5hours). At the downstream side of the bar, between locations 32 and 29, the ebb flow decelerates with 13-27% (0.1-0.26m/s). Between 3 and 5 hours after high water ebb currents at the upstream side of the bar (location 31) exceed ebb currents at the downstream side (29, 30) by 13-50% (0.1-0.3m/s). Maximum ebb currents range between 0.7 and 1m/s during the neap-spring tidal cycle. Largest ebb currents are observed at location 32.

Figure 4.49 shows ebb current patterns around the bar of the channel during mean tide in February 1996. The current pattern displays flow convergence at the downstream

side of the bar (locations 34, 35, 37,38). Current velocities at the upstream side of the bar, location 36, are 10 to 30% (0.1-0.3m/s) larger than at the downstream side of the bar (locations 35/38), indicating flow deceleration over the bar. This flow deceleration increases with time and tidal range and ranges between 20 and 65 % (0.2-0.4m/s). Current velocities in the channel, at location 33, are 15 to 35% larger than near the bar at location 34. This velocity difference is observed between 4 and 6 hours after high water and suggest advective acceleration of the ebb flow in the channel. This confirms the acceleration observed in August 1995 (see above). Largest ebb currents occur at location 36 and range between 0.88 and 1.48 m/s over the neap-spring tidal cycle.

## Detailed tidal current patterns

This section describes detailed current patterns in the channel and over the bar during mean spring tidal conditions. Current patterns are based on ADCP observations along three transects (transects 6\_1, 6\_2 and 6\_3 in Figure 4.50a). The orientation of the ADCP-transect 6\_1 was choosen parallel to general alignment of the channel axis. The cross-channel transects 6\_2 and 6\_3 intersect the along-channel transect at a distance of 700 and 1800 meters respectively.

Figure 4.50a shows time-series of the cross-sectionally averaged current velocities in the two cross-sections 6\_2 and 6\_3. The variation in the magnitude and the direction of depth-averaged current vectors along the transects are given in figures b to e.

Cross-sectionally averaged current in the central part of the channel (transect 6\_2) are about 12-25% (0.1-0.15 m/s) larger than near the bar (transect 6\_3), indicating a tendency towards flow acceleration in the channel. The increase in velocity is observed between maximum and decelerating ebb (4-6 hours after high water). Largest accelerations occur during decelerating ebb flow.

The depth-averaged current vectors are not uniformly distributed over the cross sections. In the central part of the channel (Figure 4.50b and d) maximum currents are observed in the deepest part of the cross section. The current directions in the channel gradually increase from 250° in the inner bend to about 265° in the outer bend. This change in current direction of 15° indicates a tendency towards flow convergence in the central part of the channel. Near the bar of the channel (transect 6) largest current velocities occur at the inner bend of the channel (zero distance), where the deflected ebb flow north of the bar enters the channel. Near the bar depth-averaged current directions also show an increase in current direction from about 230° in the inner bend to 250° in the outer bend, indicating a tendency towards flow convergence at the downstream side of the bar. The eulerian tidal current patterns revealed a similar pattern of flow convergence.

Figure 4.51 shows the spatial variations in the depth-averaged velocity components parallel (along-channel) and perpendicular (cross-channel) to transect 6\_1 over the ebb period. The current patterns across the flood bar channel reveal deflection of the ebb currents by the bar and major spatial differences in current velocity over the bar. The

deflection of the ebb current at the upstream side of the bar appear to be accompanied by an inclination of 15-25° of the current vectors with respect to the ADCP transect. In the channel between 0 and 1600 meters along the transect, depth-averaged current directions approximately coincide with the orientation of the ADCP transect and the channel axis. Despite the current deflection near the bar two major along-channel velocity gradients can be identified:

- largest current velocities exist at the top of the bar. On average current velocities at the top of the bar exceed currents at the upstream and downstream side of the bar by 30 % (0.4-0.5/s). These large velocity gradients indicate flow acceleration at the upstream side of the bar and flow deceleration at the downstream side of the bar.
- ebb currents at the landward side of the bar exceed ebb currents at the seaward side by 21-37% (0.2-0.4m/s). The absolute and relative magnitude of these difference in current velocity increases with decreasing water level.

The along-channel depth-averaged currents display a tendency towards flow acceleration in the channel between 1200 and 2100 meters along the transect during the period around maximum flow (2-5 hours). This tendency confirms the flow acceleration observed in the eulerian tidal current pattern and the ADCP transects 6\_2 and transect 6\_3. Strongest flow acceleration is observed near the cross-channel transect 6\_3 (intersection at a distance of 1820m), where the ebb flow converges.

## Observations of the vertical current structure

The ADCP-observations along cross-sections 6\_2 and 6\_3 were used to identify systematic patterns of veering and secondary flow in the vertical distribution of current vectors. For this purpose contourplots of the current veering and relative magnitude of secondary flow were made (for definitions see section 4.3.3, Fig.4.6). Figure 4.52 shows these plots for the conditions of maximum flow as an example. In this figure positive values indicate a veering of the current vectors with respect to the depth-averaged currents towards the inner bend of the channel. Negative values indicate the opposite direction of current veering. The figures show that major current current veering and secondary flows, like in the ebb bar channel, are absent in the the straight flood bar channel.

#### Conclusion

The ebb flow in the flood bar channel is sensibly influenced by the presence of the shallow bar and tends to flow around the bar. The depth-averaged velocity along the ADCP-transect shows velocity differences between the top of the bar and the upstream side of the bar in the order of 30 to 40%. At the downstream side of the bar the flow converges and decelerates. At the upstream side of the bar the probably accelerates. Just seaward from the bar, where the tidal flow still converges (ADCP-transect 6\_3), towards the central part of the channel the ebb flow accelerates with about 12 to 25%. This indicates a tendency towards flow acceleration as the water depth in the channel

increases. The observation of the vertical current structure in the channel does not reveal major and systematic patterns of secondary flow and current veering.

# 4.7.3 Current patterns during flood

# Eulerian tidal current patterns

Figure 4.53 depicts the depth-averaged current pattern in the flood bar channel based on the current measurements in August 1995. The flood flow is slightly deflected by the topography of the bar. The current vectors at locations 32 and 30 display a tendency towards small flow divergence. On average current directions at these two locations differ by about 10°. In the channel velocity gradients are observed between location 27 and 30. In this part of the channel, where the flood flow slightly diverges, current velocities decelerate with about 10 to 20 percent (0.1-0.15m/s). Current velocities at the downstream (landward) side of the bar (location 31) are 25 to 50 percent (0.2-0.3m/s) smaller than in the channel. On average the velocity difference amounts 30 percent. Maximum flood velocities in the channel range between 0.7 and 1.4 during the neap tide spring tide cycle. At the downstream side of the bar this temporal variation in maximum velocities ranges between 0.5 and 1m/s.

Current patterns over the bar of the channel, measured in February 1996, display a tendency towards flow acceleration and small flow divergence at the upstream side of the bar just before the top of the bar (locations 34, 35 and 38, Fig. 4.54). Current directions at locations 35 and 38 differ by about 10°. Between location 34 and 35 the current velocity increases with about 10 to 20 percent (0.1-0.2m/s). Striking are the large spatial velocity differences along the seaward side of the bar (locations 35, 37 and 38). Current velocities at the downstream side of the bar (location 36) are 40 to 15 percent smaller than at the upstream side of the bar (location 35), indicating flow deceleration over the bar. The magnitude of this deceleration is smallest during maximum flood flow. Largest flood velocities are observed at location 35, and range between 1 and 1.6 m/s during the neap tide spring tide cycle.

## Detailed tidal current patterns

This section describes detailed current patterns in the channel and across the bar during spring tidal conditions. Current patterns are based on ADCP observations along three transects (transect 4, 5 and 6 in Figure 4.5.3). The orientation of the ADCP-transect 4 was choosen parallel to general alignment of the flood channel.

Figure 4.55b shows times series of the cross-sectionally averaged current velocities in transect 6\_2 and 6\_3. The distribution of the depth-averaged velocity and current direction along the transects are shown in figures c to f. Figure b shows during steady

flood cross-sectional averaged current velocities near the bar are about 15% (0.1 m/s) smaller than in the central part of the channel, indicating a limited tendency towards flow deceleration. In the central part of the channel depth-averaged current velocities are uniformly distributed over the channel cross-section. Near the bar (Figure 4.55d) largest current velocities are observed in the inner bend and above the dune-like feature in the middle of the cross-section. The distributions of the depth-averaged current directions show a general tendency towards flow divergence as the flood flow approaches the bar: In the central part of the channel current directions are more or less uniformly distributed over the channel cross section and alligned parellel to the channel axis. Near the bar the depth-averaged current direction displays a gradual increase in current direction of about 20° between the inner bend and the outer bend.

Figure 4.56 shows the depth-averaged along-channel and cross-channel velocity components in the channel and over the bar during the flood period. The flood current is less deflected by the topography of the bar than the ebb current. The small inclination of the depth-averaged currents (6-12°, not shown) with respect to channel axis decreases over the flood period. In the channel (between 0 and 1700m) the depth-averaged along-channel velocities displays flow acceleration in the order of 12-33%. Just before the bar (between 1700 and 2200m), where the flow diverges the depth-averaged flow tends to decellerate with about 20%. This flow deceleration confirms the eulerian tidal current pattern. The flow pattern over the bar is marked by flow acceleration at the upstream side of the bar and flow deceleration at the downstream side of the bar. The increase in current velocities towards the top of the bar is observed between accelerating and decelerating flood and approximates 30% (0.3-0.4m/s). Downstream of the bar the current velocity reduces with almost 40 to 50% (0.5-0.7m/s).

### Observations of the vertical current structure

The vertical current structure is subject of this paragraph. Question is whether the vertical current structure along the ADCP-transect 6\_2 and 6\_3 is marked by systematic current veering and secondary flows.

To illustrate the characteristics of the vertical current structure, figure 4.57 shows contourplots of the secondary flow and current veering in both cross sections near maximum flood flow. The left side of the cross-sections (zero distance) may be regarded as the inner bend. The right bank of the channel is the outer bend. Positive values indicate secondary flow components and current veering directed towards the inner bend. Negative secondary flows and current veering represent current vectors deflected away from the depth-averaged flow towards the outer bend. Because the coverage of the water column by the ADCP was small near the banks of the channel, the uncertainty in the computed depth-averaged currents is relatively large. This yields the eroneous contours of secondary flow and veering near the bank in especially transect 6 3.

Systematic patterns of major secondary flow and current veering are not observed (Fig. 4.57). Near the bar, in transect 6\_3, the contourplots are very irregular (Figure c and d). Only in the central part of the channel, transect 6\_2, small positive secondary flows and current veering mark the near-bed flow, whereas small negative values are observed in the upper half of the water column. These patterns of secondary flow and current veering suggest the presence of a very weak secondary circulation.

#### Conclusion

The flood flow entering the flood bar channel initially accellerates with 12 to 33% in the central part of the channel. Just before the bar the flow diverges and decelerates with 10 to 20 percent. At the shallow upstream (seaward) side of the bar, just before the top, the flood flow accelerates (10-40%). As soon as the tidal flow cross the heighest part of the bar, current velocities rapidly decrease with about 10-50 percent. Major systematic patterns of secondary flow and current veering are not observed.

# 4.7.4 Tidal current asymmetry and residual flow

As already mentioned in the introduction of this section, the magnitude of the flood velocities tends to exceed the ebb velocities resulting in flood-dominated residual current. The spatial variation in current asymmetry and residual flow in the channel are summarized in Figure 4.58 and 4.59.

The pattern of significant current vectors and asymmetry ratios during mean tidal conditions show flood-dominated flow in the channel and at the seaward side of the bar in the channel. Flood currents are 12 to 40 % stronger than the ebb currents indicating are larger transport capacity during flood than during ebb (Fig.4.58). At the landward side of the bar ebb currents are 5 to 20% stronger than the flood currents. At this side of the bar significant current vectors are less in line than at the seaward side of the bar and in the channel. The asymmetry ratios for neap and spring tide display an increase of current asymmetry with tidal range in the channel and seaward side of the bar of about 10 to 20%. At the landward side of the bar current asymmetry decreases (6-25%) with tidal range.

The residual current pattern qualitatively resembles the pattern of current asymmetry. In the channel and at the seaward side of the bar flood-dominated residual currents are observed, whereas at the landward side residual flow is ebb-dominated. The magnitude of the residual current vector ranges between 0.06 and 0.17m/s (Fig. 4.59). Largest residual currents tend to occur near the bar in the channel.

#### 4.7.5 Discussion and conclusion

A comparison of the observed flow patterns in the flood bar channel during ebb and flood reveals similar flow features: the absence of major current veering and secondary flows, flow accelerations and decelerations, flow divergence and convergence. The intensity and and the locations with respect to channel morphology, are not exactly the same for ebb and flood.

In the channel just before the bar where channel width increases and water depth decreases, the flood flow tends to decelerate (10-20%) where the ebb flow accelerates (12-25%). The flow accelerations during ebb tends to be slightly larger than the flow deceleration during flood. Also the flow pattern over the bar displays differences. The ebb flow is more deflected by the topography of the bar than the flood flow. At the landward side of the bar the flood flow decellerates (10-50%), whereas the ebb flow accelerates (30-40%). The maximum velocity gradients during flood (deceleration) are larger than during ebb (acceleration). This phenomenom may be related to the stronger deflection of the flow during ebb. At the seaward side of the bar the opposite tends to be true: during ebb tidal flow converges and decelerates (30-40%), whereas the flood flow slightly diverges and accelerates (10-40%).

The velocity patterns alone do not allow firm conclusions which tidal conditions (ebb or flood) controls channel morphology, as the magnitude of the velocity gradients at one location during ebb and flood do not differ significantly. The discriminating factor here seems to be the magnitude of the current asymmetry. The strongly flood-dominated currents and the increase of this current asymmetry with tidal range, indicates that it is essentially the flood flow that controls the morphology of the channel. The dominating tidal at the landward side of the bar are not easily identified. The relatively small ebb-dominance and the larger velocity gradients during flood, suggest that also the morphology of the landward side of the bar is controlled by the flood flow.

#### 4.8 Discussion and conclusions

The results of the current observations in the study area, enable a preliminary discussion on:

- The flow response over the bars in the connecting channels, that revealed some intriging hydrodynamic processes.
- the flow response in relation to channel type. What are the basic differences in the hydrodynamics between the three connecting channels (question 2, section 4.1)?
- the function of the connecting channels in the system of main channels (question 1, section 4.1).

A discussion on these aspects is given below.

# Flow response over bars

The bars in the channels are the most pronounced morphological features of the channels. Near the bars channel geometry changes rapidly. Channel depth decreases and channel width increases towards the bar. In the bar channel these changes in

channel geometry are reflected in the hydrodynamics over the bars (for the cross channel not enough current information is available). The bars in these channels demarcate the transition zones between ebb-dominated and flood-dominated flow. Changes in current asymmetry with tidal range at the landward side differ from changes at the seaward side of the bar. The ebb and flood flow tend to flow around the bars of the channels. Fluid continuity across the bar may explain the observed flow pattern. Fluid continuity implies that the discharge O (m<sup>3</sup>/s) does not change much across the bar. The overall discharge Q is defined as Q=b.ū.h, where b is the width of the imaginary stream tube (m),  $\bar{u}$  is the depth-averaged current velocity and h is the water depth. The changes in channel depth over the bar may result in changes in the width of the stream tube and the depth-averaged velocity. At the upstream side of the bars the flow diverges. The width of the stream tube increases. At the downstream side the flow converges. The width of the stream tube decreases. In addition to these changes in width the depth-averaged velocity increases and decreases across the bars. The flow over the bars shows a tendency towards flow accelerations at the upstream side of the bar and deceleration at the downstream side. The pattern reverses every tidal phase. The net effect depends on the magnitude and duration of accelerations and decelerations as well as, the effect of variations in stream tube width, differences in current asymmetry and the dominant sediment transport mode. Additional sensitivity computations are necessary the identy the relative importance of the processes for the net balance.

# Flow response and channel type

As outlined in section 4.1 the three connecting channels, described in sections 4.5 to 4.7, are different from a morphological point of view. A comparison of the flow response in the three channels reveals hydrodynamic differences regarding:

- · the moment and magnitude of maximum flood flow;
- the presence of secondary circulations and current veering;
- the residual current patterns;
- · the changes in current asymmetry with tidal range.

These aspects are clarified below.

The moment and magnitude of maximum flood flow hydrodynamically distinguishes the cross channel from the bar channels. In the two bar channels maximum flood flow coincides with maximum flood flow in the main channels. The flood is marked by a short-lasting peak of maximum flood currents, which is a general feature of tidal flow in the estuary. In the cross channel maximum flood is not marked by a general flood peak. In stead, the flood flows along the entrance of the cross channel during the period of maximum flow in the other channels. As a result the (cross-sectionally averaged) flood currents in the channel are weakly developed and reach their small maximum value, 0.5 to 1 hour earlier than in the bar channels and main channels. This early maximum flood coincides with the short-lasting reversal in hydraulic gradienst along the channel, that suggests some kind of resonance. The cause of this phenomenom is not clear yet.

Sofar this is the only hydrodynamic aspect which justifies a distinction between the cross channel and the two bar channels. This is inherent to the limited amount of observations in cross channel, compared to the bar channels.

The presence of secondary circulations and systematic current veering distuiguishes the ebb bar channel from the flood bar channel. The secondary circulations and systematic current veering in the ebb bar channel and absence of these features in the flood bar channel was expected. The curved channel alignment of the ebb bar channel suggest curvature of tidal flow, whereas the relatively straight alignment of the flood channel does not.

The ebb bar channel and flood bar channel also differ with respect to the pattern of residual currents over the bar in the channels. In the ebb bar channel residual currents tend to decrease towards the top of the bar, whereas in the flood bar channels relatively large residual currents are observed. These differences may be indicative for differences in morphological behaviour of the bars. Large residual currents may be related to migration of the bars, whereas small residual currents may indicate morphological stability (Seminara, pers. comm.).

The changes in current asymmetry with tidal range is the only discriminating criterion in the hydrodynamics of the three connecting channels. In the ebb bar channel the ebb-dominated current asymmetry decrease with tidal range. In the flood bar channel the flood-dominated current asymmetry increases with tidal range. In the ebb cross channel, the ebb-dominated current asymmetry increases with tidal range. The decreasing current asymmetry in the ebb bar channel is remarkable and is probably inherent to the location of the ebb channel: The channel is located in the bar of the main flood channel, where the flow tends to be flood-dominated.

The results so far indicate that the morphological distinction in three channel types does have a foundation from a hydrodynamical point of view. The foundation is however not firm and needs a further elaboration based on computations. The same applies to the implications of the flow response for the sediment transports in in the channels.

### Function of the connecting channels

The hydrodynamic function of the connecting channels finds expression in the magnitude and assymetry of the (sediment) transport capacity of these channels relative to the main channels.

As outlined in section 4.4, the individual connecting channels conduct and redistribute 10 to 20% of the total water transports between the main ebb and flood channel. Except for the maximum flood flow in the cross channel, maximum cross-sectional

averaged current velocities in the connecting channels range between 0.9 to 1.3 m/s, depending on the neap-spring tidal cycle. The magnitude of these velocities resembles the velocities in the main channels. This indicates that the sediment transport capacity of the individual connecting channels also approximates 10 to 20% of the total transport capacity of the main channels during ebb and flood. Thus the connecting channels have the potential to redistribute a significant amount of sediment between the two main channels.

Current asymmetry is often used as a first indicator for net sediment transport directions (see section 4.1 and 4.3.3). The pattern of current asymmetry in the main channels indicate that the two channels tend to form a large-scale net circulation of water and sediment, that is related to the morphology of the channels (ebb channel or flood channel). This circulation is schematically depicted in Figure 4.60. The discharge measurements show a tendency towards an increase of the intensity of this circulation with tidal range, i.e. larger net transports with spring tide than during neap tide.

Current asymmetry in the connecting channels imply the presence of small-scale circulations within the large-scale circulation induced by the main channels. These small-scale circulations are related to presence and morphology of the connecting channel. The ebb and flood-dominated bar channels induce at least two small-scale circulations over the bar in the main flood channel (3 in Figure 4.60). The presence of the large ebb cross channel causes a larger small-scale circulation over the bar in the flood channel and the entrance in the ebb channel (2 in Figure 4.60). The increase of current asymmetry in the flood bar channels and the decrease of current asymmetry in the ebb bar channel, with increasing tidal range, has two implications for the small-scale-circulations over the bar:

- · the intensity of the circulation is not constant over the neap-spring tidal cycle;
- the circulation is not closed and is likely to have a net component in flood direction, which increases with tidal range.

The net flood component of the circulation is likely because the flood-dominated current asymmetry in the flood bar channel is larger than the ebb-dominated current asymmetry in the ebb channel. In addition the morphology of the bar is dominated by flood bar channels. The increase of the ebb-dominated current asymmetry in the cross channel indicates an increase of the intensity of the small-scale circulation 2.

To conclude, the connecting channels induce small-scale net circulations of flow within the large-scale circulation related to the main channels. The connecting channels enable small-scale redistributions of flow and sediment within the system of two main channels, thus increasing the flexibility of the channel system. The bars in the channels are important elements in these circulations, as they demarcate the areas of flood-dominated and ebb-dominated flow.

The foregoing discussion and conclusions identified the need for further elaboration on the following subjects:

- The implications of the observed flow response over the bars in the connecting channel for the patterns of sediment transport, erosion and sedimentation and the morphology of the bars;
- The cause of the small current velocities in the cross channel during flood;
- · The flow response and sediment transports over the bar in the cross;
- The effect of the temporal and spatial variations of current asymmetry in the study area on the net patterns of sediment transport.

These subject are discussed in chapter 5 on the basis of (sensitivity) computations with a 2DH-flow model and a 2DV-model for sediment transport.

#### LITERATUUR

Adler, M., 1993, Messungen von Durchflussen und Stromungsprofilen mit einem Ultraschallen-Doppler-Gerat (ADCP), Wasserwirtschaft, H.4, 192-196

Ahnert, F., 1960, Estuarine meanders in the Chesapeake Bay area, Geographical Review, 50:390-401

Allersma, E., 1994, Geulen in estuaria. 1-D modellering van evenwijdige geulen, Delft Hydraulics, report H18128 (in Dutch)

Anonymous, 1940, Westerschelde. Overzicht van de rapporten tot 1 mei 1940., Studiedienst der Zeeuwse Stroomen?, rapport 1013

Arentsen, J.D., H.C. Peters, 1986, Inventarisatie Stroommeting, Rijkswaterstaat Dienst Informatieverwerking, Nota AD 1986-136

Aubrey, D.G., 1986, Hydrodynamic controls on sediment transport in well-mixed bays and estuaries., Physics of shallow estuaries and bays. (Ed. J. van de Kreeke). Berlin. Springer Verlag. p.245-258.

Aubrey, D.G. & P.E. Speer, 1984, Updrift migration of tidal inlets, Journal of Geology, vol.92, p.531-545

Bliek, A.J., C. Storm, 1995, Bars and maintenance dredging in the Western Scheldt, Proc. 14th. World Dredging Congress, Amsterdam, The Netherlands.p.643-656. Ed. V.L. Van Dam

Bliek, A.J., H.E. Klatter, J.L.M. Konter & T. van der Meulen, 1986, Short cut channels in tidal estuaries, Third international symposium on River sedimentation, Univ. of Mississippi: 300-309

Booij, R., J.P.Th. Kalkwijk, 1983, Secondary flow in estuaries due to curvature of the main flow and to the rotation of the earth and its development., Geomor-nota: 83.05

Boon, J.D., R.J. Byrne, 1981, On basin hypsometry and the morphodynamic response of coastal inlet systems., Marine Geology 40, p.27-48.

Bray, R.N., A.D. Bates, J.M. Land, 1997, Dredging. A handbook for engineers, John Wiley & Sons, New York

Chang, H., 1987, Flow in curved river channels, Fluvial processes in river Engineering, H. Chang: 190-224

Chappell, J., C.D. Woodroffe, 1994, Macrotidal estuaries, Coastal evolution. Late Quaternary shoreline morphodynamics. R.W.G. Carter, C.D. Woodroffe (eds.). p.187-218

Claessens and Meyvis, 1994, Overzicht van de tijwaarnemingen in het Zeescheldebekken gedurende het decennium 1981-1990, Ministerie van de Vlaamse gemeenschap, Antwerpse Zeehavendienst

Cooper, J.A.G., 1993, Sedimentation in a river dominated estuary, Sedimentology, 40:979-1017

Cowell, P.J., B.G. Thom, 1994, Morphodynamics of coastal evolution, Coastal evolution. Late Quaternary shoreline morphodynamics. R.W.G. Carter, C.D. Woodroffe (eds.). p.33-86

Dalrymple, R.W., B.A. Zaitlin, R. Boyd, 1992, Estuarine facies models: conceptual basis and stratigraphic implications, Journal of Sed. Petr., vol. 62, 6: 1130-1146

Davis, J.C., 1986, Statistics and data analysis in geology, 2nd. edition, John Wiley & sons, New York., 646p.

De Jong, H., F. Gerritsen, 1984, Stability parameters of the Western Scheldt estuary, Proc. 19th. Coast.Eng.Conf., ASCE vol.III, ch. 205: 3078-3093

De Jonge, V.N., 1983, Relations between the annual dredging activities, suspended matter concentrations and the development of the tidal regime in the Ems estuary, Can. J. Fish. Aquati Sci., 40 (suppl.1), p.289-300

De Jonge, V.N., 1992, Tidal Flow and Residual Flow in the Ems Estuary, Est., Coast. and Shelf Sci. 34, 1-22

De Looff, D., J. van Malde, 1968, Over de geulontwikkelingen sinds 1800 in de Westerschelde i.v.m. trac\_ bepalingen vaste oeververbindingen, Directie Zeeland Studiedienst Vlissingen, nota 68.2

De Looff, D., J. van Malde, 1976, Over de cyclus der drempelgeulen in de oostelijke uitloop van de Zimmermangeul, Directie waterhuishouding en waterbeweging studiedienst Vlissingen, Rijkswaterstaat-serie 22.

De Vriend, H.J., 1977, A mathematical model of steady flow in curved shallow channels, Journal of Hydraulic Research, 15: 37-54

De Vriend, H.J., 1990, Morphological processes in shallow tidal seas., R.T. Cheng (ed.) Coastal and Estuarine Studies, 38: Residual Currents and Long-term Transport: 276-301

De Vriend, H.J., 1991, Mathematical modelling and large-scale coastal behaviour. Part 1: Physical processes., Journal of Hydraulic Research, vol. 29, no.6: 727-740.

De Vriend, H.J., 1991, Mathematical modelling and large-scale coastal behaviour. Part 2: Predictive models., Journal of Hydraulic Research, vol. 29, no.6: 741-753.

Dronkers, J., 1986, Tidal Asymmetry and Estuarine Morphology, Netherlands Journal of Sea Research, 20, p.117-131

Dronkers, J., W. van Leussen (eds), 1988, Physical Processes in Estuaries, Springer-Verlag, 553 p.

Dyer, K.R., 1985, Coastal and Estuarine Sediment Dynamics,

Fokkink, R.J., B. Karssen, Z.B. Wang, J.D.M. van Kerckhoven, A. Langerak, 1998, Morphological modelling of the Western Scheldt estuary., Physics of Estuaries and Coastal Seas.Eds. J.J. Dronkers, M. Scheffers. p.329-337

Gerritsen, F., H. de Jong, A. Langerak, 1990, Cross-sectional stability of estuary channels in the Netherlands., Proc. 22nd International Conference on Coastal Engineering, vol. 3, Ch.221: 2922-2935.

Geyl, W.F., 1976, Tidal Neomorphs, Z. Geomorph. N.F., 20, 3, p.308-330

Godin, G., 1972, The analysis of tides, Liverpool University Press, 264 p.

Granat, M.A., J.C. Ludwick, 1980, Perpetual shoals at the entrance of Chesapeake Bay: flow-substrate interaction and mutually evasive net currents, Marine Geology 36: 307-323

Hardisty, 1986, A morphodynamic model for beach gradients, Earth Surface Processes and Landforms, 11, 327-333

Harris, P. T., 1988, Large-scale bedforms as indicators of mutually evasive sand transport and the sequential infilling of wide-mouthed estuaries, Sedimentary geology, 57: 273-298

Harris, P.T. & M.B. Collins, 1985, Bedform distributions and sediment transport paths in the Bristol Channel and Severn Estuary, UK, Marine Geology, 62: 153-166

Heathershaw, A.D., F.D.C. Hammond, 1980, Secondary Circulations near Sand Banks and in Coastal Embayments, Dt. hydrogr. Z. 33: 135-151

Huijs, S.W.E., 1996, De ontwikkeling van de morfologie vande Westerschelde in relatie menselijke ingrepen 1995-1996, University of Utrecht, IMAU-report R96-17, 104 p.(in Dutch).

Ikeda, S. and G. Parker, 1989, River Meandering., Am. Geoph. Union, Water Res. Monograph 12, 485p

Jansen, P.Ph., 1940, Eenige aanteekeningen over het bankengebied in de Westerschelde nabij Ossenisse, Studiedienst der Zeewsche Stroomen, Hoek van Holland Jansen, P.Ph. T. Volkers, 1939, Nota inzake een onderzoek naar de oorzaken van de verdiepingen voor den oever van de zuid-watering van den polder Walcheren, Directie Benedenrivieren?, rapport D 273

Jeuken, M.C.J.L., 1993, Morfologische veranderingen van de geulen en platen in de Westerschelde gedurende de periode 1965-1990, Nota NXL-93.13

Jeuken, M.C.J.L., 1994, Morfologische ontwikkeling van de geulen en platen in het Valkenisse-gebied (Westerschelde) gedurende de periode 1986-1993, Rijkswaterstaat. Notitie NWL-94.15

Jonkers, W., 1991, De problematiek omtrend de basisgegevens voor morfologisch onderzoek naar geulveranderingen in het Oosterscheldebekken na 1987, Rijkswaterstaat, report GWAO 91.13039

Kalkwijk, J.Th., R. Booij, 1986, Adaptation of secondary flow in nearly-horizontal flow, Jour. of Hydraulic Research, Vol. 24, No.1. p.19-37

Kamminga, S., 1995, Resultaten van stromingsmetingen met een ADCP bij Everingen in de Westerschelde op 29 juni 1995, V.O.F. Aqua Vision report AV4

Kamminga, S., 1996, Resultaten van stromingsmetingen met een ADCP bij Everingen in de Westerschelde op 30 augustus 1995, V.O.F. Aqua Vision report AV9

Kleinjan, I.L., 1933, Beschouwingen en berekeningen over de ontwikkeling van de Westerschelde en haar mondingsgebied sedert 1800 op grond van de beschikbare hydrografische kaarten, Directie Benedenrivieren, rapport R 15

Kleinjan, I.L., 1934, Verslag van het onderzoek naar den toestand der tusschenwateren v\_r den aanleg van den slaakdam resp. scheldedam, alsmede naar het verschil van den toestand dier tusschenwateren v\_r 1830 en v\_r 1866, Directie Benedenrivieren, Rapport R 16a en 16b

Kleinjan, I.L., 1936, Enkele beschouwingen over plaatselijke wijzigingen in het gebied van de Westerschelde op grond van parti\_le hydrografische opnemingen, alsmede verslag over de in de jaren 1933, 1934 en 1935 verrichte dwarsprofielloodingen., Directie Benedenrivieren, rapport R 19

Kleinjan, I.L., 1938, Het gebied van de Westerschelde nabij Bath, Direktie Benedenrivieren / Directie Waterhuishouding en -beweging, rapport R 88a, 88b, 88c

Kohsiek, L.H.M., 1988, Reworking of former eb-tidal deltas into large longshore bars following the artificial closure of tidal inlets in the Southwest of the Netherlands, Tide-Influnced Sedimentary Environments and Facies. P.L. de Boer et.al. (eds.), D.Reidel Publishing Company, p.113-122

Kohsiek, L.H.M., H.J. Buist, P.Bloks, R.Misdorp, J.H. van den Berg, J.Visser, 1988, Sedimentary processes on a sandy shoal in a meso-tidal estuary (Oosterschelde, The Netherlands), Tide-Influenced Sedimentary Environments and Facies. P.L. de Boer et.al. (eds.), D.Reidel Publishing Company, p. 201-214

Kohsiek, L.H.M., J.P.M. Mulder, T. Louters, F. Berben, 1987, De Oosterschelde naar een nieuw onderwaterlandschap: eindrapport project Geomor, Nota GWAO-87.029, Geomor nota 87.02

Kroon, A., 1994, Sediment transport and morphodynamics of the beach and nearshore zone near Egmond, The Netherlands, Phd-thesis Utrecht University

Lamb, H., 1932, Hydrodynamics, Dover publications New York

Latteux, B., 1995, Techniques for long-term morphological simulation under tidal action, Marine Geology 126, 129-141

Lessa, G., G. Masselink, 1995, Morphodynamic evolution of a macrotidal barrier estuary, Marine Geology 129: 25-46

Ludwick, J. C., 1974, Tidal currents and zig-zag sand shoals in a wide estuary entrance, Geological Society of America Bulletin, v. 85: 717-726

Ludwick, J. C., 1989, Bed load transport of sand mixtures in estuaries: a review, Journal of Geophysical research, 94, C10: 14315-14326

Mosselman, E., 1992, Mathematical modelling of morphological processes in rivers with erodible cohesive banks, Phd-thesis, Delft University of Technology, 134p.

Nanninga, M., 1985, The accuracy of echo sounding. Description of a mathematical model, Rijkswaterstaat, report WWKZ 85.H016

Nichols, M.N., R.B. Biggs, 1985, Estuaries, Coastal Sedimentary Environments. R.A. Davis (ed.). 77-186

O' Brien, M.P., 1931, Estuary Tidal Prism Related to Entrance Areas., Civil Engineering, 1 (8): 738-739

Olesen, K.W., 1987, Bed topography in shallow river bends., Phd-thesis, Delft University of Technology, 265p

Parker, B.B., 1991, The relative importance of the various non-linear mechanisms in a wide range of tidal interactions (review), Tidal Hydrodynamics (B.B. Parker, ed.) John Wiley & Sons, inc.: 437-447

Perillo, G.M.E., 1995, Geomorphology and sedimentology of estuaries: an introduction, Geomorphology and Sedimentology of Estuaries. Developments in Sedimentology. G.M.E. Perillo (ed.), 53, p.1-16

Perillo, G.M.E., 1995, Definitions and geomorphologic classifications of estuaries, Geomorphology and Sedimentology of Estuaries. Developments in Sedimentology. G.M.E. Perillo (ed.), 53, p.17-47

Perillo, G.M.E. & M.E. Sequeira, 1989, Geomorphologic and sediment transport characteristics of the middle reach of the bahia blanca estuary (Argentina, Journal of Geophysical Research, 94, C10: 14351-14362

Perillo, G.M.E., G. Drapeau, M.C. Piccolo & N. Chaouq, 1993, Tidal circulation patterns on a tidal flat, Minas Basin, Canada, Marine Geology, 112: 219-236

Peters, J.J. & A. Sterling, 1978, Hydrodynamique et transports de s\_diments de l'estuaire de l'Escaut, Nat. Onderzoeks- en ontw.programma Leefmilieu Water, 10 (Projekt Zee) (Nihoul, J.C.J. & R. Wollast, eds.): 1-70

Phillips, J.D., 1992, The end of equilibrium?, Geomorphology 5, 195-201

Postma, H., 1967, Sediment Transport and Sedimentation in the Estuarine Environment, American Association of Advanced Science Publications 83, 158-179

Pugh, D.T., 1987, Tides, surges and mean sea-level. A Handbook for Engineers and Scientists, John Wiley & Sons, Chichester, 472p.

RD Instruments, 1989, Principles of Operation: A practical primer., Hydrotech, 35p.

Ridderinkhof, H., 1988, Tidal and residual flows in the western Dutch Wadden sea II: an analytical model to study the constant flow between connected tidal basins, Netherlands Journal of Sea Research, 22(3): 185-198

Ridderinkhof, H. & J.T.F. Zimmerman, 1990, Residual currents in the Dutch Wadden sea, Coastal and Estuarine Studies, 38: 93-104

Ringma, S.H., 1950, De ontwikkeling van het geulenstelsel van Ossenisse en de stroomaanval op de Nol van Molenpolder, Directie Zeeland arrondisement Vlissingen, rapport 50.4

Robinson, A.H.W., 1960, Ebb-flood Channel Systems in Sandy Bays and Estuaries, Geography 45:183-199

Robinson, I.S., 1983, Tidally induced residual flows, Physical Oceanography of Coastal and Shelf Seas. B. Johns (ed.). Ch.7: 321-356

Seminara, G., 1995, Invitation to river morphodynamics, In: Non-linear dynamics and pattern formation in the natural environment. Eds. A. Doelman and A. Van Harten (eds). Pitman Res. Notes Math. no. 335, p.269-294

Simpson, J.H., E.G. Mitchelson-Jacob, A.E. Hill, 1990, Flow structure in a channel from an acoustic doppler current profiler, Continental Shelf Research, 10: 589-603

Soulsby, R.L., 1983, The bottom boundary layer of shelf seas, Physical oceanography of coastal and shelf seas. Elsevier, Amsterdam: 189-266

Spaans, W., N. Booij, N. Praagman, R. Noorman, J. Lander, 1989, DUFLOW, a Micro-Computer Package for the Simulation of One-Dimensional Unsteady Flow in Open Channel Systems, SAMWAT, The Hague, 92 p.

Speer, P.E., D.G. Aubrey, C.T. Friedrichs, 1991, Nonlinear hydrodynamics of shallow tidal inlet/bay systems, Tidal Hydrodynamics. B.B. Parker (ed.): 321-339

Sterling, A., P. Roovers, 1967, Modelstudies aangaande de verbetering van de bevaarbaarheid van de Westerschelde, De Ingenieur, Bouw- en Waterkunde 4, 41-68

Storm, C., P. Bollebakker, J. de Jong, G. Mol, 1994, Nauwkeurigheid zandbalans Westerschelde 1965-1990, Rijkswaterstaat report RIKZ-94.008

Struiksma, N., K.W. Olesen, C. Flokstra, H.J. de Vriend, 1985, Bed deformation in curved alluvial channels., Journal of Hydraulic Research, 23, 1:?

Terwindt and Wijnberg, 1991, Thoughts on large scale coastal behaviour., Proc. Coastal Sediments '91, ASCE, New York: 1476-1488

Thorne, C.R., R.D. Hey, 1979, Direct measurements of secondary flow at a river inflexion point., Nature 280: 226-228

Uit den Bogaard, L., 1995, Resultaten zandbalans Westerschelde. 1955-1993., University of Utrecht. IMAU report R-95-08. 48 p.

Van de Kreeke, J., J. Haring, 1979, Equilibrium flow areas in the Rhine-Meuse delta, Coastal Engineering 3, p.97-111

Van de Kreeke, J., K. Robaczewska, 1993, Tide-induced residual transport of coarse sediment; application to the Ems estuary, Netherlands Journal of Sea Research, Vol. 31 (3):209-220

Van de Meene, J.W.H., 1994, The shore-face connected ridges along the central Dutch coast., Phd-thesis. Utrecht University. 222p.

Van den Berg, J.H., 1986, Aspects of sediment- and morphodynamics of subtidal deposits of the Oosterschelde (the Netherlands), Rijkswaterstaat communications no. 43

Van den Berg, J.H., D. Schouten, C.J. van Westenbrugge, 1991, Zandbalans Westerschelde 1965-"70-'75-'80-'85, Rijkswaterstaat, report NWL-91.36

Van den Berg, J.H., M.J.L. Jeuken, A.J.F. van der Spek, Hydraulical and morphological evolution of the Westerschelde estuary,

Van der Spek, A.J.F., 1994, Large-scale evolution of Holocene tidal basins in the Netherlands, Phd-thesis, Utrecht University, 191p.

Van Dongeren, A.R., H.J. De Vriend, 1994, A model of morphological behaviour of tidal basins, Coastal Engineering, 22:287-310

Van Kerckhoven, J.D.M., 1995, Morphological modelling of ebb and flood channel systems in estuaries, Masters Thesis, Delft University, Faculty of Civil Enegineering

Van Kleef, A.W., 1995, Verklaring voor de veranderingen in de grootschalige zandbalans van het gebied rond het Middelgat, Westerschelde., Rijkswatestaat. draft report

Van Munster, R.J., M. Meulblok, G. van Antwerpen, C.J. van Westenbrugge, J.C. Borst., 1995, DIGIPOL, intelligent interpolation of depth measurements., Proc. 14th World dredging Conference, Amsterdam

Van Rijn, L.C., 1984, Sediment Transport, Part II: Suspended load Transport, Journal of Hydraulic Engineering, vol.110, 11:1613-1641

Van Rijn, L.C., 1984, Sediment Transport, Part I: Bedload Transport, Journal of Hydraulic Engineering, vol.110, 11:1431-1613

Van Rijn, L.C., 1984, Sediment Transport, Part III: Bed Forms and Alluvial Roughness., Mathematical Modelling of Morphological Processes in the case of Suspended Sediment Transport, Phd-Thesis 1987 (Appendix A)

Van Rijn, L.C., 1993, Principles of sediment transport in rivers, estuaries and coastal seas, Aqua Publications, Amsterdam, The Netherlands.

Van Veen, J., 1936, Onderzoekingen in den hoofden in verband met de getseldheid der Nederlandse kust, Algemene Landsdrukkerij, Den Haag, 252 p.

Van Veen, J., 1950, Eb- en Vloedschaar Systemen in de Nederlandse Getijwateren, tijdschrift K.N.A.G., vol. 67(2): 303-325

Vroon, J., C. Storm, J. Coossen, 1997, Westerschelde, stram of struis? Eindrapport van het project Oostwest, een studie naar de beinvloeding van fysische en verwante biologische patronen in een estuarium, Rijkswaterstaat, report RIKZ-97.023

Wang, Z.B., H.J. De Vriend, T. Louters, 1991, A morphodynamic model for a tidal inlet, Computer modelling in Ocean Engineering 91, Arcilla et.al. (eds). p.235-245

Wright, L.D. B.G. Thom, 1977, Coastal depositional landforms: a morphodynamic approach, Prog. Phys. Geogr., vol. 1, 3: 412-459

Wright, L.D., J.M. Coleman & B.G. Thom, 1975, Sediment transport and deposition in a macrotidal river channel: Ord river, Western Australia, Research, Vol.II, Geology & Engineering, L.E. Cronin (ed.): ...

Zitman, T.J., 1992, Quasi-3 dimensional current modelling based on a modified version of Davies' shapefunction approach, Continental Shelf Research, 12: 143-158

